Nimbus–7 Total Ozone Mapping Spectrometer (TOMS) Data Products User's Guide

Richard D. McPeters, P. K. Bhartia,
Arlin J. Krueger, and Jay R. Herman
*NASA/Goddard Space Flight Center
Greenbelt, MD 20771*

Barry M. Schlesinger, Charles G. Wellemeyer,
Colin J. Seftor, Glen Jaross,
Steven L. Taylor, Tom Swissler,
Omar Torres, Gordon Labow,
William Byerly, and Richard P. Cebula
*Hughes STX Corporation (HSTX)
4400 Forbes Boulevard
Lanham, MD 20706*

ACKNOWLEDGMENTS

TABLE OF CONTENTS

TABLE OF CONTENTS (Continued)

LIST OF FIGURES

LIST OF TABLES

LIST OF TABLES (Continued)

1.0 INTRODUCTION

Nimbus–7 was launched on October 24, 1978; measurements began about a week later. For the purpose of obtaining daily high-resolution global maps of atmospheric ozone, TOMS measured the solar irradiance and the radiance backscattered by the Earth's atmosphere in six selected wavelength bands in the ultraviolet. TOMS scanned in 3-degree steps to 51 degrees on each side of the subsatellite point, in a direction perpendicular to the orbital plane. Consecutive cross-scans overlapped, creating a contiguous mapping of ozone.

This document is a guide to the data products derived from the measurements made by the Total Ozone Mapping Spectrometer (TOMS) experiment aboard the Nimbus–7 satellite. It discusses the calibration of the instrument, the algorithm used to derive ozone values from the measurements, the uncertainties in the data, and the organization of the data products. The data begin October 31, 1978 and end May 6, 1993. These data are archived at the Goddard Space Flight Center Distributed Active Archive Center (DAAC).

Since the previous release of TOMS data, continuing study of the TOMS data products and the process of deriving them has led to many improvements in the generation the data. A comprehensive study of the instrument properties and their variations with time has been made, producing a more accurate derivation of radiances from the raw instrument counts. Improvements have been made to the input physical data, the treatment of physical processes, and the parameterizations of atmospheric conditions used in the radiative transfer calculations that are part of the algorithm. The process of deriving ozone and reflectivity has been modified to incorporate a linear correction for wavelength dependence in the reflectivity, other wavelength-dependent physical effects, or wavelength-dependent errors. The resulting Version 7 TOMS data have a long-term 2σ calibration uncertainty of ± 1.5 percent in total ozone over 14.5 years. In addition, a number of local anomalies in the earlier data have been eliminated.

There also has been a significant change in the physical form of the TOMS products. The basic format for all earlier issues was magnetic tape, although some data have been released on CD–ROM. For Version 7, the basic format, will, for the first time, be electronic data files and CD–ROM. The new TOMS products described in this document supersede previously archived products, and this document supersedes previous TOMS data product documents.

Section 2 of this User's Guide provides a brief history of TOMS data releases, documents, and the principal modifications in the methodology used in deriving the TOMS data products between successive releases. Section 3 provides a general overview of the TOMS instrument, the algorithm, the uncertainties in the results, and other basic information required for best use of the data files. It is designed for the user who wants a basic understanding of the products but does not wish to go into all the details. Such a user may prefer to read only those parts of Sections 4 through 7 addressing questions of particular interest. In Section 4, the instrument, its calibration, and the characterization of its changes with time are discussed. The algorithm for retrieval of total ozone and its theoretical basis are described in Section 5. Section 6 describes the overall uncertainties in the ozone data and how they are estimated, while Section 7 discusses particular problems that may produce errors in specific time intervals and geographical areas. Both sections identify some anomalies remaining in the data and discuss what is known about them. The structure of the data products is presented in Section 8. Appendix A tabulates the standard atmospheric ozone and temperature profiles used in the algorithm for ozone retrieval. Appendix B provides sample software in C for reading the HDF data files, and Appendix C provides information on data availability.

2.0 HISTORICAL BACKGROUND

2.1 Releases and Documents

The 14.5 years of TOMS data (October 31, 1978 through May 6, 1993) discussed in this *User's Guide* were archived at the DAAC in February 1996. They were generated using Version 7 of the software. Other sections of this *Guide* describe the instrument and its calibration, the algorithm for ozone retrieval, and the validation. During the TOMS lifetime, there have been a number of data releases and accompanying documents. Data products are characterized by level, with higher numbers corresponding to a greater degree of processing. Level–1 consists of time-corrected, uncalibrated, Earth-located data arranged by scan, along with co-located climatological information, Level–2 consists of scene-by-scene, Earth-located products of the retrieval and calibrated data; and Level–3 consists of averages over cells in a latitude-longitude grid. The present release of data and this Version 7 *User's Guide* supersede all previous discussion of Level–2 and Level–3 products. Version 7 data should be used for any future studies based upon TOMS measurements.

The information needed for deriving data products is collected from the satellite and stored in the form of Raw Unit Files. These files are archived in tape format as the TOMS Raw Unit Tapes-TOMS (RUT-T), a Level–1 product. These tapes contain uncalibrated irradiance and radiance data, housekeeping data, calibration information, instrument field-of-view (FOV) location, and solar ephemeris information from TOMS. They also contain information on terrain pressure and snow-ice thickness, as well as some limited information on clouds. The RUT *User's Guide* [*Fleig et al., 1983*] describes the experiment, instrument calibration, operating schedules, data coverage and tape formats for the first 2 years. The material in this guide is generally still valid, except for the discussion of postlaunch instrument calibration. In particular, the tape format description still applies to the current RUT tapes. Many of the intermediate tapes discussed in the description of production have now been replaced by data files.

The first data released to the archive were the Version 4 Level–2 products, the OZONE-T tapes. Versions 1–3 of the processing software were developmental versions, and those data were not released. In June, 1982, a user's guide to the first year of TOMS data [*Fleig et al., 1982*] was produced to accompany the Version 4 release. In addition to describing the tape format, that user's guide described the algorithm used to retrieve ozone and provided a brief outline of its theoretical foundations. The present guide draws upon that description.

In 1983, the first gridded product, GRIDTOMS, a tape of daily averages of ozone over cells in a latitude-longitude grid corresponding to the current Level–3 product, was released. A tape specifications document was issued to accompany the tapes [*NASA, 1986*].

By the time 4 years of data were to be archived, a new characterization of instrument changes with time and a method for identifying ozone retrievals possibly contaminated by volcanic SO_2 had been developed. There also had been some changes in the tape format; the OZONE-T tape was replaced by the high-density TOMS (HDTOMS) tape. These issues were addressed in an addendum for the years 3 and 4 to the first-year user's guide [*NASA, 1984*]. This document included, in addition, a catalog of HDTOMS tapes for the third and fourth years of measurements.

In 1985, a new set of tapes, the result of Version 5 processing, replaced Version 4. In August 1988, Version 5 Level–3 products were made available on line at the National Space Science Data Center (NSSDC). In November 1990, Version 6 was released. The *Nimbus–7 Total Ozone Mapping Spectrometer (TOMS) Data Products User's Guide* [*McPeters et al., 1993*] was issued to describe the Version 6 products and the changes from previous versions. In December 1990, Level–3 products were issued for the first time on CD–ROM, in ASCII format. In November 1992, Level–3 near-real-time products were made available through anonymous ftp. Operational production of the Version 6 data continued for the remainder of the TOMS lifetime using an extrapolated calibration adjustment.

For Version 7, the principal release medium has been changed from tape to electronic data files. Both Level–2 and Level–3 products are being archived for distribution to the scientific community at the GSFC DAAC as Hierarchical Data Format (HDF) data sets [*NCSA, 1994*]. In addition, the Level–3 GRIDTOMS tape has been replaced by the on-line CDTOMS files, which are also available on CD–ROM. Section 2.2 describes the version-to-version processing changes. Section 8 describes the format of the Version 7 data products.

2.2 Evolution of the Processing

Analysis of the TOMS data has driven a process of continual improvement of the data. As the most significant errors have been eliminated, progressively smaller errors have been detected, investigated, and corrected. Refinement of the algorithm has been an integral part of this process. In addition, the progressively longer timespans of data have provided an improved data base for investigating changes in instrument sensitivities as the patterns of instrument change have varied over its lifetime. To incorporate these improvements, there have been three major reprocessings of the data since the original Version 4 release.

2.2.1 Versions 5 and 6

The principal reason for the first reprocessing, creating Version 5, was the adoption of improved absorption coefficients based upon the cross-section measurements of Paur and Bass [*1985*], as recommended the International Ozone Commission at its 1984 meeting in Halkidiki, Greece, replacing the absorption coefficients used for Version 4 that had been based on the results of Inn and Tanaka [*1959*]. Also, a model for degradation in the reflective properties of the diffuser plate used in weekly measurements of the solar flux was now applied to the data. These solar measurements were used to calculate the ratio of the backscattered radiance to solar irradiance for input to the algorithm. When this ratio was calculated, instrument errors other than diffuser errors would cancel; thus, the change in sensitivity of the diffuser plate was the only instrumental change component needed. This model was based on an exponential decay.

Methods for identifying scans that might be contaminated by SO_2 were developed. A third wavelength pair, especially sensitive at high latitudes and zenith angles, was added to the two that had been used for Version 4. Finally, the system of data quality flags was expanded.

As time passed, the TOMS ozone values were observed to be drifting downward relative to those measured by the ground-based Dobson network [*Fleig et al., 1988*]. Investigation of this drift and of Nimbus–7 Solar Backscatter Ultraviolet (SBUV) data identified the problem as an error in the correction for diffuser plate degradation [*Watson et al., 1988*]. To correct this error, the Pair Justification Method (PJM) [*Herman et al., 1991*] was developed. The basic principle of this method is that when two different wavelength pairs should measure the same ozone value, discrepancies in the derived values will result from differential sensitivity to instrument degradation and can be used to correct for it. Application of this correction was the principal reason for the development of Version 6.

Several other modifications were made. Radiances were calculated for ozone and temperature profiles characteristic of the severe ozone depletion in the Antarctic spring that began during the TOMS lifetime. Corrections were made to the derivation of spacecraft attitude, as described in Section 4.3. To minimize the effects of an intermittent loss of synchronization (*non-synch* conditions) between the TOMS wavelength selection/chopper wheel and the photon counting electronics [*Fleig et al., 1986*] that began in 1984, one of the original wavelength pairs was replaced by an alternate pair less affected by this problem. A more complete discussion of the changes between Versions 5 and 6 can be found in the Version 6 User's Guide [*McPeters et al., 1993*].

2.2.2 Version 7

Validation studies of the Version 6 ozone values revealed several problems. There was a systematic bias between the Version 6 TOMS total ozone values and those from SBUV and from Dobson. TOMS ozone values showed a drift with time relative to Northern Hemisphere Dobson measurements that was latitude dependent, with seasonal differences appearing toward the end of the TOMS lifetime [*McPeters and Komhyr, 1991*]. The accuracy of the ozone values retrieved at high solar zenith angles was considered unsatisfactory. Ozone values observed over partial cloud cover at low zenith angle (high sun) were systematically too low. To eliminate these problems, Version 7 was developed.

Error in the Version 6 wavelength calibration proved to be the principal source of the Version 6 TOMS total ozone bias relative to SBUV. A new wavelength calibration was determined, based on a re-examination of the original prelaunch wavelength calibration data. Also, a new method was used to correct for variations in instrument sensitivity with time. In previous versions a correction to the radiance/irradiance ratio had been derived by determining changes

in the diffuser plate reflectivity [*Herman et al., 1991*]. For Version 7, the correction is applied to the radiances and is based upon the measured wavelength dependence of surface reflectivity. Details appear in Section 4.5.

For higher path lengths, the Version 6 scheme for weighting ozone profiles from different latitudes by linear interpolation in latitude has been replaced by a weighting determined by finding the best fit to the measured radiances. This new profile weighting scheme yields more accurate ozone values and reduced noise at high solar zenith angles. In previous versions, partial cloud scenes were treated by assuming that radiation was reflected from a single effective scene pressure level with a single effective reflectivity. In Version 7, a two-layer model that accounts separately for reflection from the ground and from cloud is used. Implementing this new treatment eliminated the underestimates of ozone over partial cloud cover. In addition, adoption of a new cloud height climatology eliminated overestimates of total ozone that had been made over areas of persistent low marine stratus.

In earlier versions, ozone was derived using pairs of wavelengths, with one wavelength of each pair an ozone-absorbing wavelength. For Version 7, triplets are used, adding a longer ozone-insensitive wavelength to each pair. Using three wavelengths permits a simultaneous solution for ozone and for any additional contributions to the measured radiances, such as residual imperfections in the characterization of the changes of instrument sensitivity with time and wavelength dependence of the reflectivity caused by dust or sea glint, that are linear with wavelength.

The sulfur dioxide (SO_2) index (SOI) used for Version 6 yielded non-zero SO_2 even for scenes where SO_2 was known to be absent. Before SO_2 could be calculated, this offset value needed to be subtracted. A new SO_2 index that has no offset has been defined. In addition, because of the improvements made in the previous versions, some smaller errors under particular conditions, such as high solar zenith angle, cloudiness, or dust, have now been identified. To deal with these errors, several additional improvements have been made to the instrument calibration, the radiative transfer calculations, and the ozone retrieval algorithm. Additional details about these improvements, as well as about the other improvements described in this section appear in Section 5.

The time dependence of the ozone values from Version 7 derived from TOMS was compared with that of values derived from a set of Northern Hemisphere ground stations. Any difference was smaller than the combined uncertainties of the TOMS measurements, the surface measurements, and the comparison method.

3.0 OVERVIEW

3.1 Instrument

The Total Ozone Mapping Spectrometer (TOMS) experiment on board the Nimbus–7 satellite provided daily global coverage of the Earth's total ozone by measuring the backscattered Earth radiance in the six 1-nm bands listed in Table 4.1. The experiment used a single monochromator and scanning mirror to sample the backscattered solar ultraviolet radiation at 35 sample points at 3-degree intervals along a line perpendicular to the orbital plane. The measurements used for ozone retrieval were made during the sunlit portions of the orbit as the spacecraft moved from south to north. In normal operation, the scanner measured 35 scenes, one for each scanner view angle, stepping from right to left. It then quickly returned to the first position, not making measurements on the retrace. Eight seconds after the start of the previous scan, another would begin.

For the first 7.5 months of operation, TOMS followed a regular ON/OFF schedule for spacecraft power management, operating on 10 of each 12 days. At times, the instrument was operated on scheduled OFF days also, thus resulting in an actual duty cycle greater than 83 percent. A relay malfunction prevented any measurements from being made during the 6-day period of June 14–19, 1979. Starting June 22, 1979, TOMS operated full time. Early in 1984, a lack of synchronization between the TOMS wavelength selection/chopper wheel and the electronics began to develop. When this condition passed a defined threshold, the data were flagged. The frequency of this condition rarely exceeded 20 percent, except during summer 1990, when it reached 90 percent. However, evidence exists in the data for sporadic periods of less than a day when a subthreshold synchronization problem existed. The instrument failed on May 6, 1993.

3.2 Algorithm

Total ozone is retrieved by calculating the radiances that would be measured for different column ozone amounts and determining which column ozone amount yields the measured radiances. Detailed radiative transfer calculations are used to determine backscattered radiance as a function of total ozone and the conditions of the measurement: geometry, surface pressure, surface reflectivity, and latitude. A particular set of measured radiances is then compared with the set of calculated radiances appropriate to the conditions of the measurement.

Some of the radiation detected by the satellite has been reflected by the surface below or scattered from the atmosphere after such reflection. Thus, the reflecting properties of the surface must be known. If the reflectivity is independent of wavelength, radiances at two wavelengths, one sensitive to atmospheric ozone and one not, can be used to derive atmospheric ozone and reflectivity. This technique is the pair determination method used in previous versions. The Version 7 algorithm allows for a component of reflectivity that is linear with wavelength. It uses radiances at a third, longer, ozone insensitive wavelength to yield this linear term. The three wavelengths constitute a *triplet*.

An initial estimate of ozone is derived using a wavelength pair. Radiances are calculated for this ozone estimate. Then, the ratios of calculated and measured radiances (in practice, the difference of the logarithms) at a triplet of wavelengths can be used to solve simultaneously for the reflectivity, its wavelength dependence, and a correction to the ozone estimate. This process may be iterated. The choice of triplet wavelengths is based upon the optical path length of the measurement.

Section 5 provides a full description of the algorithm.

3.3 Data Uncertainties

Uncertainties in the ozone values derived from the TOMS measurements have several sources: errors in the measurement of the radiances, errors in the values of physical input from laboratory measurements, errors in the parameterization of atmospheric properties used as input to the radiative transfer computations, and limitations in the way the computations represent the physical processes in the atmosphere. Each of these sources of uncertainty can be manifested in one or more of four ways: random error, an absolute error that is independent of time, a time-dependent drift, or an error that will appear only under certain conditions. For TOMS total ozone, the absolute error is ±3

percent, the random error is ±2.0 percent (1σ) and the uncertainty in the drift for 14 years is ±1.5 percent (though somewhat higher at high latitudes). More detailed descriptions of the different sources of uncertainty and the extent to which each contributes to the overall uncertainty appear in Sections 4, 6, and 7. Section 4 discusses uncertainties due to errors in the characterization of the instrument sensitivity. Section 6 discusses other sources of random errors, absolute error, and drift, combining them with the instrument error to yield the overall estimates above.

The algorithm cannot retrieve correct ozone values when SO_2 is present. Values are flagged for SO_2 only when contamination is clearly present. However SO_2 can be present in other measurements but not at levels high enough to be flagged. These measurements, unlike the flagged values, are used in the calculation of the Level–3 grids. Consequently, grid means in the vicinity of high SO_2 concentrations may be affected by marginal SO_2 contamination. The SO_2 changes to sulfuric acid aerosol with time. When volcanic aerosols are present, they change the scattering properties of the atmosphere, producing a dependence of the derived ozone on satellite zenith angle that may be as large as 2 percent. Even when volcanic aerosols are not present, a solar zenith angle dependence of between one-half and one percent is observed. These effects and other errors that occur only for specific times, places, or physical conditions, are discussed in Section 7. Sections 6 and 7 also describe the remaining anomalies that have been identified in the Version 7 data, with a discussion of what is known of their origin.

Comparison between the TOMS ozone values and the ground measurements yields a TOMS-ground bias at launch that is still approximately 1 percent, with TOMS higher. This difference is within the uncertainty of the TOMS and ground measurements. Based upon comparison between the TOMS ozone values and coincident values at 30 Northern Hemisphere stations, the drift of the Version 7 TOMS ozone relative to ground measurements is 0.2 percent/ decade, or 0.3 percent over the TOMS lifetime, even though the instrument diffuser degraded by more than 30 percent at the total ozone wavelengths during its 14.5 years of continuous operation in space. The comparisons with ground measurements are discussed in Section 6.4. The calibration procedure is described in Section 4.

Data quality flags are provided with the derived ozone on the TOMS Ozone File (Level–2 data product). Only the data with quality flag values of 0 are used to compute the averages provided on the CDTOMS (Level–3) product. Larger flag values indicate retrieved ozone values that are of lower quality, allowing the users to decide whether or not they wish to accept such data for their applications. In particular, flag values of 10 or higher signify that the measurements were taken in the descending portion of the orbit, in summer midnight sun. More accurate values, from ascending parts of the orbit, are available for these locations. Table 5.4 summarizes the error flags.

3.4 Archived Products

Two kinds of TOMS total ozone products are archived at the GSFC DAAC as HDF files. The HDF Level–2 Data Product contains detailed results of the TOMS ozone retrieval for each instantaneous field of view (IFOV) in time sequence. One file contains all the data processed for a single orbit. The HDF Level–3 data product contains daily averages of the retrieved ozone and effective surface reflectivity in a 1-degree latitude by 1.25-degree longitude grid. In areas of the globe where orbital overlap occurs, the view of a given grid cell closest to nadir is used. The data for a single day are accumulated over a 24-hour period, and a temporal discontinuity exists in the vicinity of the international data line. Only good quality retrievals are included in the average. Level–3 products also are available on line and on CD–ROMs, in the form of the CDTOMS files. Each file contains one daily TOMS map (0.4 megabyte/ day). A two CD set covers the entire TOMS lifetime. Detailed descriptions of these products are provided in Section 8.

4.0 INSTRUMENT

4.1 Description

The Total Ozone Mapping Spectrometer onboard the Nimbus–7 satellite provided daily global coverage of the Earth's total ozone by measuring backscattered ultraviolet sunlight. TOMS instruments map total ozone by scanning through the subsatellite point in a direction perpendicular to the orbital plane. The Nimbus–7 TOMS instrument had a single, fixed monochromator, with exit slits at six near-UV wavelengths. The slit functions were triangular with a nominal 1-nm bandwidth. The order of individual measurements was determined by a chopper wheel. As it rotated, openings at different distances from the center of the wheel would pass over the exit slits, allowing measurements at the different wavelengths. The order was not one of monotonically increasing or decreasing wavelength; instead, the wavelengths were interleaved to minimize the effect of scene changes on the ozone retrieval. The instrument IFOV was 3 x 3 degrees. A mirror scanned perpendicular to the orbital plane in 3-degree steps from 51 degrees on the right side of spacecraft nadir to 51 degrees on the left (relative to direction of flight), for a total of 35 samples. At the end of the scan, the mirror would quickly return to the first position, not making measurements on the retrace. Eight seconds after the start of the previous scan, another would begin. Consecutive cross-scans overlapped, creating a contiguous mapping of ozone. Heath *et al.* [*1975*] provide a more complete description of the instrument and its initial calibration, along with a diagram of the system.

A ground aluminum diffuser plate was deployed to reflect sunlight into the instrument to measure the solar irradiance. This diffuser plate was shared with the Solar Backscatter Ultraviolet (SBUV) experiment. It was normally deployed once a week for TOMS solar irradiance measurements, in addition to the SBUV deployments.

The TOMS scanner had four operating modes determining data processing sequences and data formats:

- Normal scan mode.
- Single step mode.
- View diffuser mode.
- Stowed mode.

The primary operating mode of the TOMS was normal scan mode. It was in this mode that the scanning mirror sampled the 35 scenes corresponding to the scanner view angles, measuring the backscattered Earth radiances used for deriving column ozone. In the single step mode, the scanner was controlled by ground commands. Solar irradiance measurements were made in the view diffuser mode. The scanner would move to the view diffuser position and stop. In-orbit wavelength calibration occurred in the stowed mode. The scanner slowed to the stowed position and stopped, the mercury-argon lamp was turned on and the diffuser plate was deployed to reflect light from the lamp into the instrument. Wavelength calibration is discussed in greater detail in Section 4.2. Heath and Park [*1978*] describe the instrument and its operation in greater detail. Additional details are provided by Cebula, et al. [*1988*] and the RUT User's Guide [*Fleig et al., 1983*].

4.2 Wavelength Calibration

The TOMS wavelength calibration was reinvestigated for the Version 7 processing. Questions had been raised in the past about possible errors in the TOMS wavelength calibration. As early as 1979, an offset of about 0.18 nm in wavelength between the SBUV and TOMS scales had been inferred from comparisons of SBUV sweep mode and TOMS solar irradiance and reported to OPT. Subsequently, a bias of about 3 percent was observed between the total ozone derived by SBUV and by TOMS and a bias of about 4 percent between TOMS and the world standard Dobson instrument [*McPeters and Komhyr, 1991*]. The bias had a significant latitude dependence. Errors in the TOMS wavelengths were suggested as a possible origin. Because of these problems, it was decided to carry out a full reinvestigation of the wavelength calibration.

The TOMS prelaunch wavelength calibration was determined using a photographic technique wherein the positions of the images of the back-illuminated TOMS exit slit were compared to the positions of the spectral-line images of a low-pressure mercury lamp that was placed at the exit slit. None of the original film strip exposures survived, but a tracing of the strip for Nimbus–7, annotated with measured positions, is available. A tracing for the engineering

model, now the Meteor–3 TOMS instrument, also exists. An onboard wavelength monitor tracked changes in the wavelength scale between calibration and launch.

Examination of this material revealed two errors. For three of the mercury lines in the Nimbus–7 calibration, the wavelength at one edge had apparently been inaccurately measured where the line image overlapped a slit image, producing an error in the derived center wavelength. The edge wavelengths in question were corrected, using line widths from the engineering model, which did not have this problem, and new center wavelengths were derived. Secondly, the onboard wavelength monitor had recorded changes during instrument thermal vacuum tests, but the correction for this shift were applied with the wrong sign in deriving the wavelengths for the previous TOMS processing. The initial error in the sign had in fact been discovered during testing by Beckman Instruments, the instrument contractor, but for some reason the correction had not been made to the TOMS wavelengths used in processing.

The new wavelength scale was validated by comparing first day Nimbus–7 TOMS solar irradiance values on both the old and revised scales with those from other instruments. Where the solar irradiance is varying appreciably with wavelength, as at 317.5 nm, 340 nm, and 380 nm, an error in the wavelength scale will produce an error in the irradiance. In general, the effect of going to the new scale was to produce a pattern of irradiance differences between instruments that varied more smoothly with wavelength than those for the old scale. Use of the new scale also removed a latitude dependence that had been observed between radiances measured by TOMS and SBUV at 312.5 nm, where a strong gradient in the atmospheric absorption produces a significant wavelength dependence in the radiance. Table 4.1 presents the revised wavelengths. They have an estimated accuracy of ±0.1 nm.

Table 4.1. TOMS Prelaunch Calibration Constants and Gain Range Ratios

		(for Gain Range 1)	
Vacuum Wavelength (nm)	Day-1 Solar Flux at 1 A.U. $(W\text{-}m^{-2}\text{-}\mu m^{-1})$	Radiance $(W\text{-}m^{-2}\text{-}\mu m^{-1} ster^{-1}\text{-}count^{-1})$	Irradiance $(W\text{-}m^{-2}\mu m^{-1}\text{-}count^{-1})$
379.95	1109.31	2.971×10^{-4}	1.67×10^{-3}
359.88	1126.94	3.309×10^{-4}	1.871×10^{-3}
339.66	994.82	3.381×10^{-4}	1.932×10^{-3}
331.06	972.21	3.483×10^{-4}	2.001×10^{-3}
317.35	786.98	3.731×10^{-4}	2.155×10^{-3}
312.34	662.34	3.995×10^{-4}	2.314×10^{-3}

Gain Range Ratios		
Range 2/1	Range 3/2	Range 4/3
6.6	7.2	7.24

To detect any change in the wavelengths since the prelaunch calibration, wavelength calibration was monitored in orbit. Change might be produced by excessive temperature differentials or mechanical displacement of the wavelength-determining components resulting from shock, vibration, or wear. Scans of the mercury-argon lamp for in-flight monitoring of the wavelength calibration were normally made about twice a week. TOMS wavelength calibration monitoring used observations of four wavelength bands, near the center and in the wings of the 296.7-nm Hg line. The only change in the wavelength scale observed since launch is a 0.02-nm shift that appears correlated with the chopper synchronization state changes discussed in Section 4.7 and may thus be an artifact of the synchronization problems rather than a true shift. A true, uncorrected shift would result in an ozone error of about 0.6 percent. If the observed shift is not real, then the upper limit for any change in the wavelength scale is 0.005 nm, corresponding to a possible error in ozone of about 0.1–0.2 percent.

4.3 Attitude Determination

Examination of derived ozone as a function of position in the scan showed a systematic difference between the ozone values derived at the extreme ends of the scans, a cross-track bias. The size was of the order of 2–4 Dobson Units (D.

U.), generally higher at the equator, with a strong seasonal cycle developing. The effect was small in the early part of the data record, and then dramatically increased in August 1984. Investigation of the observed pattern of cross-track bias as a function of season and latitude revealed the source to be errors in the determination of the spacecraft attitude. Such errors would affect the optical path length derived for the radiation backscattered from the earth to the satellite. Because the attitude errors were not large, of the order of 0.1 degree in roll, a noticeable error in derived total ozone appeared only at the extreme off-nadir scan positions. The initial error proved to be in the derivation of the roll angle from sensor readings. Between May 1982 and February 1984, as the spacecraft attitude was gradually shifted to require less use of fuel to maneuver the satellite, the latitude dependence of this error changed. Errors in a software revision made in 1984 caused the change in cross-track bias pattern that occurred at that time. Because a full recomputation of attitude and viewing geometry would have required considerable resources, an empirical correction was developed for Version 6. The average equatorial cross-track bias and the computed sensitivities to errors in spacecraft roll angle were used to estimate a roll angle correction to the original attitude determination.

For Version 7, the attitude software was corrected and the correct roll angle computed for 2–4 orbits on each of about 50 days. The correct roll angles were then compared with those from the Version 5 processing, with the goal of deriving the time and latitude dependence of the error in the Version 5 production software. This sample proved to be insufficient for deriving the time dependence of the roll angle correction at the equator. However, the roll angles derived using the Version 6 correction proved to be consistent with the sample of roll angles derived using the corrected software. Consequently, the empirical correction from Version 6 was recomputed for the entire TOMS data record and used in production for the correction of roll angle at the equator. The sample did yield a small latitude dependence of the error in the Version 5 angles as a function of time. The correction required could be characterized as a linear function of latitude, with one slope for the initial attitude (before May 1982), a different slope for the final attitude (after August 1984), and a linear change with time in between.

4.4 Radiometric Calibration

The Earth radiance is derived from the instrument counts from the following equation:

$$I_m(t) \ = \ c_I k_I G \tag{1}$$

where

    $I_m(t)$ = derived Earth radiance
    c_I = counts detected in Earth radiance mode
    k_I = radiance calibration constant
    G = gain range correction

The solar flux at day 1 can be obtained as follows:

$$F_0 \ = \ c_0 k_F g_0 G \tag{2}$$

where

    F_0 = solar irradiance (flux) at day 1
    c_D = counts detected in solar irradiance mode at day 1
    k_F = solar irradiance calibration constant
    g_0 = goniometric correction

The calibration constants k_R and k_I were derived by using National Institute of Standards and Technology (NIST) spectral irradiance sources with the instrument. For the radiance calibration, reflection of the source off a standard diffuse reflector was used to simulate a spectral radiance standard. For the irradiance, the calibration lamp illuminated the instrument diffuser. The goniometric function, representing the angular dependence of the diffuser scattering, was also measured during these tests. The g_0 term represents the value appropriate to the geometry of the day 1

measurement. Table 4.1 gives the day-1 solar flux F_0, prelaunch calibration constants, and gain range ratios for TOMS.

The radiances measured by TOMS at 380 nm were compared with those measured by SBUV as a check on the absolute calibration. The instruments had different IFOVs, a 188-km nadir view for SBUV compared with the TOMS 49-km scan view. To ensure comparison of the same fields, radiances were derived from TOMS data for the SBUV IFOV. In addition, because differences in the instrumental wavelength bandpass will produce slightly different radiances even under the same conditions, all measurements were corrected to the SBUV prelaunch wavelengths. The details of these procedures are described by Wellemeyer, *et al.* [*1996*]. The comparisons showed that even after the TOMS wavelengths were corrected, as discussed in Section 4.2, a radiometric calibration offset remained, in the sense that the normalized radiances derived from the TOMS measurements were higher than those on the SBUV scale. It was, therefore, decided to correct the TOMS radiances to the SBUV scale by adjusting them downward by 4.2 percent at all wavelengths. This adjusted TOMS calibration yielded ocean surface reflectivities consistent with SSBUV, supporting the validity of the adjustment.

Also, because of such residual imperfections as calibration errors, errors in the quantities derived from laboratory physics, and limitations of the ability of the radiative transfer model to represent processes in the atmosphere, there will be small wavelength-to-wavelength inconsistencies in the ratio of calculated to measured radiance. By averaging over a sample of measurements covering the entire globe and all seasons, this average time-independent systematic difference could be evaluated and the radiance calibration adjusted to eliminate them. Table 4.2 gives the combined correction factors at each wavelength, which are the product of the wavelength-independent 4.2 percent adjustment and the additional correction, typically on the order of half a percent, at each wavelength, in the sense corrected/ uncorrected.

Table 4.2. Correction Factors Applied to TOMS Wavelengths

Wavelength (nm)	312	317	331	340	360	380
Factor	0.956	0.955	0.954	0.952	0.960	0.958

4.5 Changes in Instrument Sensitivity

The algorithm uses the ratio of backscattered radiance to incident solar irradiance, I(t)/F(t). The backscattered radiance I(t) depends both on the fraction of incident radiation scattered by the atmosphere and the amount of incident radiation. As the Earth-Sun distance varies over the year, the incident radiation changes, producing a component of I(t) that is independent of atmospheric processes. To eliminate this component, all radiances and irradiances are corrected to their values at 1 Astronomical Unit (A.U.). Note that this term will cancel when the ratio is calculated.

With a perfect instrument, it would be possible to measure $I_{true}(t)$, the true backscattered radiance at time t, corrected to a 1 A.U. Earth-Sun distance, and $F_{true}(t)$, the true solar flux at time t at 1 A.U. However, because of changes in the instrument sensitivity, the true radiances and changes in the solar flux received at earth are not known.

The radiance measured by TOMS $I_m(t)$ can be related to the true quantity $I_{true}(t)$ as follows:

$$I_m(t) \ = \ I_{true}(t)\, f_{inst}(t)$$
(3)

where

$I_{true}(t)$ = true backscattered radiance, corrected to 1 A.U. Earth–Sun distance.
$I_m(t)$ = radiance measured by TOMS, corrected to 1 A.U.
$f_{inst}(t)$ = changes in instrument throughput relative to day 1.

This $f_{inst}(t)$ term describes the degradation of components of the system used in both Earth radiance and solar irradiance measurements, such as the foreoptics and the photomultiplier.

The solar irradiance can be separated into the solar irradiance at day 1, which can be obtained using the prelaunch calibration, and relative changes with time:

$$F_{true}(t) = F_0 f_{true}(t) \tag{4}$$

where

F_0 = solar flux at 1 A.U. on day 1, and
$f_{true}(t)$ = solar flux at time t at 1 A.U., relative to day 1 solar flux at 1 A.U.

Because it has not been possible to accurately characterize the changes in the reflectivity of the diffuser used in the solar measurements, the true solar change cannot be directly measured to the accuracy needed. However, at the TOMS wavelengths, solar variations are very small. Solar constant measurements by Willson *et al.* [*1986*] show a long-term change in the total solar flux no greater than 0.1 percent and short-term changes no greater than 0.3 percent over a few days. At the TOMS wavelengths, rotational modulation variations measured by the Nimbus–7 SBUV are on the order of 0.1 percent or less [*Heath and Schlesinger, 1986*], and the behavior of the Mg core-to-wing ratio suggests that the solar cycle variation is of the same order [*Schlesinger and Cebula, 1992*]. Thus at the wavelengths used for the TOMS measurements, assuming a constant solar flux should introduce an error of less than 0.3 percent, small compared to the other uncertainties in the ozone derivation. With the assumption of a constant solar flux,

$$\frac{I_{true}(t)}{F_{true}} = \frac{I_m(t)}{F_0 f_{inst}(t)} \tag{5}$$

Thus, if the changes in instrument sensitivity can be determined, the true radiance/irradiance ratio can be calculated using the measured radiances and the day 1 solar flux.

For Version 7, the changes in instrument sensitivity are evaluated from the radiance measurements. At the four longest TOMS wavelengths, the backscattered radiance depends on the surface reflectivity and is insensitive to ozone. Under these conditions, differences in the derived reflectivity will be caused by errors in the calibration. Consider two wavelengths *i* and *j*, with derived reflectivities R_i and R_j respectively, and with fractional calibration errors in the measured radiance given by ε_i and ε_j. The sensitivity of the derived reflectivity to the fractional error in the measured earth radiance is defined to be

$$k = \frac{\Delta R}{\Delta \varepsilon} \tag{6}$$

Over the Pacific Ocean outside the tropics, the true reflectivity is independent of wavelength, the difference in derived reflectivity for wavelengths *i* and *j* can be written, to first order, as

$$R_i - R_j = k_i \varepsilon_i - k_j \varepsilon_j \tag{7}$$

Adding and subtracting $k_i \varepsilon_j$ allows a separation of the effects of wavelength-dependent and wavelength-independent errors:

$$R_i - R_j = k_i (\varepsilon_i - \varepsilon_j) - (k_i - k_j) \varepsilon_j \tag{8}$$

The first term is the contribution of wavelength-dependent errors; differences between the errors at wavelengths *i* and *j* cause the derived reflectivities to be different. The second term shows that wavelength-independent errors also can contribute to reflectivity differences. When two wavelengths have a different sensitivity of reflectivity to radiance, the same error in radiance will produce a different error in reflectivity.

When reflectivity is high, the sensitivity does not vary significantly with wavelength, and the sensitivity difference $k_i - k_j$ is small. Then, the second term in Equation 8 is negligible, and the relative calibration error can be derived from the reflectivity difference. At low reflectivity, most of the backscattered ultraviolet radiation comes from the atmosphere and Rayleigh scattering leads to a significant dependence of the sensitivity on wavelength. Using the difference in calibration error determined at high reflectivity, the first term in Equation 8 can be evaluated and the absolute error at wavelength j derived from measurements at low reflectivity.

The instrument changes at the two shortest wavelengths were derived from those at the longer wavelengths. For each day, a quadratic function was fit to the wavelength degradation at three of the longer wavelengths. That function was used to estimate the instrument sensitivity change for 317.3 nm and 312.3 nm for that day. The resulting instrument change estimates were then smoothed as a function of time. Wellemeyer *et al.* [*1996*] describe the procedure in greater detail.

4.6 Validation of Derived Instrument Change

Two methods were used to validate the instrument change function derived using the methods described in Section 4.5 and to estimate the errors. One was the application of the Pair Justification Method (PJM), to verify that different wavelength pairs would yield consistent ozone values when this function was used to correct the measured radiances. The other was to show that the characterization derived from a quadratic fit gave a physically plausible pattern of instrument and diffuser degradation.

4.6.1 Pair Justification

If the instrument degradation is calculated properly, then ozone values derived by different wavelength pairs under physical conditions where both are sensitive to ozone should be consistent. The difference between ozone values derived by different pairs is a measure of the error in ozone derived from an individual pair [*Herman et al., 1991*]. The A- and B′-pairs (Table 5.1) were chosen to check the calibration; the B′-pair was used for validation rather than the B-pair used for ozone retrievals because of its larger sensitivity to calibration errors and its lower sensitivity to the synchronization problems discussed in Section 4.7. The two pairs agreed to within 1 percent, with an additional 1% difference appearing in the last year. The significance of this difference can be understood by comparing it with the ozone error resulting from propagating the uncertainty in the instrument functions through the derivation. The resulting 2σ uncertainty is 1.5 percent over the entire TOMS lifetime, or about 1 percent/decade. Thus, the difference between the ozone values derived from the two pairs is smaller than any contribution from the uncertainty in the instrument calibration.

4.6.2 Inferred Diffuser Degradation

Once the instrument change is known, the relative importance of changes in the reflectivity of the diffuser plate used for solar measurements and changes in the sensitivity of the other components of the instrument can be evaluated. A plausible derived diffuser change and patterns of instrument and diffuser change that permit a coherent interpretation will support the derived instrument characterization.

The solid lines in Figure 4.1 show the derived instrument change as a function of time for all six TOMS wavelengths. Little degradation is evident before 1990; over the first 5 years, the change is almost independent of wavelength, suggesting an origin in the photomultiplier or electronics. Wavelength-dependent degradation began to appear in 1985, increasing significantly in 1990.

The variations in solar flux measured by TOMS, shown in Figure 4.2, result principally from degradation of the diffuser and of other instrumental components, with a smaller contribution from true solar variations. The toggling effect discussed in Section 4.7, seasonal goniometric errors, effects of shadowing in the last years, and other artifacts of the measurement process also make minor contributions. Because the solar irradiance is essentially constant at TOMS wavelengths, the long term change in diffuser reflectivity can be estimated by dividing the measured solar flux variations by the instrumental change derived using the techniques discussed in Section 4.5. The dashed lines in Figure 4.1 show the diffuser change so derived. In the first 5 years, the diffuser was the dominant contributor to changes in the solar flux measurements, much of the change coming during the intervals of accelerated deployment.

Version 7 TOMS Sensitivity Changes
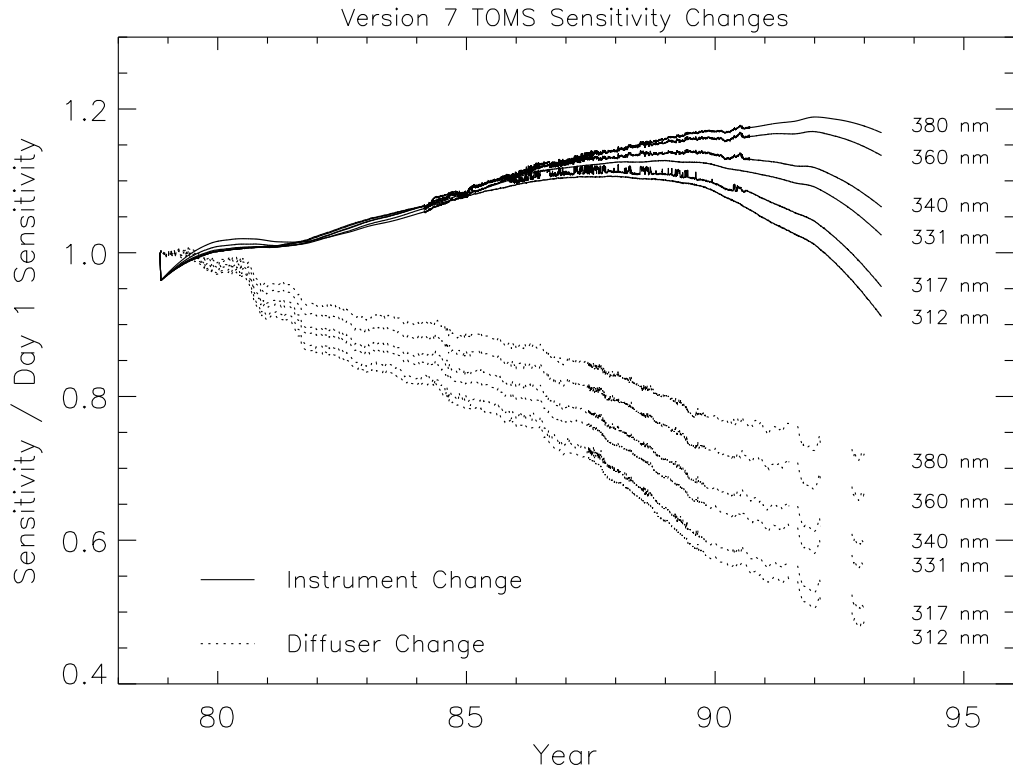
Figure 4.1. Derived changes with time in sensitivity of TOMS instrument components other than diffuser (solid lines) and diffuser (dashed lines) at the six TOMS bandpasses.

TOMS "Raw" Solar Flux: Individual Wavelengths
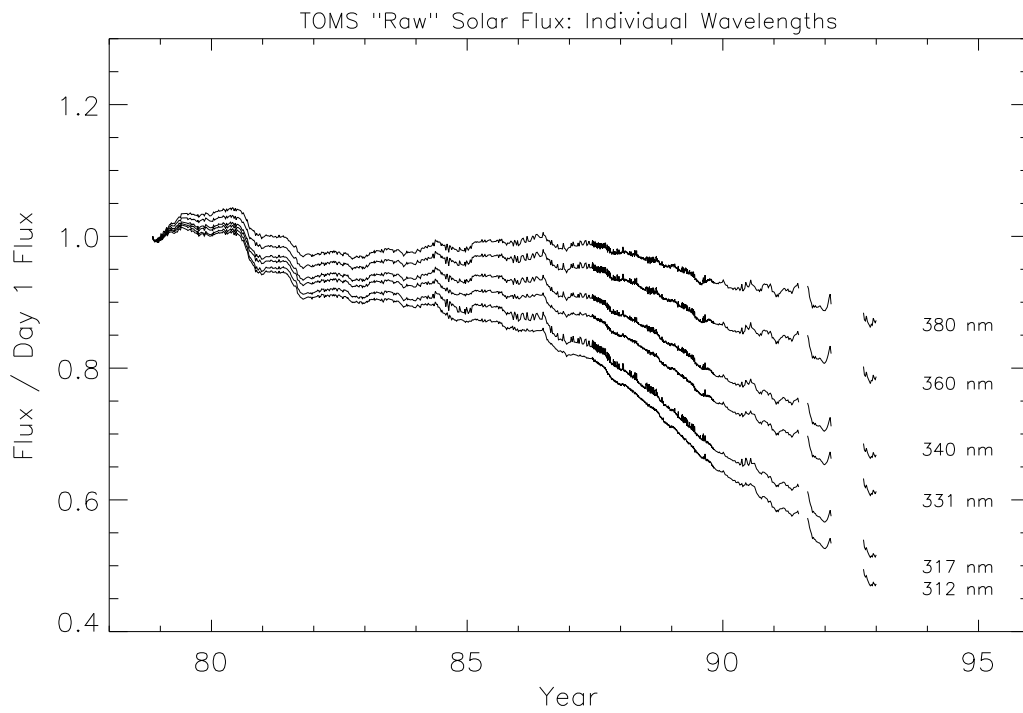
Figure 4.2. Raw TOMS solar flux as a function of time

13

Afterwards, the significance of other instrumental components increased, becoming dominant at the shorter wavelengths in 1990, particularly because there were no more intervals of accelerated exposure. Figure 4.3 shows the diffuser degradation component plotted as a function of exposure. It is nearly linear, and agrees very well in form with the diffuser degradation function derived for Version 6 using the exponential model and pair justification. Thus both the instrument and diffuser changes appear physically reasonable.
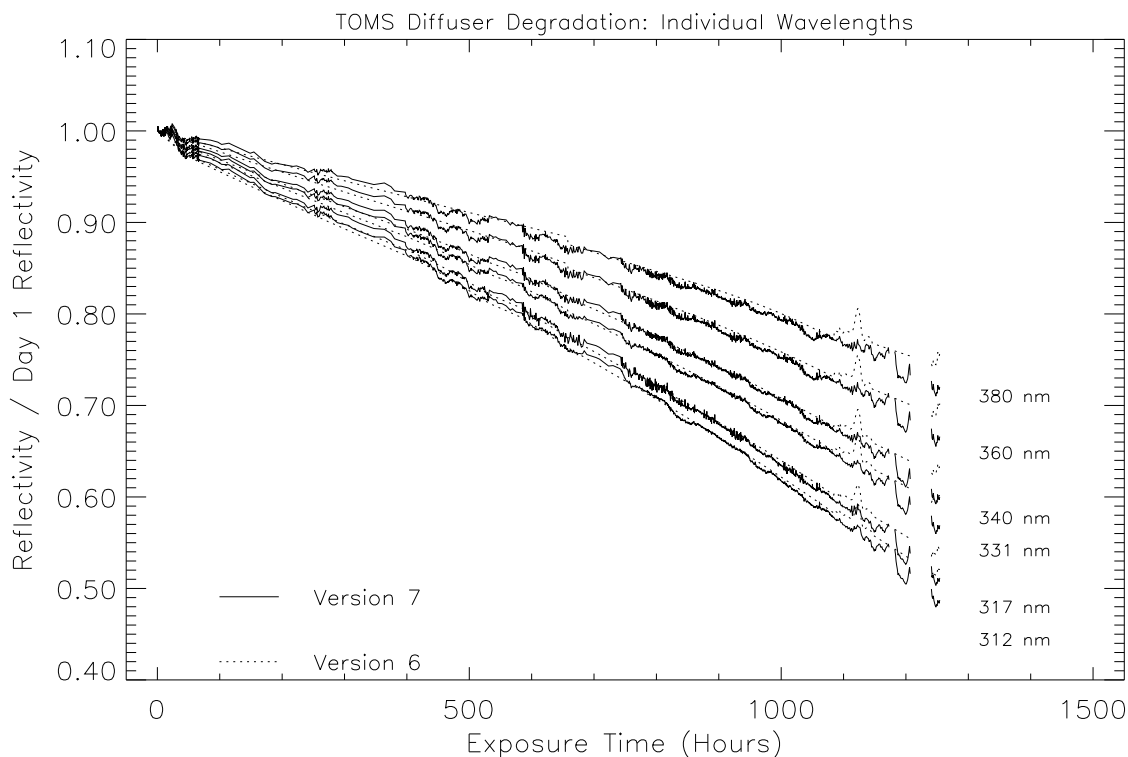
Figure 4.3. TOMS diffuser degradation as a function of exposure. (Solid line) Version 7. (Dashed line) Version 6.

4.7 Correction for Synchronization Problems

If the wavelength selection chopper wheel and the photon-counting electronics are not synchronized, part of the integration period will occur when the light on the exit slit is blocked by the chopper wheel, reducing the signal. Onboard electronics identify and flag this condition when it exceeds a preset threshold. Starting in 1984, the threshold sensor began to detect such occasional synchronization failures. At the same time, another phenomenon, *toggling*, began to appear in the TOMS data: the data would switch sporadically, on time scales ranging from less than a day to several months, between two separate states, one corresponding to the pre-1984 conditions and the other apparently a subthreshold problem with the synchronization. Figure 4.4 shows the fraction of data flagged for synchronization failure as a function of time, starting in 1984. The problem became most severe in mid-1990, decreasing in early 1991 to late 1992, and then becoming larger again until the synchronization failed completely in May, 1994. Not all triplets were affected equally; in particular there was little effect at the A-triplet. This lack of effect at A was used to estimate a correction for toggling. The A-triplet is used to derive ozone in the equatorial region. Ozone values derived using the A-triplet are used to calculate radiances at 317 nm and 340 nm, which are not used in A-triplet retrieval. The difference between the radiances so calculated and those actually measured shows a toggling signature. The magnitude and frequency of the toggling effect was estimated from daily means of these differences over an equatorial band from 15° S to 15° N and used to correct the instrument functions at 317 nm and 340 nm.
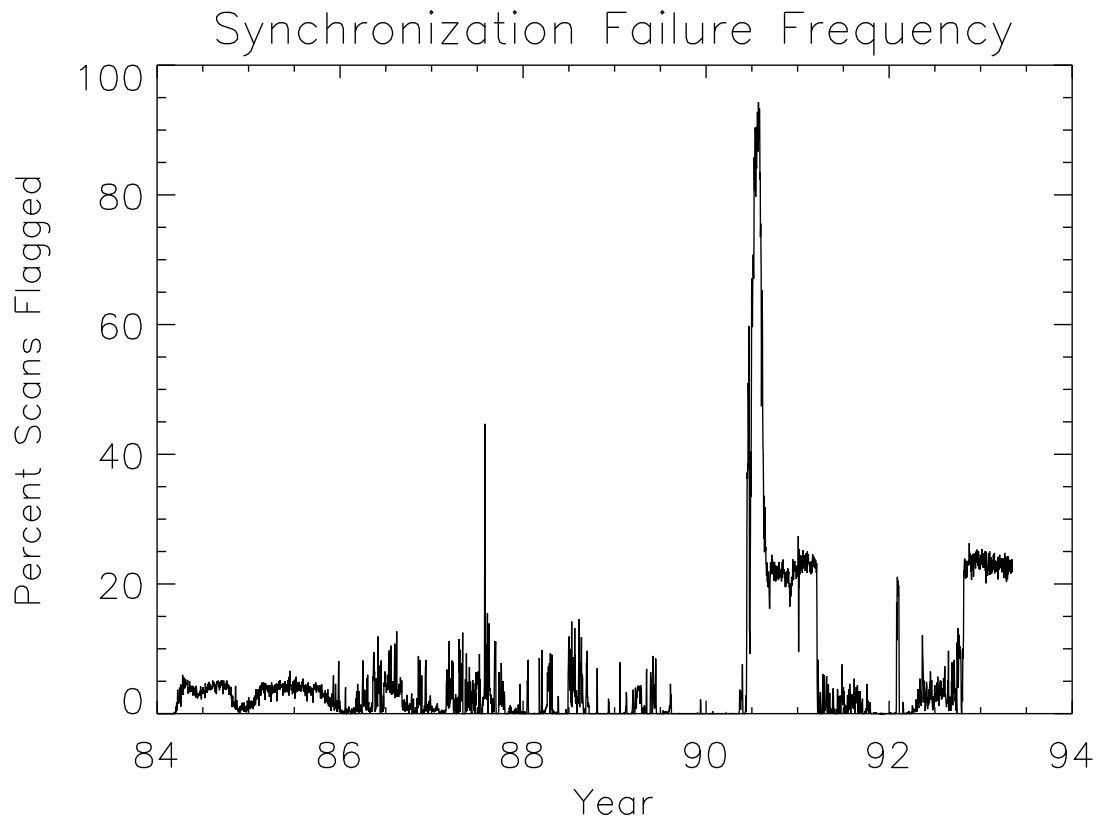
Figure 4.4. Daily frequency of synchronization failure flag

5.0 ALGORITHM

5.1 Theoretical Foundation

To interpret the radiance measurements made by the TOMS instrument requires an understanding of how the Earth's atmosphere scatters ultraviolet radiation as a function of solar zenith angle. Incoming solar radiation undergoes absorption and scattering in the atmosphere by atmospheric constituents such as ozone and aerosols and by Rayleigh scattering. Radiation that penetrates to the troposphere is scattered by clouds and aerosols, and radiation that reaches the ground is scattered by surfaces of widely varying reflectivity.

The backscattered radiance at a given wavelength depends, in principle, upon the entire ozone profile from the top of the atmosphere to the surface. The two shortest wavelengths used in the TOMS ozone measurements were selected because they are absorbed by ozone. At these wavelengths, absorption by other atmospheric components is negligible compared to that by ozone.

At wavelengths longer than approximately 310 nm, however, the backscattered radiance consists primarily of solar radiation that penetrates the stratosphere and is reflected back by the dense tropospheric air, clouds, aerosols, and the Earth's surface. The intensity is determined primarily by the total optical depth above the scattering layer in the troposphere. The amount of ozone below the scattering layer is small and can be estimated with sufficient accuracy to permit derivation of total column ozone. Because most of the ozone is in the stratosphere, the principal effect of atmospheric ozone at these wavelengths is to attenuate both the solar flux going to the troposphere and the component reflected back to the satellite.

Derivation of atmospheric ozone content from measurements of the backscattered radiances requires a treatment of the reflection from the Earth's surface and of the scattering by clouds and other aerosols. These processes are not isotropic; the amount of light scattered or reflected from a given scene to the satellite depends on both the solar zenith angle and view angle, the angle between the scene and the nadir as seen at the satellite.

The algorithm used for previous releases based its calculation of reflectivity on the treatment of Dave [*1978*], who represented the contribution of clouds and aerosols to the backscattered intensity by assuming that radiation is reflected from a particular pressure level called the "scene pressure," with a Lambert-equivalent "scene reflectivity" R. When this method was applied, at the non-ozone-absorbing wavelengths the resulting reflectivity exhibited a wavelength dependence correlated with partially clouded scenes. To remove this wavelength dependence, a new treatment has been developed, based on a simple physical model that assumes two separate reflecting surfaces, one representing the ground and the other representing clouds. The fractional contribution of each to the reflectivity is obtained by comparing the measured radiances with the values calculated for pure ground and pure cloud origin.

The calculation of radiances at each pressure level follows the formulation of Dave [*1964*]. A spherical correction for the incident beam has been incorporated, and Version 7 treats molecular anisotropy [*Ahmad and Bhartia, 1995*] Consider an atmosphere bounded below by a Lambertian reflecting surface of reflectivity R. The backscattered radiance emerging from the top of the atmosphere as seen by a TOMS instrument, I_m, is the sum of purely atmospheric backscatter I_a, and reflection of the incident radiation from the reflecting surface I_s,

$$I_m(\lambda, \theta, \theta_0, \Omega, P_0, R) = I_a(\lambda, \theta, \theta_0, \phi, \Omega, P_0) + I_s(\lambda, \theta, \theta_0, \phi, \Omega, P_0, R) \qquad (9)$$

where

λ = wavelength
θ = satellite zenith angle, as seen from the ground
θ_0 = solar zenith angle
ϕ = azimuth angle
Ω = column ozone amount
P_0 = pressure at the reflecting surface
R = effective reflectivity at the reflecting surface

The surface reflection term can be expressed as follows:

where

$$I_s(\lambda, \theta, \theta_0, \Omega, P_0, R) = \frac{RT(\lambda, \theta, \theta_0, \Omega, P_0)}{1 - RS_b(\lambda, \Omega, P_0)} \tag{10}$$

$$T(\lambda, \theta, \theta_0, \Omega, P_0) = I_d(\lambda, \theta, \theta_0, \Omega, P_0)\, f(\lambda, \theta, \Omega, P_0) \tag{11}$$

where

S_b = fraction of radiation reflected from surface that atmosphere reflects back to surface
I_d = total amount of direct and diffuse radiation reaching surface at P_0
f = fraction of radiation reflected toward satellite in direction θ that reaches satellite,

and the other symbols have the same meaning as before. The denominator of Equation 10 accounts for multiple reflections between the ground and the atmosphere.

The intensity of radiation as it passes through a region where it is absorbed and scattered can be described in general terms as having a dependence $I \propto \exp(-\tau)$. For a simplified case, where all processes can be treated as absorption, the optical depth τ depends on the number of absorbers n in a column and the absorption efficiency α of the absorbers; that is, $I \propto \exp(-n\alpha)$. The column number should thus scale approximately as -log I. The ozone algorithm therefore uses ratio of radiance to irradiance in the form of the N-value, defined as follows:

$$N = -100 \log_{10}\left(\frac{I}{F}\right) \tag{12}$$

The N-value provides a unit for backscattered radiance that has a scaling comparable to the column ozone; the factor of 100 is to produce a convenient numerical range.

The basic approach of the algorithm is to use a radiative transfer model to calculate the N-values that should be measured for different ozone amounts, given the location of the measurement, viewing conditions, and surface properties, and then to find the column ozone that yields the measured N-values. In practical application, rather than calculate N-values separately for each scene, detailed calculations are performed for a grid of total column ozone amounts, vertical distributions of ozone, solar and satellite zenith angles, and two choices of pressure at the reflecting surface. The calculated N-value for a given scene is then obtained by interpolation in this grid of theoretical N-values.

The ozone derivation is a two-step process. In the first step, an initial estimate is derived using the difference between N-values at a *pair* of wavelengths; one wavelength is significantly absorbed by ozone, and the other is insensitive to ozone. Use of a difference provides a retrieval insensitive to wavelength-independent errors, in particular, any in the zero-point calibration of the instrument. In deriving the initial estimate, the same pair is always used.

In the second step, N-values are calculated using this ozone estimate. In general, these calculated values will not equal the measured N-values. The differences, in the sense $N_{meas}-N_{calc}$, are called the *residues*. Using the residues at a properly chosen *triplet* of wavelengths, it is possible to simultaneously solve for a correction to the original ozone estimate and for an additional contribution to the radiances that is linear with wavelength, arising primarily from wavelength dependence in the surface reflectivity but also possibly originating in the instrument calibration. The triplet consists of two pair wavelengths, as described above, plus 380 nm, which is insensitive to ozone. The pair wavelengths used are those most sensitive to ozone at the optical path length of the measurement. The separation of the 380-nm wavelength from the pair wavelengths is far larger than the separation between the pairs; thus, the 380-nm measurement provides a long baseline for deriving wavelength dependence. This process may be iterated, using the results of the first triplet calculation as the new initial estimate. Table 5.1 lists the wavelengths of the pairs and triplets.

Table 5.1. Pair/Triplet Wavelengths

Pair/Triplet Designation	Ozone Sensitive Wavelength (nm)	Ozone Insensitive Wavelength (nm)	Reflectivity Wavelength (nm)	Range of Application (optical path s)
A	312.3	331.0	380.0	$1 \geq s$
B	317.4	331.0	380.0	$3 \geq s > 1$
B′	317.4	339.7	not used	validation only
C	331.0	339.7	380.0	$s > 3$

5.2 Calculation of Radiances

To carry out the calculation described in Section 5.1 requires the following information:

- Ozone absorption coefficients as a function of temperature for the wavelengths in the TOMS bandpasses.
- Atmospheric Rayleigh scattering coefficients.
- Climatological temperature profiles.
- Climatological ozone profiles.
- Solar zenith angle.
- Satellite zenith angle at the IFOV.
- Angle between the solar vector and the TOMS scan plane at the IFOV.
- Pressure at the reflecting surface.

Because of the its finite bandwidth, TOMS does not measure a monochromatic radiance. For comparison with the TOMS measurements, radiances are calculated at approximately 0.05-nm intervals across each of the TOMS slits, using the appropriate absorption coefficient and temperature dependence [*Paur and Bass, 1985*] for each wavelength. The I/F for the entire band, $A(\lambda_0)$, is then given by the following expression:

$$A(\lambda_0) = \int A(\lambda) F(\lambda) S(\lambda) \, d\lambda / \int F(\lambda) S(\lambda) \, d\lambda \tag{13}$$

where

$A(\lambda) = \dfrac{I(\lambda)}{F(\lambda)}$ at wavelength λ,

$F(\lambda)$ = solar flux at wavelength λ,
$I(\lambda)$ = earth radiance at wavelength λ, and
$S(\lambda)$ = Instrument response function at wavelength λ.

The wavelength dependence of the solar flux is based on SOLSTICE measurements (Woods *et al.*, 1996). This detailed calculation replaces the effective absorption coefficients used in Version 6.

Because of the revised TOMS wavelength calibration, the ozone absorption for the TOMS bandpasses will not be the same for Version 7 as it was for Version 6. To permit a comparison, effective absorption coefficients like those of Version 6 were calculated for the TOMS bands using the Version 7 wavelengths. The same method was used, integrating the monochromatic laboratory values over the TOMS bandpass for the following conditions: a mid-latitude profile for $\Omega = 350$, a path length of 2.5, and a wavelength-independent solar flux. These effective absorption coefficients are given in Table 5.2. Because the effective absorption coefficient depends on the ozone profile, optical path length, and solar flux spectrum, the Version 7 technique of calculating I/F at individual wavelengths and then integrating over the TOMS bandpass eliminates the imprecision arising from using one set of effective absorption coefficients, derived for a particular set of conditions, for all calculations. Table 5.2 also contains the Rayleigh scattering coefficients and the regression equations used for the temperature dependence of the ozone coefficients. The values shown in the table are purely to illustrate the magnitude of the change; they have not been used in the algorithm.

Table 5.2. Effective Absorption and Scattering Coefficients

Vacuum Wavelength (nm)	Effective Ozone Absorption Coefficient (atm-cm^{-1}) at 0°C (C_0)	Temperature Dependence Coefficients		Rayleigh Scattering Coefficient (atm^{-1})
		C_1	C_2	
312.34	1.9000	5.507×10^{-3}	2.922×10^{-5}	1.0220
317.35	0.9915	3.167×10^{-3}	1.768×10^{-5}	0.9543
331.06	0.1703	7.117×10^{-4}	4.199×10^{-6}	0.7967
339.66	0.0390	3.938×10^{-4}	2.816×10^{-6}	0.7145
359.96	$< 10^{-8}$	–	–	0.5597
380.01	$< 10^{-8}$	–	–	0.4458

Correction to ozone absorption for temperature:
Ozone absorption = $C_0 + C_1 T + C_2 T_2$
(where T is in degrees C)

Ozone and temperature profiles were constructed using a climatology based on SBUV measurements above 15 km and on balloon ozonesonde measurements [*Klenk et al., 1983*] for lower altitudes. Each standard profile represents a yearly average for a given total ozone and latitude. Profiles have been constructed for three latitude bands: low latitude (15 degrees), mid-latitude (45 degrees), and high latitude (75 degrees). There are 6 profiles at low latitudes and 10profiles each at middle and high latitudes, for a total of 26. These profiles cover a range of 225–475 D.Us. for low latitudes and 125–575 for middle and high latitudes, in steps of 50 D.Us. The profiles are given in Appendix A.

To use the new Version 7 ozone profile weighting scheme for high path lengths, outlined in Section 3.2, it was necessary to extend the standard profiles beyond the available climatology. To minimize the use of extrapolation in this process, profile shapes were derived by applying a Principal Component Analysis to a separate ozone profile climatology derived from SAGE II and balloon measurements [*Chu et al., 1989*] to derive Empirical Orthogonal Functions (EOFs). The EOFs corresponding to the two largest eigenvalues represented more than 90 percent of the variance. The EOF with the greatest contribution to the variance was associated with variation in total ozone. The second most important EOF was associated with the height of the ozone maximum and correlated well with latitude, showing a lower maximum at higher latitude. This correlation was used as the basis for lowering the heights of the ozone maxima at high latitudes and raising them in the tropics when extending the original climatology to represent the more extreme profile shapes.

Given the wavelength, total ozone and ozone profile, surface pressure, satellite zenith angle at the field of view, and solar zenith angle, the quantities I_m, I_a, T, and S_b of Equations 9 and 10 can then be calculated at the six TOMS wavelengths. For the tables used in the algorithm, these terms are computed at the TOMS wavelengths for all 26 standard profiles and two reflecting surface pressure levels (1.0 atm and 0.4 atm). For each of these cases, I_m, I_a, T are calculated for ten choices of solar zenith angle from 0–88 degrees, spaced with a coarser grid at lower zenith angles and a finer grid for higher zenith angles, and for six choices of satellite zenith angle, five equally spaced from 0–60 degrees and one at 70 degrees. In Version 6, the tables extended only to a satellite zenith angle of 63.33 degree. The fraction of reflected radiation scattered back to the surface, S_b, does not depend on solar or satellite zenith angle.

5.3 Surface Reflection

To calculate the radiances for deriving ozone from a given measurement requires that the height and reflectivity of the reflecting surface be known. The TOMS algorithm assumes that reflected radiation can come from two levels, ground and cloud. The average ground terrain heights are from the National Oceanic and Atmospheric Administration National Meteorological Center (NOAA/NMC), provided in km for a 0.5 x 0.5-degree latitude and longitude grid, a finer resolution than the 2.5 x 2.5-degree grid used for Version 6. These heights are converted to units of pressure using a U.S. Standard Atmosphere [*ESSA, 1966*] and interpolated to the TOMS IFOVs to establish the pressure at the Earth's surface. Probabilities of snow/ice cover from around the globe are collected by the Air Force Global Weather Center and mapped on a polar stereographic projection. These data have been averaged to provide a monthly snow/

ice climatology mapped onto a 1 x 1-degree latitude-longitude grid and used to determine the presence or absence of snow in the TOMS IFOV. If the probability is 50 percent or greater, snow/ice is assumed to be present. For cloud heights, a climatology based upon the International Satellite Cloud Climatology Project (ISCCP) data set is used. It consists of the climatological monthly averages over a 0.5 x 0.5-degree latitude-longitude grid. This climatology replaces the purely latitude-based climatology derived from Temperature-Humidity Infrared Radiometer (THIR) measurements used for Version 6, which placed the cloud layer at higher altitude closer to the equator. In particular, the ISSCP-based climatology better represents the low marine stratus over oceans and continental west coasts.

Reflectivity is determined from the measurements at 380 nm. For a given TOMS measurement, the first step is to determine calculated radiances at 380 nm for reflection off the ground and reflection from cloud, based on the tables of calculated 380 nm radiances. For reflection from the ground, the terrain height pressure is used, and the reflectivity is assumed to be 0.08, unless snow/ice is present, in which case 0.5 is used. For cloud radiances, a pressure corresponding to the cloud height from the ISCCP-based climatology is used, and the reflectivity is assumed to be 0.80. The ground and cloud radiances are then compared with the measured radiance. If $I_{ground} \leq I_{measured} \leq I_{cloud}$, and snow/ice is assumed not to be present, an effective cloud fraction f is derived using

$$f = \frac{I_{measured} - I_{ground}}{I_{cloud} - I_{ground}}$$

(14)

If snow/ice is assumed to be present, then the value of f is divided by 2, based on the assumption that there is a 50-50 chance that the high reflectivity arises from cloud. The decrease in f means that there is a smaller contribution from cloud and a higher contribution from ground with a high reflectivity off snow and ice. Equation 14 is solved for a revised value of I_{ground}, and the ground reflectivity is calculated from Equation 10. For the ozone retrieval, the calculated radiances are determined assuming that a fraction f of the reflected radiance comes from cloud with reflectivity 0.80, and a fraction $1-f$ from the ground, with reflectivity 0.08 when snow/ice is absent and with the recalculated reflectivity when snow/ice is present. An effective reflectivity is derived from the cloud fraction using the following expression:

$$R = R_g (1 - f) + R_c f$$

(15)

where R_g is 0.08 when snow/ice cover is assumed absent and has the recalculated value when it is assumed present. This reflectivity is included in the TOMS data products but plays no role in the retrieval.

If the measured radiance is less than the ground radiance, then the radiation is considered to be entirely from surface terrain with a reflectivity less than 0.08. Equations 9 and 10 can be combined to yield:

$$R = \frac{I - I_a}{T - S_b (I - I_a)}$$

(16)

The ground reflectivity can be derived using an I_a obtained assuming ground conditions. Similarly, if the measured radiance is greater than the cloud radiance, when snow/ice are absent, the reflected radiance is assumed to be entirely from cloud with reflectivity greater than 0.80, and an I_a derived using the cloud conditions is used in Equation 16 to derive the effective reflectivity. If snow/ice are present, the cloud and ground are assumed to contribute equally to I_m at 380 nm. Equation 16 can then be used to calculate new values of both ground and cloud reflectivities from these radiances. Radiances at the shorter wavelengths are calculated using these reflectivities and a value of 0.5 for f.

5.4 Initial B-Pair Estimate

The initial ozone is calculated by a modification of the Version 6 method, using the B-pair, which provides good ozone values over the largest range of conditions of any of the pairs.

The first step is to calculate radiances for the conditions of the measurement—geometry, latitude, cloud and terrain height, and cloud fraction. For each ozone value in the table, radiances are calculated for the 1.0 atm and 0.4 atm levels, using ground reflectivity and the values of I_a, T, and S_b from the tables for the geometry of the measurement and a single ozone profile—the low latitude profile for measurements at latitudes 15 degrees and lower, the mid latitude profile for 15 degrees < latitude ≤ 60 degree, and the high latitude profile at latitudes higher than 60 degrees. These radiances are then corrected for rotational Raman scattering (the Ring effect). The correction factors, based on the results of Joiner *et al.* [*1995*], are shown in Table 5.3. They were computed using a solar zenith angle of 45 degrees and a nadir scan. The dependences on solar and scan angles, which are small under most conditions, are neglected. Two sets were calculated, one at 1 atm and the assumed 8 percent ground reflectivity for use with the 1-atm radiance tables and the other at 0.4 atm and the assumed 80 percent cloud reflectivity for use with the 0.4-atm tables. This correction, new for Version 7, greatly reduces the biases that had been seen between ozone values derived from different pairs in the Version 6 retrievals.

Table 5.3. Rotational Raman Scattering Corrections

	Radiance Correction (%)	
Actual Wavelength (nm)	Pressure = 1.0 atm Reflectivity = 8%	Pressure = 0.4 atm Reflectivity = 80%
312.34	0.27	0.17
317.35	–0.92	–0.47
331.06	0.16	0.09
339.66	–0.18	–0.08
359.88	–0.94	–0.39
379.95	0.34	0.14

The ground radiance is then derived by interpolating between values for the two pressures to derive the radiance for the pressure at the terrain height from the grid. A similar process is carried out for both pressures using cloud reflectivity, and the cloud radiance is derived by linear interpolation for the pressure level at the height given by the ISCCP cloud height climatology. Finally, the appropriate fractions of ground and cloud radiances, determined as described in Section 5.3, are added to yield I/F for all ozone values. These results are then converted to N-values.

The next step is to compare the measured radiance with the calculated radiance. The two tabulated ozone values whose calculated B-pair N-value differences bracket the measured N-value difference are identified in the table. A climatological ozone amount below the terrain pressure level is subtracted from these two bracketing table ozone values, and the initial ozone estimate is derived by linearly interpolating between the two resultant values, using the measured N-value and the two calculated N-values.

5.5 Best Ozone

Once an initial estimate of ozone has been obtained, it is used to calculate N-values at all TOMS wavelengths in the way described in Section 5.2, applying the rotational Raman scattering correction described in Section 5.4. N-values are calculated for each measurement, using one profile or two, depending upon the latitude. For latitude ≤ 15 degrees, only the low latitude profiles are used, for 15 degrees< latitudes ≤ 45 degrees, one set each is calculated using low and middle latitude profiles, for 45 degrees< latitudes < 75 degrees, N-values are calculated using middle and high latitude profiles; and for latitude ≥ 75 degrees, only N-values for high latitude profiles are calculated. Values of dN/dΩ are calculated, as well.

In general, these calculated N-values will not equal the measured N-values. In the derivation of the initial ozone estimate, reflectivity is assumed to be independent of wavelength, but for some surface conditions, such as sea glint, desert dust, or ice, the reflectivity will be wavelength dependent. In addition, residual errors in the instrument calibration can produce a wavelength dependent artifact in the measured N-value Because of these effects on the spectrum of backscattered radiation and because of the simplifications used in its derivation, the initial ozone estimate will not be equal to the true ozone value. This error in ozone will also contribute to the discrepancy between the measured N-value N_m and the value N_0 calculated from the initial ozone estimate. The initial ozone estimate should,

however, be sufficiently close to the true value to derive a correction using a first order Taylor expansion in the difference. The wavelength-dependent contribution from factors other than ozone, such as reflectivity and residual errors in the instrument characterization, is assumed to be a linear function of wavelength, $a + b\lambda$. Then,

$$N_m = N_0 + (\Omega - \Omega_0)\left(\frac{dN}{d\Omega}\right)_0 + a + b\lambda. \tag{17}$$

Let

$r_\lambda \quad = (N_m - N_0)_\lambda$ be the residue at wavelength λ, and

$s_\lambda \quad = \left(\frac{dN}{d\Omega}\right)_\lambda$ be the sensitivity at wavelength λ.

Equation 17 becomes:

$$r_\lambda = s_\lambda (\Omega - \Omega_0) + a + b\lambda. \tag{18}$$

The radiation at 380 nm is insensitive to ozone, and therefore $s_{380} = 0$. Further, since the reflectivity was derived at 380 nm, the residue is zero at that wavelength. Substituting into Equation 18 and solving yields:

$$a = -380b \tag{19}$$

and therefore, for the ozone-sensitive wavelengths,

$$r_\lambda = s_\lambda (\Omega - \Omega_0) + b (\lambda - 380) . \tag{20}$$

There are two unknowns, Ω and b. Let $\Delta\lambda = \lambda - 380$. Using measurements at two wavelengths, labeled λ_1 and λ_2, it is possible to solve for Ω:

$$\Omega = \Omega_0 + \frac{r_1 \Delta\lambda_2 - r_2 \Delta\lambda_1}{s_1 \Delta\lambda_2 - s_2 \Delta\lambda_1} \tag{21}$$

Equation 21 is the form in which the algorithm applies the correction. Ozone values are derived for each of the two profiles selected.

Another form of this equation is:

$$\frac{\Delta\lambda_2}{\Delta\lambda_1} = \frac{r_1 - s_1 (\Omega - \Omega_0)}{r_2 - s_2 (\Omega - \Omega_0)} \tag{22}$$

This form illustrates how the correction is equivalent to assuming that the size of that part of the residual not arising from ozone error is linear with wavelength.

For retrievals at latitudes where two profiles are used, an ozone value appropriate to the latitude of the measurement is then derived from the ozone values for the two profiles, using an equation of the following form:

$$\Omega = (1 - f_{prof}) \Omega_{lower} + f_{prof} \Omega_{higher} \tag{23}$$

where

$\Omega \quad$ = best ozone,
Ω_{lower} = ozone retrieved using lower latitude profile,
Ω_{higher} = ozone retrieved using higher latitude profile, and

f_{prof} = weight given to higher latitude profile.

Thus, f_{prof} will be 0 if only the lower latitude profile is selected, 1 if only the higher latitude profile is selected, and in between for a combination of the two profiles. The choice of pairs and f_{prof} depends upon the optical path length $\Omega_0(\sec\theta_0 + \sec\theta)$, in atm-cm.

For path lengths less than 1.5, a value of f_{prof} obtained by simple linear interpolation in latitude,

$$f_{prof} = \frac{|latitude| - |latitude|_{lower}}{|latitude|_{higher} - |latitude|_{lower}} \qquad (24)$$

is used for latitudes between 15 and 75 degrees using the two profiles appropriate to the latitude. The low latitude profile alone is used from the equator to 15 degree, and the high latitude profile alone is used from 75 degree to the pole. For a path length less than or equal to 1.0, the A-triplet wavelengths are used in Equation 21; for a path length greater than 1 and no greater than 1.5, the B-triplet is used with the same latitude interpolation.

For longer path lengths, a different treatment is used for latitude interpolation. The basic principle is to require consistency between two triplets. For an arbitrary value of f_{prof}, the two triplets will give different ozone values. The value of f_{prof} is determined by finding the factor that yields the same ozone value for both triplets. For path lengths greater than 1.5 but no greater than 3, the B-triplet is used for the retrieval, and the profile is determined by requiring the A-triplet to be consistent, and for path lengths greater than 3, the C-triplet is used for the retrieval and a consistent B-triplet required. If the value derived using the low and middle latitudes is greater than one, the middle and high latitudes profiles are used; similarly if using the middle and high latitudes gives a value less than zero, the low and middle latitudes are used. The minimum value accepted using the two lower-latitude profiles is –0.5, and the maximum accepted using the two higher is 1.5, to avoid extreme extrapolation in either case.

The implementation of this approach uses residues. First, ozone values Ω_1 are calculated using Equation 21 for the two appropriate latitude profiles and interpolation in latitude as specified by Equation 24. The B-triplet is used for path lengths below 3, and the C-triplet is used for higher path lengths. Sensitivities are also calculated using latitude interpolation between the sensitivities for the standard profiles.

Rather than computing the radiances for the new set of ozone values Ω_1 to obtain the residues r_1 for this new ozone value, the following equation is used to adjust the residues for the change in ozone:

$$r_i = r_0 - s_i(\Omega_i - \Omega_0), \qquad (25)$$

with i equal to 1. By Equation 20,

$$r_{1,\lambda} = b(\lambda - 380), \qquad (26)$$

for the wavelengths used in the triplet ozone determination. For other wavelengths λ, the *triplet residue* can be defined as the difference between the residue at that wavelength and the value that would fall on the line defined by

$$r_{trip} = r - \frac{\lambda - 380}{\lambda' - 380} r', \qquad (27)$$

where λ' is a wavelength used in the derivation of Ω_1 and r' is the value of r_1 at that wavelength. If two triplets differ only in one wavelength, a consistent result requires that the residues for all wavelengths in both triplets fall on the same line. For example, when ozone is calculated using the B-triplet, a consistent A-triplet ozone value requires that the triplet residue at 312 nm, which is used for the A-triplet but not for the B triplet, be zero; similarly, for B-triplet ozone to be consistent with ozone derived using the C-triplet, the 317 nm triplet residue must be zero. To find the

profile that will yield consistency, the triplet residue for the appropriate wavelength is calculated for each of the two standard profiles. Then f_{prof} is set to be

$$f_{prof} = \frac{r_{trip}(lower)}{r_{trip}(lower) - r_{trip}(higher)} \tag{28}$$

where lower and higher refer to latitudes of the two profiles used. In most cases, the appropriate profile will be between the higher and lower latitude profiles, and the residues will be of opposite sign; thus the denominator represents a distance between the residues and the numerator a fraction of this distance. If, for example, the lower-latitude residue has a significantly larger absolute value, the value of f_{prof} is close to one; the profile chosen is close to the higher latitude profile. The value of f_{prof} derived from Equation 28 is then used to calculate a new ozone value Ω_2. Adjusted residues are calculated using Equation 25, and a new triplet residue is derived, using Equation 27. If this triplet residue is 0.10 or less in N-value units, then Ω_2 is adopted as the Best ozone value; otherwise, the process is repeated, beginning with the derivation of residues for the new ozone value using Equation 25 with i equal to 2. This second result (Ω_3) is then accepted as Best ozone. When the low- and mid-latitude profiles are used, if the derived value of f_{prof} is greater than 1, the process is repeated using the mid- and high-latitude profiles; similarly, if $f_{prof} < 0$ when using mid- and high-latitude profiles, the process is repeated using the low- and mid-latitude profiles. Finally, if the first derived Ω_{best} differs from the estimated value from the B-pair calculation by more than 50 D.Us., then the procedure starting with Equation 21 is repeated, using this initial Ω_{best} as the Ω_0. The result of this recalculation is adopted as Best ozone. After a Best ozone value has been accepted, residues are calculated from Equation 25 for each of the latitude profiles used, and final residues are derived by interpolating using f_{prof}.

The final step is to estimate the amount of the derived ozone that is beneath clouds. Estimates of the ozone amount under the cloud level pressure level are obtained for each of the two latitude profiles used to derive Best ozone and the two tabulated ozone values on either side of the derived Best ozone. The column ozone beneath cloud is then derived by interpolating in ozone and using f_{prof} to weight the latitudes. Finally, this ozone amount is multiplied by the cloud fraction f to derive the ozone in a particular field of view that is under cloud. The sensitivities are calculated from the sensitivities for the two profiles using the same weighting as for ozone.

5.6 Validity Checks

The algorithm contains several validity checks for maintaining data quality. Before measured radiances are accepted for use in ozone determination, the solar zenith angle, satellite attitude, and instrument status are checked to ensure the suitability of the radiances and other geophysical input to the algorithm. This section describes the quality checks performed to identify invalid and lower quality ozone values caused either by bad input data that passed preprocessing checks or by limitations of the ozone algorithm. It also explains the significance of the error flags that are set.

The principal tool used to investigate the validity and quality of a total ozone value is the set of residues. The residues measure how well radiances calculated based on the ozone derived using one set of wavelengths match the radiances measured at the other wavelengths. The usual significance of a large residue is that the atmospheric or surface conditions deviate significantly from those assumed in the algorithm, for example, if reflectivity has a non-linear dependence on wavelength. The final triplet residues for wavelengths used in the retrieval will be zero.

The first check is of all the non-zero residues; if any is greater than 12.5 in units of N-value, the error flag is set to 5. This condition usually arises when problems in the data stream lead to incorrect values for the measured radiance or when the atmospheric conditions are so unusual that the assumptions used in the calculation of radiances do not hold.

Data that pass flag 5 are checked for sulfur dioxide contamination. The SO_2 index (SOI) is defined by the following equation:

$$r = SOI\left[\frac{dN}{d(SO_2)}\right] + \Delta\Omega\left(\frac{dN}{d\Omega}\right) + b(\lambda - 380) \tag{29}$$

This equation is formulated in the same way as Equation 18, the basic equation for the ozone correction, with an additional term for sulfur dioxide contamination. The physical interpretation is that the mismatch between calculated and measured radiance has a component due to SO_2 in addition to the components due to ozone error, wavelength-dependent reflectivity, and residual calibration error accounted for in Equation 20. Using three wavelengths provides three equations, which can be solved for SOI as a function of the residues, the sensitivities, and the wavelengths. The algorithm uses the residues at 317 nm, 331 nm, and 340 nm. The 312-nm wavelength is not used because it is more affected by aerosols. If the SOI is greater than 24, the error flag is set to 4. The limit corresponds approximately to a 4σ departure from zero, as determined from examination of a day of data that is known not to be contaminated. Since the triplet residues at the wavelengths used to derive the SOI are all zero when the C-triplet is used to derive ozone with the B-triplet to select the profile, SOI is not evaluated for path lengths greater than 3; the output data set will contain a fill value. SO_2-contaminated data will still be likely to be flagged by the remaining residue tests, but the presence of SO_2 will not be identified.

In principle, Equation 29 could be used to simultaneously solve for ozone and SOI. However, the wavelengths best for ozone determination at a given path length are not necessarily the best for SOI determination. Also, the more complicated expression for ozone that would result would significantly increase the computer time required.

The next check assesses triplet consistency. If a single triplet is used, the triplet residue defined in Equation 27 is checked for the ozone-sensitive wavelength not used in the ozone determination: 317 nm in the case of the A-triplet, and 312 nm for the B-triplet. The maximum residues allowed, in N-value units, are 1.1 at 317 nm when an A-triplet determination is checked and 0.9 at 312 nm when a B-triplet determination is checked. If a second triplet is used to determine the profile, then the requirement is that a value of f_{prof} can be found such that $-0.5 \le f_{prof} \le 1.5$. Values of f_{prof} outside this limit require such a degree of extrapolation that the profile is not considered highly reliable. If the data fail the relevant test, the error flag is set to 3. The next check uses the 331-nm residue. If this residue exceeds 4 in N-value units, the error flag is set to 2. Flag values of 3 or 2 resulting from large residues imply that the values of I/F are inconsistent with the assumption that the linear correction can be used.

For solar zenith angles greater than 84 degrees, the algorithm loses accuracy. Most retrievals must make use of the C-pair, which is not highly sensitive to ozone. In addition, the conditions depart from those for which the radiative transfer code was designed, in particular the geometry. For this case, the error flag is set to 1. Finally, because of the summer high zenith angle B/C pair bias discussed in Section 7.6, the value 10 is added to the flag value for the data that are taken in polar summer on the descending (north to south) part of the orbit. While all flagged ozone values appear on the Level–2 data sets, only ozone values with the flag set to 0 for a good retrieval from the ascending part of the orbit are used to derive the gridded means of Level–3.

Table 5.4 summarizes the error flags, when they are set, and their significance.

Table 5.4. Error Flags

Flag	Criterion	Significance
0	No other flag set	Good value
1	Solar zenith angle > 84˚	Algorithm less accurate
2	r(331) > 4 (N-value)	Linear correction inadequate
3	$r_{trip}(317)$ > 1.1 (N-value) (if A-triplet alone used) $r_{trip}(312)$ > 0.9 (N-value) (if B-triplet alone used) f_{prof} < -0.5 or f_{prof} > 1.5 (profile selection)	Linear correction inadequate
4	SOI > 24	Sulfur dioxide contamination
5	any residue > 12.5	Unusual atmospheric conditions or data stream problems
+10	Descending orbit	High zenith angle; redundant

6.0 GENERAL UNCERTAINTIES

There are three areas in which uncertainties can be introduced into the ozone derived from TOMS: the accuracy and precision of the measurements, the value of the radiances calculated from the radiative transfer model, and the process of comparing the measured and calculated radiances to derive ozone. In each of these areas, errors of three kinds are possible: random errors, time-invariant systematic errors, and time-dependent systematic errors.

Table 6.1 summarizes the estimated uncertainties in the retrieved TOMS ozone. They are organized by kind of error rather than by where they originate in the ozone retrieval process. This organization makes it clearer how the errors are to be combined to derive a total error for the retrieval. However, the following discussion will be organized by where the error arises in the retrieval process, to make clearer the relation between the individual uncertainties and how they arise.

Table 6.1. Errors in Retrieved TOMS Ozone

Source	Error (%)
Random - not applicable to long-term change	
(typical values - may be larger in winter months	
or under disturbed atmospheric conditions)	
Instrument noise (including digitization)	0.3
Atmospheric temperature	1
Retrieval error	1^1
Tropospheric ozone	1.5
Net (Root sum of squares)	2.0
Time Invariant	
Rayleigh scattering	< 0.5
Ozone absorption cross-section	$< 2^2$
Wavelength calibration	< 2
Radiometric calibration	1
Retrieval error	< 1
Time Dependent	
Radiometric calibration	< 1.0/decade
Wavelength calibration	< 0.07/decade
Atmospheric temperature	$0.16/°K$
Tropospheric ozone	0.05/percent change

[1] May by 5 percent or higher at very high solar zenith angles.
[2] Value for comparisons with non-UV instruments or UV measurements evaluated using different ozone absorption cross-sections.

It is important to recognize that the use of a single number to describe the uncertainty from any source is an oversimplification. In all cases, the uncertainty in total ozone depends upon the wavelengths used in determining ozone, the uncertainty in the measurement at those wavelengths, and the sensitivity of the retrieved ozone to a change in the value of I/F at that wavelength. In addition, the error from a particular source will depend on the conditions of measurement, with values much above the usual values under certain conditions. The entries in Table 6.1 represent values for the most common conditions. Some cases where the uncertainty may differ significantly from the values in the table are noted.

6.1 Accuracy and Precision of TOMS Measurements

There are three separate components to determining the accuracy and precision of the normalized radiances that are used in the total ozone retrieval from TOMS. First is the precision of the radiances, which is governed by instrument noise and by the digitization of the TOMS output. These factors produce random errors in the value that is given for measured radiance. The second is the initial laboratory calibration. An error in the absolute radiometric calibration or in the wavelength calibration may lead to a time invariant, systematic zero-point error or bias in the retrieved ozone. The third is possible changes with time in the instrument sensitivity. An error here will cause a drift with time of the derived total ozone values.

The largest contributor to random instrumental error, resulting from reporting of raw radiances only at discrete values from the digitized instrument, is less than 0.2 percent at all wavelengths. The total random instrumental error is 0.3 percent. This error is the first entry under random errors in Table 6.1.

The accuracy of the initial albedo derived from TOMS measurements depends on the accuracy of the prelaunch radiance and irradiance calibration constants. These constants depend primarily upon the radiometric accuracy (±3 percent) of the standard calibration lamp supplied by the National Institute for Standards and Technology (NIST) and, for the radiance calibration constants only, upon the accuracy with which the reflecting properties of the NIST-calibrated standard barium sulfate-coated diffuser plates are known. However, the ratio of radiance and irradiance calibration constants, which enters into the determination of I_m/F_0 discussed in Section 4.5, is not affected by the lamp calibration and is known to be better than ±3 percent. The error in ozone that will result can be a systematic error of 1 percent that does not change with time.

Errors in the instrument wavelength scale also can generate uncertainties in the retrieved ozone. The radiances that are calculated for comparison with measurements must be derived for the wavelengths and slit sensitivity of the TOMS instrument. If there is an error in the wavelengths assumed for the TOMS instrument, then the calculated radiances will not be the same as those for the actual TOMS instrument, leading to an error in the retrieved ozone. As discussed in Section 4.2, it is estimated that the initial TOMS wavelength calibration was known to ±0.1-nm accuracy. This uncertainty corresponds to a possible systematic error of 2 percent in derived ozone, constant with time.

A wavelength calibration drift could produce a time dependent error in ozone. As noted in Section 4.2, the wavelength calibration drifted by less than 0.005 nm over the life of the instrument, corresponding to a possible drift of less than 0.07 percent/decade in ozone. The upper limit to the possible change appears on the first line under the time-dependent changes of Table 6.1.

The principal long-term error of instrumental origin lies in the uncertainty in the characterization of the long-term changes in instrument sensitivity. The TOMS instrument sensitivity changed significantly during its lifetime of operation in orbit. A concerted effort by NASA's Ozone Processing Team to understand the TOMS long-term calibration changes has led to the methods, described in Section 4.5, used to assess these changes. The derived radiometric calibration of TOMS over time is accurate to about 1.0 percent/decade and is the first source of time-dependent error listed in Table 6.1. Section 6.4 discusses the additional insight gained from comparisons with ground-based ozone measurements.

6.2 Calculated Radiances and Their Use in the Algorithm

Errors in the calculation of radiances have two principal origins: in the physical quantities whose values are obtained from laboratory physics and in the atmospheric properties assumed for the radiative transfer calculations. Calculation of the scattering of atmospheric radiation by ozone and the other constituents of the atmosphere requires values for the ozone absorption and Rayleigh scattering coefficients. The values used in the algorithm are obtained from laboratory measurements. Any error in the laboratory values will propagate through the algorithm to produce a systematic error in the derived ozone. The first two lines in the time-invariant error group of Table 6.1 show the effect of the uncertainties in these quantities on derived ozone. In addition, the absorptivity of ozone is a function of the temperature. The calculated radiances are based upon a climatological temperature; however, if the temperature structure departs from the climatology, the absorption coefficient may change from that assumed in the algorithm, producing an error in retrieved ozone. The size of this error is shown in the second line of the random error group.

The third random error component listed in Table 6.1, called retrieval error, arises from variations of the properties of the real atmosphere about those assumed for the calculation of radiances. The most important of these is the difference between the actual vertical distribution of ozone and the standard profile used to compute the look-up tables. At low to moderate solar zenith angles, the TOMS derived total ozone is not significantly dependent on the ozone profile used. At high solar zenith angles, however, profile sensitivity is a significant source of error. Other contributors included in retrieval error are variations in cloudiness about the climatology, and non-volcanic aerosols.

The fourth random error in Table 6.1 arises from possible variations in tropospheric ozone, in particular from cases where changes in tropospheric ozone do not affect the measured radiance. TOMS cannot measure ozone that is hidden from the instrument by thick cloud. In the TOMS algorithm, a climatological tropospheric ozone amount is assumed to be present beneath the cloud fraction identified by the reflectivity channel of TOMS. Thus, the error from hiding by clouds in a given measurement is equal to the error in tropospheric ozone times the cloud fraction, and the algorithm will, in general, be less sensitive to errors in tropospheric ozone if the cloud fraction is low. About 6 percent of total ozone is in the lowest 5 km, with a 50 percent variability. The radiation from the troposphere has both surface and atmospheric components: the surface component traverses the troposphere and provides a measure of tropospheric ozone, while the atmospheric component, arising from Rayleigh scattering, is not sensitive to the ozone amount. Over surfaces with low reflectivity, the Rayleigh scattering component dominates, and the measured radiance will not be sensitive to departures from the standard tropospheric ozone profile. When the surface is highly reflective, the ozone-sensitive surface component is more important, and the TOMS estimate of tropospheric ozone improves; thus, the problem of tropospheric ozone is less significant over ice-covered regions such as the Antarctic. The retrieval also improves at low solar zenith angles when incident UV penetrates further into the troposhpere [*Klenk et al. 1982*]. Overall, TOMS measures roughly half of the trophospheric ozone variation.

Assignment of the temperature, retrieval, and tropospheric ozone errors as random is based upon an approach in which the atmospheric variations are not known and are treated as random variability about the climatology. However, if independent measurements of any of these quantities are available for a scan, then such measurements can be used to correct the ozone values derived from TOMS, and the error would no longer be random. The next section discusses such corrections.

6.3 Estimating Sensitivities to Atmospheric Conditions

Independent measurements of tropospheric ozone or atmospheric temperature make it possible to evaluate the contribution of these changes to the derived ozone. This contribution may then be treated as a systematic, time-dependent contribution, whose size is given by the sensitivity of the derived ozone to the known variations in these quantities, rather than as a random error. The last two entries under time-dependent error show the sensitivities that can be used to determine the corrections to ozone that should applied for known changes in atmospheric temperature and tropospheric ozone.

The combination of long-term decreases in upper level ozone measured by SBUV and Umkehr and a small increase in solar zenith angle associated with the drift in the Nimbus–7 orbit can produce a systematic time-dependence in the error due to profile shape. Most of the time dependence in the Version 6 data that arose in this way has been eliminated by the new Version 7 profile interpolation for path lengths greater than 1.5, as described in Section 5.5.

6.4 Comparison with Ground-Based Total Ozone Measurements

The TOMS Version 7 data have been compared with ground-based measurements made by a network composed of 30 mid-northern latitude stations with Dobson and Brewer ozone measuring instruments. A station was included if it had homogeneous data coverage over the 14.5 year TOMS lifetime. Each ground measurement was paired with the TOMS scan whose center was closest to the station; if two measurements were equally near, the one closest to nadir was used. A weekly mean was then calculated of the daily TOMS-ground differences at each station. These means were then averaged to derive a weekly average TOMS-ground difference.

Figure 6.1 shows the percentage difference between TOMS and ground ozone measurements as a function of time. Except at the very beginning, in the northern winter of 1978–1979, this difference is smaller than the combined uncertainty of the TOMS and ground-based measurements and of the comparison technique, as is the overall trend of 0.2 percent/decade. The two methods thus agree to within the uncertainties.

For the 1978–1979 period, the standard deviations of the weekly means are not significantly larger than those during the remainder of the TOMS lifetime, suggesting that the origin of this difference is probably a change in the TOMS instrument sensitivity that has not been characterized properly rather than anomalies in the ground measurements or

the comparison. Two apparent discontinuities, one in late 1982 and one in the middle of 1988, have not been identified with any known events in the TOMS history.

Version 7 TOMS − Ground Based
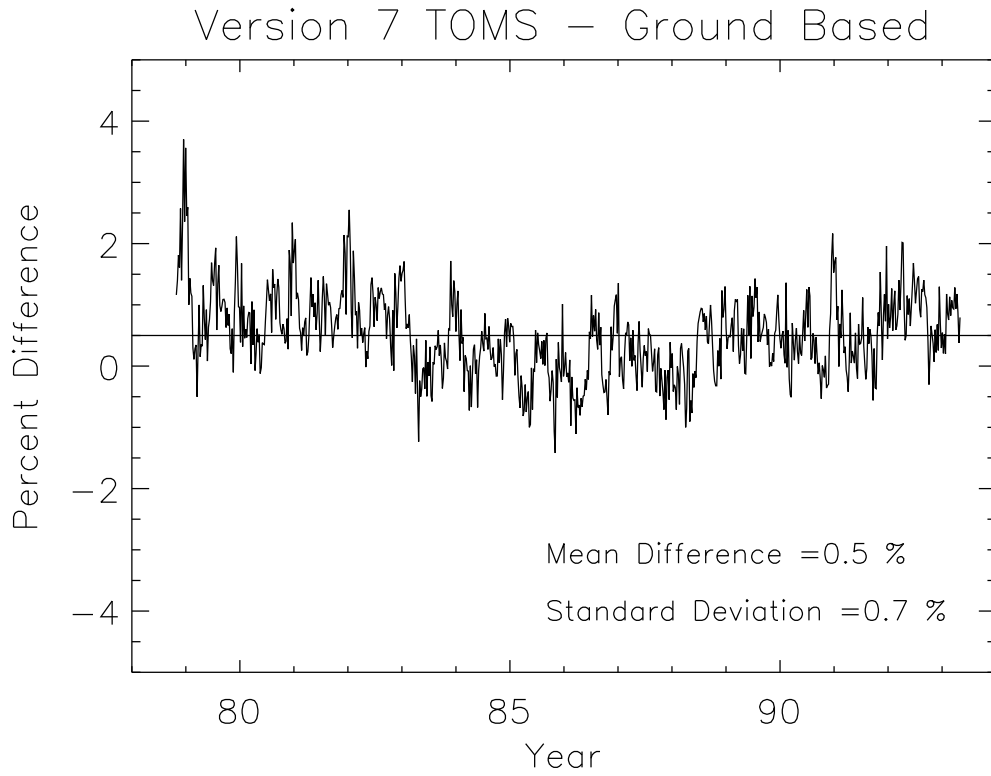
Figure 6.1. Percentage difference between TOMS and ground ozone. Solid line is linear fit trend.

7.0 PROBLEMS LOCALIZED IN SPACE AND TIME

7.1 Volcanic SO$_2$ and Aerosol Contamination

Prior to the eruption of El Chichón April 1982, ozone was thought to be the only significant atmospheric absorber at the near ultraviolet wavelengths. However, the El Chichón cloud appeared in TOMS data as anomalously high ozone amounts. The excess absorption was found to be from sulfur dioxide [*Krueger 1983*], which was contained together with water and carbon dioxide in the volatile portion of the plume in magmatic eruptions. With two absorbing constituents, the TOMS algorithm could no longer be used to accurately measure total ozone when volcanic clouds were present. However, an algorithm to detect the presence of sulfur dioxide was developed so that contaminated ozone data could be flagged with a sulfur dioxide index (SOI). The algorithm is based on a simultaneous solution of the absorption optical depth equations at four of the TOMS wavelengths, coupled with an empirical correction developed in background areas where the sulfur dioxide absorption is neglibible [*Krueger, et al., 1995*]. The El Chichón plume was tracked for nearly four weeks using the SO$_2$ estimates from this algorithm. Radiative transfer simulations of volcanic clouds under low latitude conditions show that these SO$_2$ estimates are accurate (5 percent) in ash-free clouds, but overestimate the SO$_2$ by up to 3 percent when ash and aerosols are present [*Krueger, et al., 1995*]. The current TOMS measurements of SO$_2$ production in large volcanic eruptions are far more accurate than the order of magnitude accuracy of previous methods. Much of this gain in accuracy comes from the contiguous, synoptic view of entire volcanic clouds with areas of millions of square kilometers from the satellite orbit. Consequently, the SOI data have found wide use in the volcanology, chemistry, and climate communities. Over 100 eruptions have been detected and measured in the Nimbus–7 TOMS data base [*Bluth et al., 1993*]. The most recent major eruption is that of Mt. Pinatubo in the Phillipine Islands on June 15, 1991, in which 20 million tons of SO$_2$ were produced [*Bluth et al., 1992*].

Gaseous SO$_2$ absorbs in bands throughout the 290-nm to 320-nm range. Some bands at longer wavelengths coincide with wavelengths used by TOMS to measure ozone. The effect of this absorption is to produce a false enhancement in the ozone measured by TOMS after a major eruption. These effects are short lived, because the SO$_2$ is converted rapidly to sulfuric acid aerosols. Sweep mode spectral scans of the backscattered Earth radiance made every 24 days by SBUV show clear evidence of structure attributable to SO$_2$ on April 15, 1982, a marginally detectable level on May 9, and no evidence of SO$_2$ in the albedos for June 2 [*McPeters et al., 1984*]. Following Mt. Pinatubo, SO$_2$ was detectable through at least mid-July 1991 [*Bluth et al., 1992*].

The SOI defined in Section 5.6 uses the radiances at one ozone wavelength and two comparison wavelengths to identify affected scans. It is used to flag contaminated ozone values and appears on the Level–2 data set. Because the SOI is not derived from a complete radiative transfer calculation like that used to obtain ozone, a value for column SO$_2$ cannot be obtained definitively from the SOI. The screening limit, an SOI of 24, corresponds to a 4σ departure from the mean of a set of uncontaminated measurements, chosen on a day when no known volcanic contamination was present and showing a Gaussian distribution of SOI values. As the ozone error that results when SO$_2$ modifies the backscattered spectrum is, in matm-cm, about twice the SOI, this limit corresponds to an estimated error on the order of 50 matm-cm. In the vicinity of flagged values, SOI values just below the threshold suggest the likelihood of errors that are non-negligible but below the flagging limit. Isolated points with such values could be either very localized infusions of SO$_2$ or only noise; they must be evaluated individually. The maximum value of the SOI stored on the Level–2 data set is 200; if larger values are calculated, the value is set to 200. At such high levels of SO$_2$ contamination, differences in the SOI are not meaningful.

Values that are flagged for SO$_2$ contamination are not used to calculate the Level–3 grid means. Because the error of ozone values with subthreshold SOI contamination may be as large as 50 D.Us., grid means in the vicinity of high SO$_2$ concentrations may be affected by the inclusion of these scans.

Increased Mie scattering by sulfuric acid aerosols in the atmosphere modifies its radiative transfer properties and may significantly affect the backscattered ultraviolet radiances measured by TOMS. Depending on the solar and satellite zenith angles, the effect may be either an enhancement or a decrease in the measured radiances. The magnitude of the effect depends upon the optical depth of the aerosol layer and its altitude with respect to the ozone peak, being greatest for those wavelengths whose contribution functions peak in the vicinity of the densest part of the ozone layer

[*Torres and Bhartia, 1995*]. The SBUV spectral scans of Earth radiance show this effect to be most significant at wavelengths shorter than those used by TOMS for the retrieval of total ozone. The impact of any anomalous increase in radiance from the aerosol is further reduced by the use of wavelength triplets in the calculation of total ozone. Still, following the eruptions of El Chichón and Mt. Pinatubo, anomalies in the TOMS total ozone retrievals became apparent [*Bhartia et al., 1993*]. The top panel of Figure 7.1 shows ozone as a function of satellite zenith angle for a scan following the eruption of Mt. Pinatubo. The tic marks on the abscissa correspond to individual scan positions. The second panel shows ozone as a function of scan position for an unaffected scan, during 1980. The scan angle dependence of less than 1 percent arises from scattering by normal background aerosols and by cirrus cloud that is not fully treated in the radiative transfer calculation. The scan following the Mt. Pinatubo eruption shows the anomalies, apparent depressions in the tropical ozone amount near the center of each track (satellite zenith angles 0–32 degrees on the right) and higher ozone values toward the wings of the scan. These effects are of the order of 2 percent. The observed structure is related to the sulfuric acid aerosol scattering phase function [*Torres et al., 1995*]. When aerosols are present, they change the scattering properties of the atmosphere from those assumed in the calculation of radiances described in section 5.2; thus, the radiances in the tables are not correct for the case where aerosols are present.

7.2 Additional Scan Angle Dependence

The second panel of Figure 7.1 shows that even in the absence of volcanic aerosols, a small scan angle dependence, on the order of 1 percent, remains in TOMS retrieved ozone. In the presence of sun glint, a stronger scan angle dependence of about 2 percent is seen, as shown in the third panel of Figure 7.1. For the Nimbus–7 sun-synchronous orbit with a noon equator crossing time, sun glint occurs only for clear sky with direct overhead sun over water. Under these conditions, the derived surface reflectivity is enhanced, a result of scattering by the stratospheric background of this extra radiation reflected from the surface. The consequence is that derived ozone is about 1 percent low under these conditions near nadir in the vicinity of the center sample. Near the end of the TOMS data record, as the local equator crossing time drifted toward morning, the glint effect moved slightly off nadir.

7.3 Solar Eclipses

When the Sun is eclipsed, the decrease in incoming solar irradiance leads to a decrease in the backscattered Earth radiance, because the reflection and scattering processes are not affected. However, because the solar irradiance used for the ozone retrieval is derived from measurements of the uneclipsed Sun, the derived I/F will not be correct during times of eclipse. Consequently, ozone values are not retrieved for periods of time and ranges of latitude where the radiances are affected by a solar eclipse. In actual production, tabulated eclipse information is part of the input stream for the job run and is used by the software to exclude the eclipse periods and regions.

7.4 Polar Stratospheric Clouds

The effect of anomalously high clouds can be a significant error source for localized regions in the Arctic and Antarctic. Polar Stratospheric Clouds (PSCs) above the ozone peak may cause the TOMS retrieved total ozone to be underestimated for solar zenith angles larger than 70 degrees. Models indicate that the impact of these clouds on TOMS retrieved total ozone is a strong function of optical depth. Type I PSCs of optical depth 0.01 (composed of $HNO_3/3H_2O$, particle mean radius ~0.5 μm) may produce an underestimate of up to 2 percent at solar zenith angles greater than 80 degrees. Larger errors (up to 6 percent) may be introduced by Type II PSCs of optical depth 0.05 (water ice, particle mean radius ~5-50 μm). Underestimates as large as 50 percent may occur when Type II PSCs of optical depth 0.4 (associated with lee-waves) are present. No corrections have been made for the presence of PSCs, but they tend to be very localized in time and space, lasting 3–5 days with typical sizes of 1000–3000 km [*Torres et al., 1992*].

7.5 High Terrain

Users may note an apparent anticorrelation of ozone with terrain height, particularly in the form of ozone dips above high mountain ranges. These dips occur because the algorithm retrieves the actual column ozone above the surface, not above sea level. The atmospheric ozone that would normally be present between sea level and the actual terrain height is missing. Column ozone actually is lower above the mountains, in the same way as other atmospheric
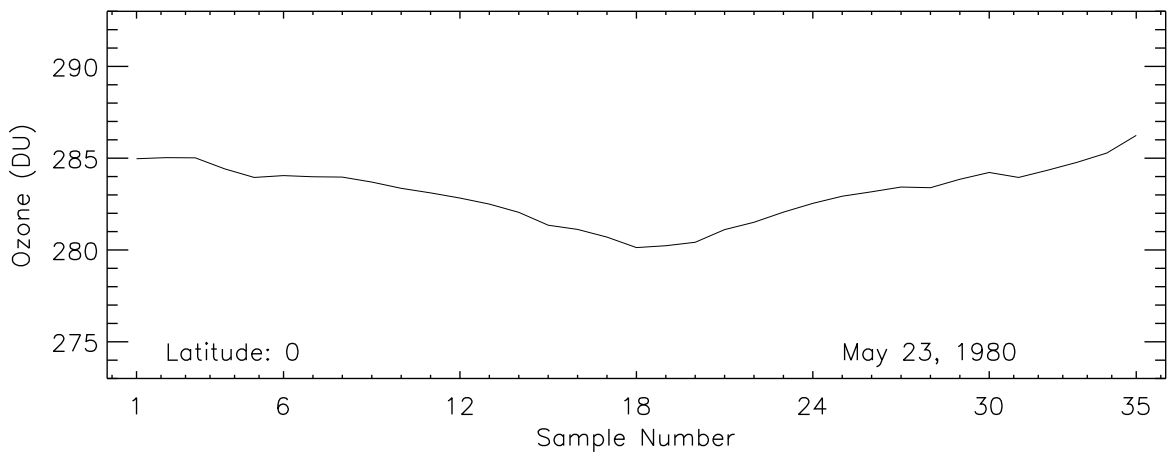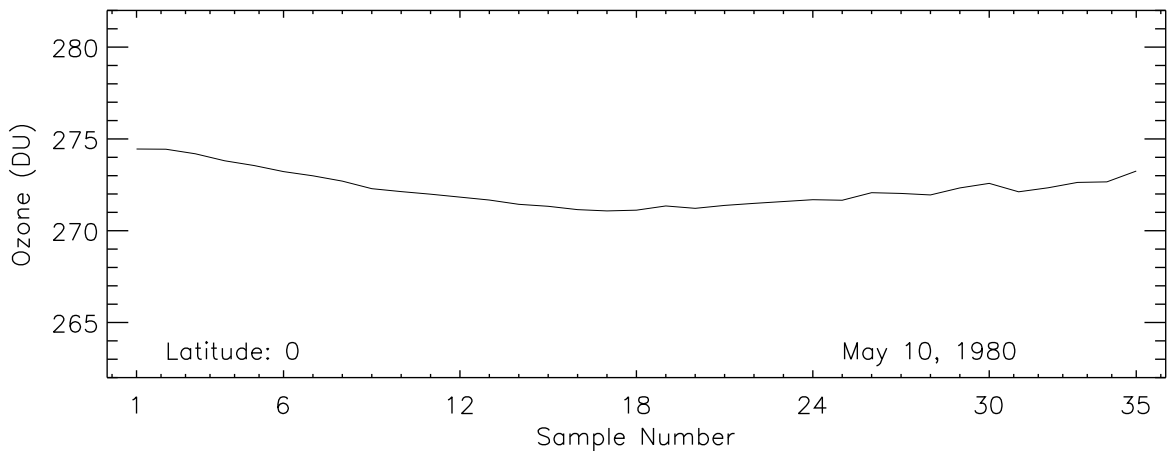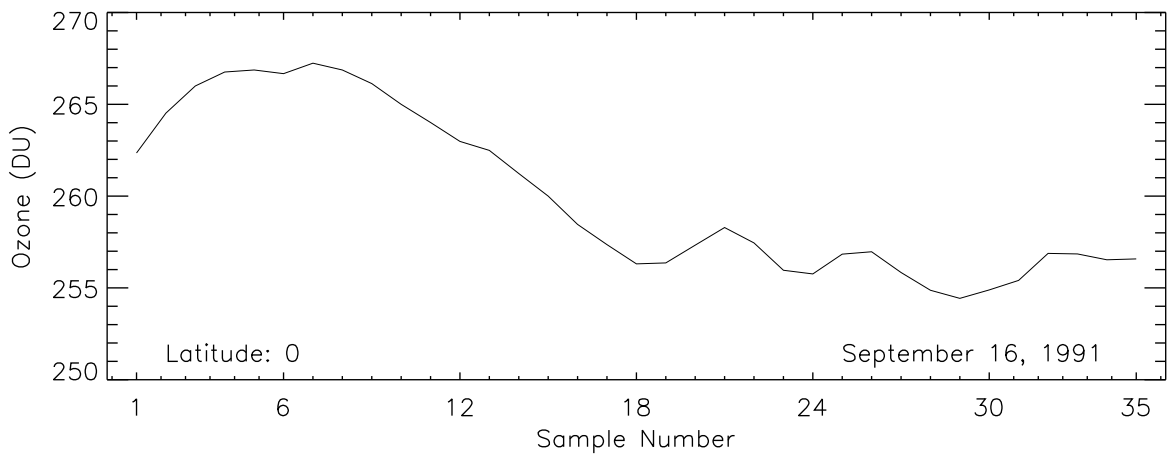
Figure 7.1. Derived total ozone as a function of satellite zenith angle. (Top) Shortly after the eruption of Mt. Pinatubo. (Middle) Typical scan. (Bottom) Scan affected by sea glint.

constituents. The relation between column ozone and altitude is thus not an artifact of the measurement but simply reflects the fact that when the surface is higher, there is less atmosphere above it.

7.6 Descending Portion of Orbit

For a period around the summer solstice for each pole, TOMS is able to measure backscattered sunlight from the regions on the descending (north to south) part of the orbit lit by the midnight sun. The ozone values so derived are biased low at high zenith angle. As zenith angle increases, so does the path length, and the algorithm switches from the B-triplet to the C-triplet. The C-triplet has proven to have a seasonally dependent bias relative to the B-triplet, with the C-triplet approximately 2.5 percent lower in summer and with the bias approximately zero in winter. Thus, the low values for high zenith angle reflect the shift to the C-triplet and its biasing low. The origin of this bias is not currently understood. Fortunately, this problem does not affect the TOMS coverage or the Level–3 map product. In summer, better views of the same polar region are available from the ascending, noon portion of the orbit. In winter, when the high zenith angle data must be used, the bias is small. When the Level–3 product is created, the descending orbit retrievals are not used. However, users of the Level–2 product should be aware of this problem and avoid the use of data flagged as being taken during the descending portion of the orbit.

8.0 DATA FORMATS

8.1 Hierarchical Data Format

TOMS data products will be available electronically from the Distributed Active Archive Center (DAAC) in the form of Hierarchical Data Format (HDF) files [*Ilg et al., 1993; Kalman, 1994*]. Along with the files, the DAAC will distribute HDF software tools for reading the files.

8.1.1 Level–2 Hierarchical Data Format Product

The standard archival Level–2 products are stored in HDF files, one for each orbit, at the GSFC DAAC. They are generated using the most recent version of HDF available from the University of Illinois' National Center for Supercomputing Applications (NCSA) and endorsed by the EOSDIS Project. The Level–2 file contains all output from the Version 7 ozone processing, including ozone and reflectivity products, as well as diagnostic parameters and a SOI, on a scan-by-scan basis for each TOMS daylit FOV.

The Level–2 HDF file consists of the following components:

1. A File Label
2. A File Description
3. Metadata (stored as a second file description)
4. Network Common Data Form (netCDF) style attributes
5. Multiple Data Scientific Data Sets (SDSs)
6. Multiple Coordinate SDSs

The File Label is a string that identifies the instrument, the spacecraft, date, and orbit number of the data within the Level–2 HDF. It has the following form: "TOMS_NIMBUS-7_yyddd.nxxxxx", where yy is the (two digit) year, ddd is the three-digit day of year, and xxxxx is the lifetime orbit number (i.e., revolution since launch, where orbit 1 is defined to start with the first ascending node equator crossing). Leading zeroes are used for yy, ddd, and xxxxx when applicable.

The File Description is a field of up to 40,000 ASCII characters which describes, in free form text, the Level–2 product and its generation algorithm.

Metadata include the following:

1. Data set name
2. Data product name
3. Granule size (bytes)
4. Time of first scan of orbit (year, month, day, hour, minute, second, GMT)
5. Time of last scan of orbit (year, month, day, hour, minute, second, GMT)
6. Number of scans (including fill) in orbit
7. Date and time of ascending node equator crossing (year, month, day, hour, minute, second, GMT)
8. Longitude of ascending node equator crossing (degrees; –7777 when unavailable)
9. Altitude of spacecraft during last TOMS scan of orbit (km)
10. Orbit number
11. Geographical flag - o (orbit) for Level–2
12. Day/night flag
13. Granule version
14. Producer granule ID
15. 4 byte signed decimal integer that represents missing value
16. 2 byte signed decimal integer that represents missing value
17. 1 byte unsigned decimal integer that represents missing value

The following NetCDF style attributes are included:

1. Quality flag counters (32)
   1   Number of input/output errors for this orbit
   2   Number of scans read for orbit
   3   Number of scans written for orbit
   4   Number of samples out of range (total)
   Number of samples out of range for
   5   Zenith angle > 88 degrees
   6   Latitude
   7   Instrument counts (negative)
   8   Number of samples written that were bad (total)
   Numbers of individual error flags for Algorithm Flag = 1 (see Table 8.2 for description of error and algorithm flags):
   9   Number of samples that had error flag = 0 or 10
   10   Number of samples that had error flag = 1 or 11
   11   Number of samples that had error flag = 2 or 12
   12   Number of samples that had error flag = 3 or 13
   13   Number of samples that had error flag = 4 or 14
   14   Number of samples that had error flag = 5 or 15
   15–20 Same as 9–14 for Algorithm Flag = 2
   21–26 Same as 9–14 for Algorithm Flag = 3
   27–32 Same as 9–14 for Algorithm Flag = 4
2. TOMS band center wavelengths (nm), shortest first
3. Solar irradiance F-values at 1 A. U. (watts/cm^3) for the current day at the six TOMS wavelengths, shortest first
4. Count-to-radiance conversion factors (watts/cm^3/steradian/count) for each of the four gain ranges for each of the six wavelengths, shortest first
5. Nominal spacecraft zenith angle (degrees) at each scan position

There are 27 Data SDSs stored in the Level–2 product. Their names, dimensions and data types are listed in Table 8.1. More detailed descriptions, units, offsets, and scale factors are listed in Table 8.2. The data are stored as integers; to convert to the physical units, they must be added to the offset and then multiplied by the scale factor. Table 8.3 lists the fill values used for different data types for missing scans. One-dimensional SDSs are stored in a TOMS scan number domain. Two-dimensional SDSs are stored in a TOMS scan number by TOMS scene number domain. Three-dimensional SDSs are stored in a TOMS scan number by TOMS scene number by TOMS wavelength domain.

The four Coordinate SDSs stored in the Level–2 product are listed in Table 8.4.

8.1.2 Level–3 Hierarchical Data Format Product

The standard archival Level–3 product contains global arrays of total ozone and effective surface reflectivity stored as daily HDF files. A Level–3 file is generated from each complete daily set of Level–2 files.

The Level–3 HDF file is comprised of the following elements:

1. a File Label,
2. a File Description,
3. Metadata (stored as a second file description),
4. 2 Data Scientific Data Sets (SDS),
5. 2 Coordinate SDS's.

Table 8.1. Nimbus–7/TOMS Level–2 HDF SDSs

Name of SDS	Dimensions	Data Type
LSEQNO	575	2 byte integer
YEAR	575	2 byte integer
DAY	575	2 byte integer
GMT	575	4 byte integer
ALTITUDE	575	2 byte integer
NADIR	575	2 byte integer
SYNC	575	2 byte integer
LATITUDE	575 x 35	2 byte integer
LONGITUDE	575 x 35	2 byte integer
SOLAR_ZENITH_ANGLE	575 x 35	2 byte integer
PHI	575 x 35	2 byte integer
NVALUE	575 x 35 x 6	2 byte integer
SENSITIVITY	575 x 35 x 5	2 byte integer
dN/dR	575 x 35 x 6	1 byte unsigned integer
RESIDUE	575 x 35 x 5	1 byte unsigned integer
TOTAL_OZONE	575 x 35	2 byte integer
REFLECTIVITY	575 x 35	2 byte integer
ERROR_FLAG	575 x 35	2 byte integer
OZONE_BELOW_CLOUD	575 x 35	1 byte unsigned integer
TERRAIN_PRESSURE	575 x 35	1 byte unsigned integer
CLOUD_PRESSURE	575 x 35	1 byte unsigned integer
SOI	575 x 35	1 byte unsigned integer
ALGORITHM_FLAG	575 x 35	1 byte unsigned integer
CLOUD_FRACTION	575 x 35	1 byte unsigned integer
MIXING_FRACTION	575 x 35	1 byte unsigned integer
CATEGORY	575 x 35	1 byte unsigned integer
THIR_CLOUD_PRESSURE	575 x 35	1 byte unsigned integer

The last index varies most rapidly in all arrays.

Table 8.2. Detailed Description of Nimbus–7/TOMS Level–2 SDSs

SDS Name	Description
LSEQNO	Sequence number of scan within orbit
YEAR	Year (four digits) at start of scan, GMT.
DAY	Day of year (1–366) at start of scan, GMT.
GMT	Greenwich Mean Time in seconds of day at start of scan (1–86,400).
ALTITUDE	Spacecraft altitude at start of scan (km).
NADIR	Nadir scan angle, used to express the spacecraft's attitude error, the angle between the vectors from the S/C to the local normal and from the S/C to the FOV (0 ≤ nadir angle ≤ 180) (x 100).
SYNC	Flag for chopper non-synchronization occurrence:
	0: Does not occur in current or next scan
	1: Occurs in current scan, not in next
	2: Occurs in next scan, not current
	3: Occurs in both current and next scan
LATITUDE	IFOV latitude, from 90˚ S–90˚ N (degrees x 100).
LONGITUDE	IFOV longitude, from 180˚ W–180˚ E (degrees x 100).
SOLAR_ZENITH_ANGLE	IFOV solar zenith angle (degrees x 100).
PHI	Angle ϕ between sun and satellite measured at IFOV, (degrees x 100).

Table 8.2. Detailed Description of Nimbus–7/TOMS Level–2 SDSs (Continued)

SDS Name	Description
NVALUE	N-values (as defined in Section 4.5) at 6 wavelengths, shortest first (x 50).
SENSITIVITY	Sensitivity $dN/d\Omega$ at 5 shortest wavelengths, shortest first, obtained by table interpolation (matm-cm x 10,000).
dN/dR	N-value sensitivity to reflectivity dN/dR at 6 wavelengths, shortest first (% x –50).
RESIDUE	Adjusted residues (see Sections 5.5) at 5 shortest wavelengths, shortest first (x 10 + 127).
TOTAL_OZONE	Total Ozone (matm-cm), x 10.
REFLECTIVITY	Effective reflectivity assuming Lambertian surface (% x 100).

ERROR_FLAG	Error Flag
	0 good data
	1 good data, $84° <$ solar zenith angle $< 88°$
	2 residue at 331 nm greater than 4 in N-value units
	3 triplet residue too large
	     (A-triplet: $r_{317} > 1.1$ N-value units)
	     (B-triplet: $r_{312} > 0.9$ N-value units)
	     (f_{prof}: $< –0.5$ or > 3.5)
	4 $SOI > 24$ (SO_2 contamination)
	5 At least one residue has absolute value larger than 12.5
	A value of 10 is added to the error flag for all scans on descending (midnight) part of orbit.

OZONE_BELOW_CLOUD	Estimated ozone below cloud layer (matm-cm).
TERRAIN_PRESSURE	Ground pressure derived from NOAA/NMC grid (atm x 100).
CLOUD_PRESSURE	Cloud pressure from ISCCP climatology (atm x 100).
SOI	Sulphur dioxide index (SOI), (matm-cm + 50).
ALGORITHM_FLAG	Algorithm flag - identifies triplet(s) used 1: A-triplet alone used 2: B-triplet alone used 3: B-triplet with A-triplet to select profile 4: C-triplet with B-triplet to select profile
CLOUD_FRACTION	Effective cloud fraction, as defined in Section 5.3 (percent).
MIXING_FRACTION	Mixing fraction f_{prof}, which parameterizes contributions of lower and higher latitude profiles in ozone determination, as described in Section 5.5; values range from 0.5 to 3.5 (x 10). 1: pure low latitude 2: pure mid latitude 3: pure high latitude
CATEGORY	Surface Category code 0: ocean 1: land 2: low inland (below sea level) 3: mixed land and ocean 4: mixed land and low inland 5: mixed ocean, land, and low inland
THIR_CLOUD_PRESSURE	Cloud pressure measured from Temperature-Humidity Infrared Radiometer, where available, (atm).

Table 8.3. Fill Values for Missing Scans

Data Type	Decimal	Hexadecimal
1 byte unsigned integer:	255	xFF
2 byte integers:	32767	x7FFF
4 byte integers:	2147483647	x7FFFFFFF

Table 8.4. Nimbus–7/TOMS Level–2 HDF Coordinate SDSs

Name	Type	Scaletype	Scalemin	Scalemax
time_of_orbit	2 byte int	regular	0	#scans-1
scan_position	2 byte int	regular	0	#scans-1
wavelength_6	4 byte real	irregular	n/a (6 TOMS wavelengths	
wavelength_5	4 byte real	irregular	n/a (5 shortest wavelengths)	

The Level–3 file names have the following form:

   n7gYYDDD.hdf

where YY is a 2-digit year and DDD is day of year.

The File Description provides background on the TOMS instrument, processing algorithms and data products, in free format. The following metadata are included:

1. Data set name
2. Data product name
3. Granule size (bytes)
4. Begin date and time (year, month, day, hour, minute, second, GMT)
5. End date and time (year, month, day, hour, minute, second, GMT)
6. Geographical flag - G (grid) for Level–3
7. Locations (latitude and longitude) of 4 corner points
8. Day/night flag
9. Granule version
10. Producer granule ID
11. Value representing missing data for ozone
12. Value representing missing data for reflectivity
13. Equator crossing time of first orbit (year, month, day, hour, minute, second, local mean solar time)

The data stored in the SDSs are on a fixed 1-degree latitude by 1.25-degree longitude grid. The gridded ozone values are stored as 3-digit integers in units of matm-cm. Reflectivity in percent, times 10, is also stored as 2-byte integers. Grid cells that are missing data due to lack of sunlight or other problems will be filled with 0 if ozone, 999 if reflectivity.

The two Coordinate SDSs stored in the Level–3 product are listed in Table 8.5.

Table 8.5. Nimbus–7/TOMS Level–3 HDF Coordinate SDSs

Name	Type	Scaletype	Scalemin	Scalemax
Latitude	4 byte real	regular	–89.5	89.5
Longitude	4 byte real	regular	–179.375	179.375

8.2 Native Format

8.2.1 TOMS Ozone File (Level–2 Data Product)

The TOMS Ozone File, also called the Level–2 Data Product, is a binary file, written as FORTRAN unformatted records. It is generated under UNIX. These files are used primarily as part of the TOMS processing. They are not normally distributed but may be obtained by special arrangement.

Each file contains all of the data processed for a single day. The first record of the file is a header, written in character format, containing information on the production hardware and software for both the Level–2 product and the Level–1 product used to generate it, the date and time the Level–2 file was generated, and the time period that the data on the file cover. The data records follow, ordered chronologically by time (GMT) of observation, and grouped by TOMS orbit. Each data record contains the information processed from one scan of the TOMS instrument. Only daylight scans, where the solar zenith angle at the nadir view for the scan is less than or equal to 92 degrees, have been processed by the ozone algorithm and written to the ozone file. The end of an orbit is indicated by a record called the orbital summary record, which contains the date, time, and location of the start and end of the orbit and of the equator crossing, counts of the number of scans processed and those flagged for various reasons, and other summary and ancillary information for the orbit. The last record of the file, called the trailer record, contains the time and date of the first and last scan of the last orbit of the day and the total number of the scans processed and flagged for various reasons for all orbits.

Each type of record, other than the header, can be identified by the logical sequence number, which is stored as an integer in the two most significant bytes of the third word of the record. All data records have a positive logical sequence number that counts the order of that record within the orbit to which it belongs, starting with a value of 1 for the first data record of the orbit. The orbital summary record for each orbit has a *negative* logical sequence number whose absolute value is one greater than that of the last data record of the orbit. The trailer record contains the unique logical sequence number of –1, which may be used to identify the end of the file.

The Tables 8.6–8.10 following contain, in order, the format of the header record, the format of the data records, a detailed description of selected words in the data record, the format of the orbital summary record, and the format of the trailer record.

Table 8.6. Format of TOMS Ozone File Header Record

Bytes	Character Representation[*]	Description
1–9	NIMBUS–7$_b$	Spacecraft identification.
10–14	FM-1$_b$	Flight model identifier. 1= Nimbus
15–22	LEVEL–2$_b$	Data product identification
23–38	BY$_b$XXXXXXXXXXXX$_b$	Program name in 12 characters, e.g., ozt.f
39–51	VERSION$_b$XXXX$_b$	Program version in 4 characters, e.g., 1.0
52–63	MMM$_b$DD$_b$YYYY$_b$	Program date in month-day-year, e.g., JUL 01 1994
64–83	ON$_b$XXXXXXXXXXXXXXX$_b$	Processing environment, 16 char., e.g., ALPHA UNIX V
84–106	GEN$_b$MMM$_b$DD$_b$YYYY$_b$HHMMSS$_b$	Time in month, day, year, hours, minutes, and seconds, corresponding to generation time of file.
107–135	DATA$_b$SPAN$_b$MMM$_b$DD$_b$YYYY$_b$HHMMSS$_b$	Time in month, day, year, hours, minutes, and seconds, corresponding to start of data span on file.
136–159	TO$_b$MMM$_b$DD$_b$YYYY$_b$HHMMSS$_{bbb}$	Time in month, day, year, hours, minutes, and seconds, corresponding to end of data span on file.
160–174	LEVEL–1$_b$HEADER:$_b$	Indicates that actual Level-1 header follows.
175–2100	[Level–1 header]$_b$...$_b$	Actual text of Level-1 header, followed by spares.

* Character "$_b$" is used to indicate a blank character.

Table 8.7. Format of Data Records

Word	Byte 1	Byte 2	Byte 3	Byte 4
1	Orbit number			
2	GMT (seconds of day) at start of scan			
3	Logical sequence number		Chopper synchronization flag	
4	Day of year at start of scan		Year at start of scan	
5	Altitude		Sample 1 view angle	
6	Latitude		Longitude	
7	Solar Zenith Angle		ϕ Angle	
8	N_{312}		N_{317}	
9	N_{331}		N_{340}	
10	N_{360}		N_{380}	
11	$(dN/d\Omega)_{312}$		$(dN/d\Omega)_{317}$	
12	$(dN/d\Omega)_{331}$		$(dN/d\Omega)_{340}$	
13	$SENS_{360}$		Reflectivity	
14	Total Ozone		Error Flag	
15	$(dN/dR)_{312}$	$(dN/dR)_{317}$	$(dN/dR)_{331}$	$(dN/dR)_{340}$
16	$(dN/dR)_{360}$	$(dN/dR)_{380}$	THIR cloud pressure	Terrain pressure
17	$RES(N_{331})$	$RES(N_{317})$	$RES(N_{331})$	$RES(N_{340})$
18	$RES(N_{360})$	Ozone Below Cloud	SOI	Cloud pressure
19	Algorithm Flag	Eff. Cloud Fraction	Mixing Fraction	Surface Category
20-523	Same as 6 through 19 for samples 2 to 35			
524-525	Spares			

Notes:

All values are stored in INTEGER format, MSB first. Values stored in one byte are always positive, with a value of 255 indicating missing data. Values stored in two bytes can be either positive or negative, with values of 32767 indicating missing data. Some values have had constants added or multiplied to accommodate integer storage.

Table 8.8. Detailed Descriptions

Word	Bytes	Description
1		Orbit number, starting at ascending node
2		Greenwich Mean Time at start of scan in seconds (1–86,400)
3	1–2	Sequence number of record in file
	3–4	Flag for chopper non-synchronization:
		0 Does not occur in current or next scan
		1 Occurs in current scan, not in next
		2 Occurs in next scan, not current
		3 Occurs in current and next scan
4	1–2	Day of the (1–366) at start of scan
	3–4	Year at start of scan (4 digits)
5	1–2	Spacecraft altitude in kilometers at start of scan

Table 8.8. Detailed Descriptions (Continued)

Word	Bytes	Description
	3–4	Sample 1 view angle can be used to calculate the nominal spacecraft roll error and the 35 view angles within each scan. The view angle is the angle between the FOV local normal vector and the vector from the FOV to the spacecraft. The relationship between roll angle and the 35 view angles in a scan is given by

$$V_n^* \;=\; V_n + \; \frac{r_e + h_s}{r_e} \frac{\cos(S_n)}{\cos(V_n)} \; \Delta R$$

		where V_n^* is the actual view angle for sample number n, V_n is the nominal view angle for sample n (given in the orbital summary trailer record), S_n is the nominal scan angle for sample number n, ΔR is the roll angle, r_e is the radius of the earth (6,380 km), h_s is the height of the satellite (955 km). The scan angle is the angle between the vectors from the S/C to the local normal and from the S/C to the FOV, and ranges in 3-degree steps from 51 degrees at sample 1 to 0 degrees at nadir back to 51 degrees at sample 35.
6	1–2	IFOV latitude, from 90° S–90° N, in degrees x 100
	3–4	IFOV longitude, from 180° W–180° E, in degrees x 100
7	1–2	IFOV solar zenith angle, in degrees x 100
	3–4	Angle φ between sun and satellite measured at IFOV, in degrees x 100
8	1–2	213 nm N-value x 50 (N-value is defined in Section 4.5)
	3–4	317 nm N-value x 50
9	1–2	331 nm N-value x 50
	3–4	340 nm N-value x 50
10	1–2	360 nm N-value x 50
	3–4	380 nm N-value x 50
11	1–2	312 nm sensitivity $dN/d\Omega$, in $(matm\text{-}cm)^{-1}$ x 10,000
	3–4	317 nm sensitivity $dN/d\Omega$, in $(matm\text{-}cm)^{-1}$ x 10,000
12	1–2	331 nm sensitivity $dN/d\Omega$, in $(matm\text{-}cm)^{-1}$ x 10,000
	3–4	340 nm sensitivity $dN/d\Omega$, in $(matm\text{-}cm)^{-1}$ x 10,000
13	1–2	360 nm sensitivity $dN/d\Omega$, in $(matm\text{-}cm)^{-1}$ x 10,000
	3–4	Effective Reflectivity, in percent x 100
14	1–2	Total Ozone, in matm-cm x 10
14	3–4	Error Flag (flag = flag + 10 for data taken during descending, N–S, orbit):
		0 (10) good data
		1 (11) good data, 84° < SZA < 88°
		2 (12) pair residue too large
		3 (13) triplet residue too large:
		use: 318 and 331 nm for A-triplet
		331 and 340 nm for B-triplet
		318 and 340 nm for C-triplet
		4 (14) SOI flag set (SO_2 is present)
		5 (15) fatal: set when the absolute value of any residue is larger than 12.5; ozone and SOI set to fill values
15	1	312 nm dN/dR (reflectivity sensitivity), in $percent^{-1}$ x –50
	2	317 nm dN/dR, in $percent^{-1}$ x –50
	3	331 nm dN/dR, in $percent^{-1}$ x –50
	4	340 nm dN/dR, in $percent^{-1}$ x –50
16	1	360 nm dN/dR, in $percent^{-1}$ x –50
	2	380 nm dN/dR, in $percent^{-1}$ x –50
	3	Cloud pressure measured by THIR, where available, in atm x 100
	4	Terrain pressure, in atm x 100
17	1	312 nm residue x 10 + 127

41

Table 8.8. Detailed Descriptions (Continued)

Word	Bytes	Description
	2	317 nm residue x 10 + 127
	3	331 nm residue x 10 + 127
	4	340 nm residue x 10 + 127
18	1	360 nm residue x 10 + 127
	2	Amount of ozone added below cloud layer, in matm-cm
	3	SOI, in matm-cm + 50
	4	Pressure derived from ISCCP cloud climatology, in atm x 100
19	1	Algorithm flag (flag = flag + 10 for snow assumed present):
		1 (11) A-triplet used
		2 (12) B-triplet used
		3 (13) B-triplet used with profile selection
		4 (14) C-triplet used with profile selection
	2	Effective cloud fraction x 100
	3	Profile mixing fraction x 10:
		$1 < f_p < 2$ profile between low and mid latitudes
		$2 < f_p < 3$ profile between low and mid latitudes
	4	Surface category code:
		0 water
		1 land
		2 low inland (below sea level)
		3 land and water
		4 land and low-inland
		5 water, land and low-inland
20–523		Same as 6–19 for samples 2–35
523–525		Spares

Table 8.9. Format of Orbital Summary Record

Word	Description
1	Orbit number
2	GMT (seconds) of first scan of orbit
3	Negative logical sequence number (2 most significant bytes)[*]
4	Day of year of first scan of orbit
5	Year of first scan of orbit (4 digits)
6	Latitude (90˚ S–90˚ N) for first scan, nadir view (degrees x 100)
7	Longitude (180˚ W–180˚ E) for first scan, nadir view (degrees x 100)
8	GMT (seconds) of last scan of orbit
9	Day of year of last scan of orbit
10	Year of last scan of orbit (4 digits)
11	Latitude (90˚ S–90˚ N) for last scan, nadir view (degrees x 100)
12	Longitude (180˚ W–180˚ E) for last scan, nadir view (degrees x 100)
13	Local time (seconds) at equator crossing (or –77 if unavailable)
14	Day of year (local time) at equator crossing
15	Year (local time) at equator crossing
16	GMT (seconds) at equator crossing (or –77 if unavailable)
17	Day of year (GMT) at equator crossing
18	Year (GMT) at equator crossing
19	Longitude at equator crossing (or –77777 if unavailable), nadir view (degrees x 100)
20	Altitude (km) at last scan
21	Number of input/output errors for this orbit

Table 8.9. Format of Orbital Summary Record (Continued)

Word	Description
22	Number of scans read for orbit\
23	Number of scans written for orbit
24	Number of samples out of range (total)
	Number of samples out of range for:
25	Zenith angle > 88 degrees
26	Latitude out of range (> 90 degrees)
27	Counts negative
28	Number of bad samples written: algorithm flag not 0, 1, 10, or 11 (total)
29–34	Counts of error flags for Algorithm Flag = 1 (see data record for description of error flags):
29	number of samples that had error flag = 0 or 10
30	number of samples that had error flag = 1 or 11
31	number of samples that had error flag = 2 or 12
32	number of samples that had error flag = 3 or 13
33	number of samples that had error flag = 4 or 14
34	number of samples that had error flag = 5 or 15
35–40	Same as 29–34 for Algorithm Flag = 2
41–46	Same as 29–34 for Algorithm Flag = 3
47–52	Same as 29–34 for Algorithm Flag = 4
53	Minimum ozone for orbit.
54	Maximum ozone for orbit.
55–60	The six instrument wavelengths.
61–66	Solar irradiance F-values at 1 AU (watts/cm^3) for current day at the six instrument wavelengths, shortest first.
67–90	Calibration constants: The counts to radiance conversion factors, in units of watts/cm^3/steradian/count, given for each of the four gain ranges for each of the six wavelengths in order: words 63–66, 312 nm; ...; words 83–86, 380 nm.
91–127	Nominal spacecraft zenith angle (0–80 degrees) at each scan position.

* Notes: The logical sequence number is a 16-bit integer that occupies the left half (two most significant bytes) of word 3. Words 53–127 are stored in IEEE-754 32-bit floating-point format (REAL*4); all others are 4-byte (32-bit) integer format with the most significant byte first.

Table 8.10. Format of Trailer Record

Word	Description
1	Orbit number of last scan
2	GMT (seconds) of first scan of last orbit of day
3	Logical sequence number (= –1) (2 most significant bytes)[*]
4	Day of year of first scan of last orbit of day
5	Year of first scan of last orbit of day
6	Latitude (90˚ S–90˚ N) for first scan, nadir view (degrees x 100)
7	Longitude (180˚ W–180˚ E) for last scan, nadir view (degrees x 100)
8	GMT (seconds) of last scan of last orbit of day
9	Day of year of last scan of last orbit of day
10	Year of last scan of last orbit of day
11	Latitude (90˚ S–90˚ N) for first scan, nadir view (degrees x 100)
12	Longitude (180˚ W–180˚ E) for last scan, nadir view (degrees x 100)
13	Total number of input/output errors
14	Total number of scans read
15	Total number of scans written

Table 8.10. Format of Trailer Record (Continued)

Word	Description
16	Total number of good samples written
17	Total number of samples out of range
	Total number of samples out of range for:
18	Zenith angle > 85.7 degrees
19	Latitude out of range (absolute value > 90 degrees)—normally zero
20	Counts out of range (negative)
21	Number of samples written that were bad: algorithm flag not 0, 1, 10, or 11 (total)
22–27	Totals of error flag counts for algorithm flag = 1:
22	Total number of samples that had error flag = 0 to 10
23	Total number of samples that had error flag = 1 to 11
24	Total number of samples that had error flag = 2 to 12
25	Total number of samples that had error flag = 3 to 13
26	Total number of samples that had error flag = 4 to 14
27	Total number of samples that had error flag = 5 to 15
28–33	Same as 22–27 for Algorithm Flag = 2
34–39	Same as 22–27 for Algorithm Flag = 3
40–45	Same as 22–27 for Algorithm Flag = 4
46–525	Spare

* The trailer record identifier (= –1) is a 16-bit integer that occupies the left half (two most significant bytes) of word 3. All other values are stored as 4-byte integers, MSB first.

8.2.2   CDTOMS (Level–3 Data Product)

The CDTOMS Level–3 product contains global total ozone on a fixed 1-degree latitude by 1.25-degree longitude grid. It is available at URL ftp://jwocky.gsfc.nasa.gov/pub/nimbus7/ or in the form of CD–ROMs. Except for some changes in the header line, the Version 7 Level–3 product is identical to the Nimbus–7/TOMS Version 6 CD–ROM product and the CDTOMS ozone product that was available by ftp.

One global grid is stored in each CDTOMS file. The first three lines in a CDTOMS daily grid file contain header information:

 a) the date of observations (line 1; characters 2–22),
 b) the processing version (line 1; characters 24–37),
 c) the satellite/instrument name (line 1; characters 39–51),
 d) the product name (line 1; 53–57),
 e) local time of the ascending node equator crossing (line 1; characters 62–79), and
 f) a description of the grid (lines 2 and 3).

Table 8.11 provides a detailed description of the first line of a daily grid file. The remaining lines contain the gridded ozone values, stored as 3-digit integers in units of matm-cm. Each of the 180 latitude zones requires 12 lines. They are ordered from south to north with the first zone centered at –89.5 degrees. Within each latitude zone, values are given for each of 288 longitude zones from 180° W through 0° (Greenwich) to 180° E. The first longitude zone is centered at –179.375 degrees. As shown in Figure 8.1an annotation is present after all values are given for a latitude zone. Zeroes denote flagged data; that is data that could not be collected due to lack of sunlight or other problems.

Figure 8.1 shows an example of the header and the first two latitude zones in a CDTOMS daily file

Table 8.11. Format of Header Line of CDTOMS Daily Grid

Character	Contents
1	ASCII blank (HEX 20)
2–5	"Day:" (quotes indicate fixed content)
6	ASCII blank
7–9	day of year
10	ASCII blank
11–13	month ("Jan," "Feb," "Mar" ...)
14	ASCII blank
15–16	day of month
17	","
18	ASCII blank
19–22	year
23	ASCII blank
24–37	"Production V07"
38	ASCII blank
39–51	"NIMBUS–7/TOMS"
52	ASCII blank
53–57	"OZONE"
58–61	ASCII blanks
62–70	"Asc LECT:"
71	ASCII blank
72–73	hour (local) of ascending node equator crossing
74	ASCII blank
75–76	minute (local) of ascending node equator crossing
77	ASCII blank
78–79	"AM" or "PM" indicating morning or afternoon/evening ascending node equator crossing
80	ASCII blank
81<	If > (line feed character; i.e., HEX 0A)

```
Day: 289 Oct 15, 1980 Production V70 NIMBUS-7/TOMS OZONE   Asc LECT: 11:51 AM
Longitudes:  288 bins centered on 179.375 W to 179.375 E  (1.25 degree steps)
Latitudes :  180 bins centered on  89.5   S to  89.5   N  (1.00 degree steps)
208208208208208208208208208207207207207207207207207207207207207207207207207213
213213213213213213213213213213213213214214214214214214214214214214214214214214
214214205205205205205205205205205205205205205205205205205205205205205205205205
205205205205205205205205205205205205205205205205205205205205205205205205205205
208208208208208208208208208208208208208208208208208208208208208208208208208208
208208208208208208208214214214214214214214214214214214214214214214214214214214
214214214214214214214214214214214214214214214214214214214214214214214214214214
214214214214214215215215215212212212212208208208208208208208208208208208208208
208208208208208208208208208208208208208208208208208209209209209209209209209209
209209209209217217217217217217217217217217217217217217217217217217211211211211
211211211211211208208208208208208208208208208208208208208208208208208208208208
208208208208208208208208208208208208208   lat =  -89.5
205205205205205205205205205205205205205206206206206207207207207208208208208207
207207207207207207207207207207207207207207207207207207207207207210210210210210
210210210210210210210210210210210210210210205205205205206206206206207207207207
207207207207207207207207207207207212212212212212212212212211211211211211211211
210210210210210210210210210209209209209209209209209209209209209209209209209209
209209209209209209209209209209209209209209209209209209208208208208208208208208
208208208208208208208208208208208208208208208208208208208214214214214214214214
214214214214214214214214214212212212212214214214214213213213213213213213213213
213213213213213213213213217217217217216216216216215215215215214214214214214217
217217217215215215215214214214214214214214214214214214214214214214214214214214
214214212212212212212212212212212212212212212212212215215215215205205205205205
205205205205205205205205205205205205205   lat =  -88.5
```

Figure 8.1. Sample CDTOMS Daily Grid File Excerpt

REFERENCES

Ahmad, Z. and P. K. Bhartia, 1995, "Effect of Molecular Anisotropy on the Backscattered UV Radiance," submitted to *Applied Optics*.

Bhartia, P. K., J. R. Herman, R. D. McPeters, and O. Torres, 1993, "Effect of Mount Pinatubo Aerosols on Total Ozone Measurements From Backscatter Ultraviolet (BUV) Experiments," *J. Geophys. Res.*, *98*, 18547–18554.

Bluth, G. J. S., S. D. Doiron, C. C. Schnetzler, A. J. Krueger, and L. S. Walter, 1992, "Global Tracking of the SO_2 Clouds From the June 1991 Mount Pinatubo Eruptions," *Geophys. Res. Lett., 19*, 151–154.

Bluth, G. J. S., S. D. Doiron, C. C. Schnetzler, A. J. Krueger, and L. S. Walter, 1993, "New Constraints on Sulfur Dioxide Emissions From Global Volcanism," *Nature*, 366, 327–329.

Cebula, R. P., H. Park, and D. F. Heath, 1988, "Characterization of the Nimbus–7 SBUV Radiometer for the Long-Term Monitoring of Stratospheric Ozone," *J. Atm. Ocean. Tech., 5*, 215–227.

Chu, W. P., M. P. McCormick, J. Lenoble, C. Brogniez, and P. Pruvost, 1989, "SAGE II Inversion Algorithm," J. Geophys. Res., *94*, 8339–8351.

Dave, J. V., 1964, "Meaning of Successive Iteration of the Auxiliary Equation of Radiative Transfer," *Astrophys. J., 140*, 1292–1303.

Dave, J. V., 1978, "Effect of Aerosols on the Estimation of Total Ozone in an Atmospheric Column From the Measurement of its Ultraviolet Radiance," *J. Atmos. Sci.*, *35*, 899–911.

Environmental Science Services Administration, National Aeronautics and Space Administration, and United States Air Force, 1966, *U. S. Standard Atmosphere Supplements*, U.S. Government Printing Office, Washington, DC.

Fleig, A. J., K. F. Klenk, P. K. Bhartia, and D. Gordon, 1982, "User's Guide for the Total Ozone Mapping Spectrometer (TOMS) Instrument First Year OZONE-T Data Set," *NASA Reference Publication 1096*, National Aeronautics and Space Administration, Washington, DC.

Fleig, A. J., D. F. Heath, K. F. Klenk, N. Oslik, K. D. Lee, H. Park, P. K. Bhartia, and D. Gordon, 1983, "User's Guide for the Solar Backscattered Ultraviolet (SBUV) and the Total Ozone Mapping Spectrometer (TOMS) RUT-S and RUT-T Data Sets, October 31, 1978 to November 1, 1980," *NASA Reference Publication 1112*, National Aeronautics and Space Administration, Washington, DC.

Fleig, A. J., P. K. Bhartia, C. G. Wellemeyer, and D. S. Silberstein, 1986, "Seven Years Of Total Ozone From the TOMS Instrument—A Report on Data Quality," *Geophys. Res. Lett., 13*, 1355–1358.

Fleig, A. J., D. S. Silberstein, C. G. Wellemeyer, R. P. Cebula, and P. K. Bhartia, 1988, "An Assessment of the Long–Term Drift in TOMS Total Ozone Data, Based on Comparison with the Dobson Network," *Geophys Res. Lett.*, *15*, 1133–1136.

Heath, D. F., A. J. Krueger, H. R. Roeder, and B. D. Henderson, 1975, "The Solar Backscatter Ultraviolet and Total Ozone Mapping Spectrometer (SBUV/TOMS) for Nimbus G," *Opt. Eng., 14*, 323–331.

Heath, D. F., and H. Park, 1978, "The Solar Backscatter Ultraviolet (SBUV) and Total Ozone Mapping Spectrometer (TOMS) Experiment," in *The Nimbus–7 Users' Guide*, edited by C. R. Madrid, 175–211, NASA Goddard Space Flight Center, Greenbelt, MD.

Heath, D. F., and B. Schlesinger, 1986, "The Mg 280-nm Doublet as a Monitor of Changes in the Solar Ultraviolet Irradiance," *J. Geophys. Res., 91*, 8672–8682.

Herman, J. R., R. Hudson, R. McPeters, R. Stolarski, Z. Ahmad, X.-Y. Gu, S. Taylor, and C. Wellemeyer, 1991, "A New Self-Calibration Method Applied to TOMS/SBUV Backscattered Ultraviolet Data to Determine Long-Term Global Ozone Change," *J. Geophys. Res., 96*, 7531–7545.

Hilsenrath, E., R.P. Cebula, M. T. DeLand, K. Laamann, S. Taylor, C. Wellemeyer, and P. K. Bhartia, 1995, "Calibration of the NOAA–11 Solar Backscatter Ultraviolet (SBUV/2) Ozone Data Set From 1989 to 1983 Using In-Flight Calibration Data and SSBUV," *J. Geophys. Res., 100*, 1351–1366.

Ilg, D., F. Baker, and M. Folk, 1993, "HDF Specification and Developer's Guide, Version 3.2," National Center for Supercomputing Applications, Champaign, IL.

Inn, E. C. Y., and Y. Tanaka, 1959, "Ozone Chemistry and Technology," ACS Appl. Publ. American Chemical Society, Washington DC, 263–268.

Joiner, J., P. K. Bhartia, R. P. Cebula, E. Hilsenrath, and R. D. McPeters, 1995, "Rotational Raman Scattering (Ring Effect) in Satellite Backscatter Ultraviolet Measurements," *Applied Optics*, *34*, 4513-4525.

REFERENCES (Continued)

Kalman, L., 1994,"HDF Reference Manual, Version 3.3," National Center for Supercomputing Applications, Champaign, IL.

Klenk, K. F., P. K. Bhartia, A. J. Fleig, V. G. Kaveeshwar, R. D. McPeters, and P. M. Smith, 1982, "Total Ozone Determination From the Backscattered Ultraviolet (BUV) Experiment," *J. Appl. Meteorol., 21*, 1672–1684.

Klenk, K. F., P. K. Bhartia, E. Hilsenrath, and A. J. Fleig, "Standard Ozone Profiles From Balloon and Satellite Data Sets,"*J. Climate Appl. Meteorol.*, *22*, 2012–2022, 1983.

Krueger, A. J., 1983, Sighting of El Chichon Sulfur Dioxide Clouds With the Nimbus–7 Total Ozone Mapping Spectrometer. Science, 220, 1377–1378, 1983.

Krueger, A.J., L.S. Walter, P.K. Bhartia, C.C. Schnetzler, N.A. Krotkov, I. Sprod, and G.J.S. Bluth, 1995, Volcanic Sulfur Dioxide Measurements from the Toal Ozone Mapping Spectrometer Instruments, J. Geophys. Res., 100, 14057–14076.

McPeters, R. D., D. F. Heath, and B. M. Schlesinger, 1984, "Satellite Observation of SO_2 from El Chichón: Identification and Measurement," *Geophys. Res. Lett., 11*, 1203–1206.

McPeters, R., and W. D. Komhyr, 1991, "Long-Term Changes in the Total Ozone Mapping Spectrometer Relative to World Primary Standard Dobson Spectrometer 83," *J. Geophys. Res., 96*, 2987–2993.

McPeters, R., D., A. J. Krueger, P. K. Bhartia, J. R. Herman, A. Oakes, Z. Ahmad, R. P. Cebula, B. M. Schlesinger, T. Swissler, S. L. Taylor, O. Torres, and C. G. Wellemeyer, 1993, "Nimbus–7 Total Ozone Mapping Spectrometer (TOMS Data Products User's Guide," *NASA Reference Publication, 1323*, National Aeronautics and Space Administration, Washington, DC.

National Aeronautics and Space Administration, 1984, "Third and Fourth Year Addendum to the User's Guide for the Total Ozone Mapping Spectrometer (TOMS) Instrument First Year Ozone-T Data Set," Goddard Space Flight Center, Greenbelt, MD.

National Aeronautics and Space Administration, 1986, "Nimbus–7 Solar Backscattered Ultraviolet and Total Ozone Mapping Spectrometer (SBUV/TOMS) GRIDTOMS Tape Specifications," Goddard Space Flight Center, Greenbelt, MD.

National Center for Supercomputing Applications, 1994, "Hierarchical Data Format," http://www.ncsa.uiuc.edu/SDG/software/HDF/HDFIntro.html, hypertext file.

Paur, R. J., and A. M. Bass, 1985, "The Ultraviolet Cross-Sections of Ozone: II. Results and Temperature Dependence," *Atmospheric Ozone*, edited by C.S. Zerefos and A. Ghazi, 611–616, D. Reidel, Dordrecht.

Schlesinger, B. M., and R.P. Cebula, 1985, "Solar Variation 1979–1987 Estimated From an Empirical Model For Changes With Time in the Sensitivity of the Solar Backscatter Ultraviolet Instrument," *J. Geophys. Res., 97*, 10,199–10,134.

Torres, O., Z. Ahmad, and J. R. Herman, 1992, "Optical Effects of Polar Stratospheric Clouds on the Retrieval of TOMS Total Ozone," *J. Geophys. Res., 97*, 13,015–13,024.

Torres, O., and P. K. Bhartia, 1995, "Effect of Stratospheric Aerosol on Ozone Profile From BUV Measurements," *Geophys. Res. Lett.*, *22*, 235–238.

Torres, O., J. R. Herman, P. K. Bhartia, and Z. Ahmad, 1995, "Properties of Mount Pinatubo Aerosols as Derived From Nimbus–7 Total Ozone Mapping Spectrometer Measurements," *J. Geophys. Res., 100*, 14,043–14,055.

Watson, R. T., and Ozone Trends Panel, M. J. Prather and Ad Hoc Theory Panel, and M. J. Kurylo and NASA Panel for Data Evaluation, 1988, "Present State of Knowledge of the Upper Atmosphere 1988; An Assessment Report," *NASA Reference Publication 1208*, 33–47.

Wellemeyer, C. G., S. L. Taylor, G. Jaross, M. T. DeLand, C. J. Seftor, G. Labow, T. J. Swissler, and R. P. Cebula, 1996, "Final Report on Nimbus–7 TOMS Version 7 Calibration,"*NASA Contractor Report ###-####*, National Aeronautics and Space Administration, Washington, DC.

Willson, R. C., H. S. Hudson, C. Frohlich, and R. W. Brusa, 1986, "Long-Term Downward Trend In Solar Irradiance,"*Science, 234*, 1114–1117.

Woods, T. N., *et al.*, 1996, "Validation of the UARS Solar Ultraviolet Irradiance: Comparison With the Atlas 1–2 Measurements," *J. Geophys. Res.*, in press.

RELATED LITERATURE

Bates, D. R., 1984, "Rayleigh Scattering by Air," *Planet. Sp. Sci., 32,* 785–790.

Bhartia, P. K., K. F. Klenk, D. Gordon, and A. J. Fleig, "Nimbus–7 total Ozone Algorithm," 1983, *Proceedings, 5th Conference on Atmospheric Radiation,* American Meteorological Society, Baltimore, MD.

Bhartia, P. K., K. F. Klenk, C. K. Wong, D. Gordon, and A. J. Fleig, 1984, "Intercomparison of the Nimbus–7 SBUV/TOMS Total Ozone Data Sets With Dobson and M83 Results," *J. Geophys. Res., 89,* 5239–5247.

Bhartia, P. K., D. Silberstein, B. Monosmith, and Albert J. Fleig, 1985, "Standard Profiles of Ozone From Ground to 60 km Obtained by Combining Satellite and Ground Based Measurements," *Atmospheric Ozone,* edited by C. S. Zerefos and A. Ghazi, 243–247, D. Reidel, Dordrecht.

Bowman, K. P., 1986, "Interannual Variability of Total Ozone During the Breakdown of the Antarctic Circumpolar Vortex," *Geophys. Res. Lett., 13,* 1193–1196.

Bowman, K. P. and A. J. Krueger, 1985, "A Global Climatology of Total Ozone From the Nimbus–7 Total Ozone Mapping Spectrometer," *J. Geophys. Res., 90,* 7967–7976.

Bowman, K. P., 1988, "Global Trends in Total Ozone," *Science, 239,* 48–50.

Chandra, S., 1986, "The Solar and Dynamically Induced Oscillations in the Stratosphere," *J. Geophys. Res., 91,* 2719–2734.

Chandra, S., 1993, "Changes in Stratospheric Ozone and Temperature Due to the Eruption of Mt. Pinatubo," *Geophys. Res. Lett.,* 20, 33–36.

Chandra, S., and R. S. Stolarski, 1991, "Recent Trends In Stratospheric Total Ozone: Implications of Dynamical and El Chichón Perturbation," *Geophys. Res. Lett., 18,* 2277–2280.

Dave, J. V., 1965, "Multiple Scattering in a Non-Homogeneous, Rayleigh Atmosphere," *J. Atmos. Sci., 22,* 273–279.

Dave, J. V., and Carlton L. Mateer, 1967, "A Preliminary Study on the Possibility of Estimating Total Atmospheric Ozone From Satellite Measurements," *J. Atmos. Sci., 24,* 414–427.

Eck, T. F., P. K. Bhartia, P. H. Hwang and L. L. Stowe, 1987, "Reflectivity of Earth's surface and Clouds in Ultraviolet From Satellite Observations," *J. Geophys. Res., 92,* 4287–4296.

Fraser, R. S., and Z. Ahmad, 1978, "The Effect Of Surface Reflection and Clouds on the Estimation of Total Ozone From Satellite Measurements." Fourth NASA Weather and Climate Program Science Review, *NASA Conf. Publ. 2076,* 247–252, National Aeronautics and Space Administration, Washington, DC, [NTIS N7920633].

Fleig, A. J., P. K. Bhartia, and David S. Silberstein, 1986, "An Assessment of the Long-Term Drift in SBUV Total Ozone Data, Based on Comparison With the Dobson Network," *Geophys. Res. Lett., 13,* 1359–1362.

Fleig, A. J., R. D. McPeters, P. K. Bhartia, Barry M. Schlesinger, Richard P. Cebula, K. F. Klenk, Steven L. Taylor, and D. F. Heath, 1990, "Nimbus–7 Solar Backscatter Ultraviolet (SBUV) Ozone Products User's Guide," *NASA Reference Publication, 1234,* National Aeronautics and Space Administration, Washington, DC.

Fleig, A. J., D. S. Silberstein, R. P. Cebula, C. G. Wellemeyer, P. K. Bhartia, and J. J. DeLuisi, 1989, "An Assessment of the SBUV/TOMS Ozone Data Quality, Based on Comparison With External Data," *Ozone in the Atmosphere, Proceedings of the Quadrennial Ozone Symposium 1988 and Tropospheric Ozone Workshops,* edited by R. D. Bojkov and P. Fabian, 232–237, A. Deepak, Hampton, VA.

Gleason, J. F., P. K. Bhartia, J. R. Herman, R. McPeters, P. Newman, R. S. Stolarski, L. Flynn, G. Labow, D. Larko, C. Seftor, C. Wellemeyer, W. D. Komhyr, A. J. Miller, and W. Planet, 1993, "Record Low Global Ozone in 1992," *Science, 260,* 523–526.

Heath, D. F., 1988, "Non-Seasonal Changes in Total Column Ozone From Satellite Observations," 1970–1986, *Nature, 332,* 219–227.

Heath, D. F., 1990, "Changes in the Vertical Distribution of Stratospheric Ozone and the Associated Global Scale Changes in Total Ozone From Observations With the Nimbus–7 SBUV Instrument; 1978-1986," *Proceedings of the International Ozone Symposium 1988 and Tropospheric Ozone Workshops,* edited by R. Bojkov and P. Fabian, 810, A. Deepak, Hampton, VA.

Herman, J. R., R. D. Hudson, and G. Serafino, 1990, "Analysis of the Eight-Year Trend in Ozone Depletion From Empirical Models of Solar Backscattered Ultraviolet Instrument Degradation," *J. Geophys. Res., 95,* 7403–7416.

Herman, J. R., R. McPeters, R. Stolarski, D. Larko, and R. Hudson, 1991, "Global Average Ozone Change From November 1978 to May 1990," *J. Geophys. Res., 96,* 17,279–17,305.

Herman, J. R., R. McPeters, and D. Larko, 1993, "Ozone Depletion at Northern and Southern Latitudes Derived From January 1979 to December 1991 Total Ozone Mapping Spectrometer Data," *J. Geophys. Res., 98,* 12,783–12,793.

RELATED LITERATURE (Continued)

Herman, J. R. and D. Larko, 1993, "Global Ozone Change As A Function of Latitude and Longitude: January 1979 to December 1991," submitted to *J. Geophys. Res.*

Herman, J. R., D. Larko, 1994, "Nimbus–7/TOMS-November 1, 1978 to May 6, 1993: Low Ozone Amounts During 1992–1993 From Nimbus–7 and Meteor–3 Total Ozone Mapping Spectrometer," *J. Geophys. Res.*, *99*, 3483–3496.

Hudson, R. D., J. R. Herman, and G. Serafino, 1989, "On the Determination of Long-Term Trends From SBUV Ozone Data," *Ozone in the Atmosphere, Proceedings of the Quadrennial Ozone Symposium 1988 and Tropospheric Ozone Workshops*, edited by R. Bojkov and P. Fabian, 189–192. A. Deepak, Hampton, VA.

Klenk, K. F., 1980, "Absorption Coefficients of Ozone for the Backscatter UV Experiment," *Applied Optics, 19,* 236–242.

Komhyr, W. D., R. D. Grass, and R. K. Leonard, 1989, "Total Ozone, Ozone Vertical Distributions, and Stratospheric Temperatures at South Pole, Antarctica, in 1986 and 1987," *J. Geophys. Res., 94*, 11,429–11,436.

Krueger, A. J., M. R. Schoeberl, and R. S. Stolarski, 1987, "TOMS Observations of Total Ozone in the 1986 Antarctic Spring," *Geophys. Res. Lett., 14*, 527–530.

Larko, D. E., L. W. Uccellini, and A. J. Krueger, 1986, "Atlas of TOMS Ozone Data Collected During the Genesis of Atlantic Lows Experiment (GALE)" *NASA-TM-87809,* 99 pp.

Lienesch, J. H. and P. K. K. Pandey, 1985, "The Use of TOMS Data in Evaluating And Improving The Total Ozone from TOVS Measurements," *Rep. NOAA-TR-NESDIS-23, Issue 22*, 3814–3828.

Logan, J. A., 1985, "Tropospheric Ozone: Seasonal Behavior, Trends, and Anthropogenic Influence," *J. Geophys. Res., 90*, 10,463–10,482.

Pommereau, J. P., F. Goutail, H. LeTexier, and T. S. Jorgensen, 1989, "Stratospheric Ozone and Nitrogen Dioxide Monitoring at Southern and Northern Polar Latitudes," *Our Changing Atmosphere, Proceedings of the 28th Liege International Astrophysical Colloquium*, edited by P. Crutzen. J.-C. Gerard, and R. Zander, University de Liege, Liege, Belgium.

Schoeberl, M. R., A. J. Krueger, and P. A. Newman, 1986, "The Morphology of Antarctic Total Ozone as Seen by TOMS—Total Ozone Mapping Spectrometer," *Geophys. Res. Lett., 13*, 1217–1220.

Schoeberl, M. R., P. K. Bhartia, E. Hilsenrath, and O. Torres, 1993, "Tropical Ozone Loss Following the Eruption of Mt. Pinatubo," *Geophys. Res. Lett., 20*, 29–32.

Solomon, S., 1990, "Antarctic Ozone: Progress Towards a Quantitative Understanding," *Nature, 347*, 347–354.

Stolarski, R. S., A. J. Krueger, M. R. Schoeberl, R. D. McPeters, P. A. Newman, and J. C. Alpert, 1986, "Nimbus–7 Satellite Measurements of the Springtime Antarctic Ozone Decrease," *Nature, 322*, 808–811.

Stolarski, R. S., 1992, "Observations of Global Stratospheric Ozone Change," *Ber. Bunsen Ges. Phys. Chem., 96,* 258–263.

Stolarski, R. S., P. Bloomfield, R. D. McPeters, and J. R. Herman, 1991, "Total Ozone Trends Deduced From Nimbus–7 TOMS Data," *Geophys. Res. Lett., 18*, 1015–1018.

Stolarski, R. S., L. Bishop, R. Bojkov, M. L. Chanin, V. Fioletev, V. Kircchoff, J. Zawodny, and C. Zerefos, 1992, "Ozone and Temperature Trends," in Scientific Assessment of Ozone Depletion; 1991, *WMO Rep. 25*, 2.1–2.30, World Meteorol. Organ., Geneva.

Stolarski, R. S., R. Bojkov, L. Bishop, C. Zerefos, J. Staehelin, and J. Zawodny, 1992, "Measured Trends in Stratospheric Ozone," *Science, 256*, 342–349.

Vigroux, Ernest, 1953, "Contribution a l'Etude Experimental de l'Aabsorption de l'Ozone," *Ann. Phys., Ser. 12, 8*, 709–762.

Vigroux, E., 1967, "Determination des Coefficients Moyen d'Absorption de l'Ozone en vue des Observations Concernant L'ozone Atmospherique a l'Aide Du Spectrometre Dobson," *Ann. Phys., Ser. 14, 2*, 209–215.

Watson, R. T., and Ozone Trends Panel, 1990, "Report of the International Ozone Trends Panel 1988," *Rep. 18.* Global Ozone Res. and Monit. Proj., World Meteorol. Organ., Geneva.

Wellemeyer, C. G., A. J. Fleig, and P. K. Bhartia, 1989, "Internal Comparisons of SBUV and TOMS Total Ozone Measurements," *Ozone in the Atmosphere, Proceedings of the International Ozone Symposium and Tropospheric Ozone Workshops*, edited by R. Bojkov and P. Fabian, 193–197, A. Deepak, Hampton, VA.

Wellemeyer, C. G., S. L. Taylor, R. R. Singh, and R. D. McPeters, 1992, "External Comparisons Of Reprocessed SBUV/TOMS Ozone Data," *Ozone in the Troposphere and Stratosphere, Proceedings of the Quadrennial Ozone Symposium*, edited by R. D. Hudson, 911–914, *NASA Conference Publication 3266,* Greenbelt, MD.

LIST OF ACRONYMS, INITIALS, AND ABBREVIATIONS

ASCII	American Standard Code for Information Interchange
A.U.	Astronomical Unit
CD–ROM	Compact Disk–Read Only Memory
CDTOMS	Compact Disk TOMS Gridded Data
DAAC	Distributed Active Archive Center
D. U.	Dobson Units (= milliatmosphere-centimeters)
EOF	Empirical Orthogonal Functions
ESSA	Environmental Science Services Administration
FOV	Field-of-View
ftp	file transfer protocol
GMT	Greenwich Mean Time
GRIDTOMS	Gridded TOMS Tape
GSFC	Goddard Space Flight Center
HDF	Hierarchical Data Format
HDTOMS	High Density TOMS Tape
IFOV	Instantaneous Field-of-View
ISCCP	International Satellite Cloud Climatology Project
MSB	Most Significant Bit
NASA	National Aeronautics and Space Administration
NCSA	National Center for Supercomputing Applications
NET	Nimbus Experiment Team
netCDF	Network Common Data Form
NIST	National Institute of Standards and Technology
NMC	National Meteorological Center
NOAA	National Oceanic and Atmospheric Administration
NSSDC	National Space Science Data Center
OPT	Ozone Processing Team
PSC	Polar Stratospheric Cloud
RUT	Raw Unit Tape
SAGE	Stratospheric Aerosol and Gas Experiment
SBUV	Solar Backscatter Ultraviolet
SDS	Scientific Data Set
SOI	Sulfur Dioxide Index
SSBUV	Shuttle Solar Backscatter Ultraviolet

LIST OF ACRONYMS, INITIALS, AND ABBREVIATIONS (Continued)

SZA   Solar Zenith Angle

THIR   Temperature-Humidity Infrared Radiometer

TOMS   Total Ozone Mapping Spectrometer

URL   Uniform Resource Locator

UV   Ultraviolet

APPENDIX A STANDARD TEMPERATURE AND OZONE PROFILES

This appendix contains the standard temperature and ozone profiles used in the calculation of radiances discussed in Section 5. The profiles are described as a function of Umkehr layers. The boundaries of the layers, in pressure units, and the location of the midpoints of the layers are given in Table A.1. Table A.2 gives the temperature at the midpoint of each layer, and Table A.3 gives the column ozone, in units of matm-cm, for each layer. The three-digit and one-letter code identifies the total ozone and latitude of the profile. Profiles are provided for three latitude zones: 15 degrees, denoted L for low, 45 degrees, denoted M for mid, and 75 degrees, denoted H for high. The three-digit number is the total ozone, in units of matm-cm.

Table A.1. Umkehr Layers

Umkehr Layer Number	Layer Pressure (mb)	Pressure at Altitude of Midpoint	Layer Midpoint (km)
12	0.000–0.247	–	–
11	0.247–0.495	.350	56.5
10	0.495–0.990	.700	51.0
9	0.990–1.980	1.40	45.5
8	1.980–3.960	2.80	40.2
7	3.960–7.920	5.60	35.2
6	7.920–15.80	11.2	30.4
5	15.80–31.70	22.4	25.8
4	31.70–63.30	44.8	21.3
3	63.30–127.0	89.6	17.0
2	127.0–253.0	179.0	12.5
1	253.0–506.0	358.0	7.9
0	506.0–1013	716.0	2.8

Table A.2. TOMS Version 7 Standard Temperature Profiles

Profile	Umkehr Layer Number										
	0	1	2	3	4	5	6	7	8	9	> 9
225L	283.0	251.0	215.6	200.7	210.7	221.6	231.1	245.3	258.7	267.4	265.4
275L	283.0	251.0	215.9	203.5	211.9	222.5	231.1	245.3	258.7	267.4	265.4
325L	283.0	251.0	216.5	207.0	213.6	223.0	231.1	245.3	258.7	267.4	265.4
375L	283.0	251.0	216.0	210.0	216.0	224.0	231.1	245.3	258.7	267.4	265.4
425L	283.0	251.0	216.0	213.0	217.0	224.5	231.1	245.3	258.7	267.4	265.4
475L	283.0	251.0	216.0	216.0	219.0	225.0	231.1	245.3	258.7	267.4	265.4
125M	237.0	218.0	196.0	191.0	193.0	210.0	227.6	239.4	253.6	263.9	262.6
175M	260.0	228.0	201.7	198.0	202.1	214.3	227.6	239.4	253.6	263.9	262.6
225M	273.0	239.0	213.3	207.5	211.7	219.1	227.6	239.4	253.6	263.9	262.6
275M	273.0	239.0	217.1	212.2	214.9	220.4	227.6	239.4	253.6	263.9	262.6
325M	273.0	239.0	219.1	216.6	217.0	220.8	227.6	239.4	253.6	263.9	262.6
375M	273.0	239.0	220.2	219.0	219.0	221.9	227.6	239.4	253.6	263.9	262.6
425M	273.0	239.0	220.9	220.7	221.0	223.7	227.6	239.4	253.6	263.9	262.6
475M	273.0	239.0	221.5	222.5	222.7	224.4	227.6	239.4	253.6	263.9	262.6
525M	273.0	239.0	222.3	224.8	225.5	225.8	227.6	239.4	253.6	263.9	262.6
575M	273.0	239.0	225.0	227.0	227.0	227.0	227.6	239.4	253.5	263.9	262.6
125H	237.0	218.0	196.0	191.0	193.0	210.0	223.3	237.1	251.6	262.4	265.6
175H	260.0	228.0	201.7	198.0	202.1	214.3	223.3	237.1	251.6	262.4	265.6
225H	260.0	228.0	209.7	208.5	212.5	222.0	228.0	237.1	251.6	262.4	265.6

Table A.2. TOMS Version 7 Standard Temperature Profiles (Continued)

Profile	Umkehr Layer Number										
	0	1	2	3	4	5	6	7	8	9	> 9
275H	260.0	228.0	222.6	223.4	223.8	226.5	231.6	237.1	251.6	262.4	265.6
325H	260.0	228.0	222.6	223.4	223.8	226.5	231.6	237.1	251.5	262.4	265.6
375H	260.0	228.0	222.6	223.4	223.8	226.5	231.6	237.1	251.5	262.4	265.6
425H	260.0	228.0	222.6	223.4	223.8	226.5	231.6	237.1	251.5	262.4	265.6
475H	260.0	228.0	222.6	223.4	223.8	226.5	231.6	237.1	251.5	262.4	265.6
525H	260.0	228.0	222.6	223.4	223.8	226.5	231.6	237.1	251.5	262.4	265.6
575H	260.0	228.0	222.6	223.4	223.8	226.5	231.6	237.1	251.5	262.4	265.6

Table A.3. TOMS Version 7 Standard Ozone Profiles

Profile	Umkehr Layer Number										
	0	1	2	3	4	5	6	7	8	9	> 9
225L	15.0	9.0	5.0	7.0	25.0	62.2	57.0	29.4	10.9	3.2	1.3
275L	15.0	9.0	6.0	12.0	52.0	79.2	57.0	29.4	10.9	3.2	1.3
325L	15.0	9.0	10.0	31.0	71.0	87.2	57.0	29.4	10.9	3.2	1.3
375L	15.0	9.0	21.0	53.0	88.0	87.2	57.0	29.4	10.9	3.2	1.3
425L	15.0	9.0	37.0	81.0	94.0	87.2	57.0	29.4	10.9	3.2	1.3
475L	15.0	9.0	54.0	108.0	100.0	87.2	57.0	29.4	10.9	3.2	1.3
125M	6.0	5.0	4.0	6.0	8.0	31.8	28.0	20.0	11.1	3.7	1.4
175M	8.0	7.0	8.0	12.0	26.0	41.9	33.6	22.3	11.1	3.7	1.4
225M	10.0	9.0	12.0	18.0	44.0	52.1	39.2	24.5	11.1	3.7	1.4
275M	16.0	12.0	15.0	29.0	58.0	63.7	40.6	24.5	11.1	3.7	1.4
325M	16.0	14.0	26.0	45.0	74.7	66.9	41.7	24.5	11.1	3.7	1.4
375M	16.0	16.0	39.0	64.0	85.7	71.1	42.5	24.5	11.1	3.7	1.4
425M	16.0	18.0	54.0	84.0	97.7	71.7	42.9	24.5	11.1	3.7	1.4
475M	16.0	22.0	72.0	107.7	101.0	72.6	43.0	24.5	11.1	3.7	1.4
525M	16.0	26.0	91.0	127.7	108.0	72.6	43.0	24.5	11.1	3.7	1.4
575M	16.0	30.0	110.0	147.7	115.0	72.6	43.0	24.5	11.1	3.7	1.4
125H	9.5	7.0	18.3	7.6	8.2	28.6	22.0	12.4	7.7	2.5	1.2
175H	9.5	8.0	22.8	22.0	26.9	32.3	26.8	15.0	8.0	2.5	1.2
225H	10.0	9.0	27.6	45.7	41.0	35.0	28.8	15.4	8.3	2.9	1.3
275H	14.0	12.0	34.0	66.9	54.2	36.0	28.8	15.4	8.9	3.4	1.4
325H	14.0	15.0	46.8	82.6	65.2	41.7	28.8	17.2	8.9	3.4	1.4
375H	14.0	20.0	61.2	93.8	75.2	45.9	32.5	18.7	8.9	3.4	1.4
425H	14.0	25.0	76.2	104.9	84.2	51.4	35.6	20.0	8.9	3.4	1.4
475H	14.0	32.0	91.0	117.1	93.0	55.8	37.5	20.9	8.9	3.4	1.4
525H	14.0	41.0	107.1	128.1	101.0	60.2	38.2	21.7	8.9	3.4	1.4
575H	14.0	49.0	123.2	142.2	111.0	60.6	38.8	22.5	8.9	3.4	1.4

APPENDIX B. SAMPLE SOFTWARE TO READ HDF OZONE DATA

This appendix provides software that can be used to read the TOMS HDF Level–2 and Level–3 data files. The software is written in C. It is available through the Goddard DAAC.

The program v2hdfread.c can be used to read the TOMS Level–2 HDF file. It is executed using the command `v2hdfread.exe level2-hdf-filename`, where v2hdfread.exe is the compiled version of v2hdfread.c.

Immediately after execution, the program will display the following information:

- File label
- Text: "File description is stored in the file: filedesc.v2"
- (This description may be large.)
- Metadata

The next keystroke will display netCDF-style global attributes.

The next keystroke will display a numbered list of all the SDS's providing the name and dimensions of the SDS corresponding to each number. The user can select any SDS to display by entering its number or can exit the program by entering q. For the selected SDS, the program will display a description of the axis or axes, the physical units, and offsets and scale factors used to convert the values in the HDF data set to physical values. The user can then press q to go back to the SDS list or any other key to browse the data. After the user enters the number of the desired SDS, the following will be displayed:

- For a 1-D SDS: All data
- For a 2-D SDS: Data from five consecutive scans, with the starting scan chosen by the user. The default value is one. The user can then enter a new starting scan number to browse five consecutive scans starting with that number, enter q to return to the SDS list, or any other key to browse the next five consecutive scans. If there are fewer than five scans starting with the selected scan, they will be the only ones displayed.
- For a 3-D SDS: Data from one scan, with data from all wavelengths in a scene in one line. The user can then enter a scan number to browse that scan, enter q to go back to the SDS list, or press any other key to browse the next scan.

The program displays the unscaled data in the HDF file. To display the physical values for an SDS, users will require software to apply the offsets and scale factors shown when the SDS is selected.

```
Program: v2hdfread.c
*******************************************************************/
#include <stdio.h>
#include "hdf.h"
#define maxscan1000
#define maxlen100
#define maxattr20

char *to_strtype(intype)
int intype;
{char *str;
 switch (intype)
 {case DFNT_UINT8:  str="UINT8";  break;
  case DFNT_INT8:  str="INT8";  break;
  case DFNT_INT16: str="INT16"; break;
  case DFNT_INT32: str="INT32"; break;
  case DFNT_FLOAT32: str="FLOAT32"; break;
  otherwise: str="unknown"; break;
 }
```

```
  return(str);
}

main(argc,argv)
int argc;
char *argv[];
{
 FILE *desc;
 int sd_id, sdsid;
 static char *attrname[]=
   {"Quality flag counters (vector of 32)",
    "Six wavelengths nm",
    "Solar irradiance F-values watts/cm^3/AU",
    "Calibration constants (vector of 24) watts/cm^3/steradian/count",
    "Nominal spacecraft zenith angles (vector of 37) (r*4) degrees"
   };
 int ret, num, i, j, k, m;
 char *hdf_file, filelabel[maxlen];
 char filedesc1[maxlen*400], filedesc2[maxlen*100];
 int file_id, ndatasets,nglobal_attr, filelabellen, filedesclen;
 int attrvalue[maxattr], attridx;
 float tmpattr, floatattr[73];
 int intattr[32];
 char sdsname[40];
 int rank, dims[3];
 int i4fillval, i4arr[maxscan*37*6], i4_tmp[maxscan][37][6];
 short int i2fillval, i2arr[maxscan*37*6], i2_tmp[maxscan][37][6];
 unsigned char i1fillval, i1arr[maxscan*37*6], i1_tmp[maxscan][37][6];
 double cal, cal_err, offset, offset_err;
 int xdimscale[maxscan], ydimscale[37];
 float zdimscale[6];
 int i4max, i4min;
 short int i2max, i2min;
 unsigned char i1max, i1min;
 unsigned short int sdsref;
 char dimnamebk[maxlen],dimlabelbk[maxlen], dimunitbk[maxlen],
     dimfmtbk[maxlen], datalabelbk[maxlen], dataunitbk[maxlen],
     datafmtbk[maxlen], coordsysbk[maxlen], datadescbk[10*maxlen];
 int num_datatype, num_caltype, dimsize, num_dimtype;
 int dimid[3], nlocal_attr, dimnattrs, datadesclen;
 int start[3], stride[3], edge[3];
 int want, ext;
 char ch, buf[maxlen*50], str[maxlen];

 system("clear");
 if (argc<2) {printf("usage: v2hdfread.exe level2-hdf-filename\n"); exit(1);}
 hdf_file = argv[1];
 /* open hdf file to read annotation */
 file_id = Hopen(hdf_file, DFACC_RDONLY, 0);
 if (file_id==-1) {printf("error from Hopen\n"); exit(1);}
 /* get file label length and file label and display it */
 filelabellen = DFANgetfidlen(file_id,1);
 if (filelabellen==-1) {printf("error from DFANgetfidlen\n"); exit(1);}
 ret = DFANgetfid(file_id,filelabel,filelabellen+1,1);
 if (ret==-1) {printf("error from DFANgetfid\n"); exit(1);}
 filelabel[filelabellen+1]='\0';
 printf("filelabel=%s\n",filelabel);
 /* get file description length and file description for 1st */
 filedesclen = DFANgetfdslen(file_id,1);
 if (filedesclen==-1) {printf("error from DFANgetfdslen\n"); exit(1);}
 ret = DFANgetfds(file_id,filedesc1,filedesclen+1,1);
 if (ret==-1) {printf("error from DFANgetfds\n"); exit(1);}
 filedesc1[filedesclen+1]='\0';
 /* write 1st file description to an external file */
```

```c
printf("file description is in: filedesc.v2\n");
desc=fopen("filedesc.v2","w");
fprintf(desc,"%s\n",filedesc1);
fclose(desc);
/* get file description length and file description for 2nd and display it */
filedesclen = DFANgetfdslen(file_id,0);
if (filedesclen==-1) {printf("error from DFANgetfdslen\n"); exit(1);}
ret = DFANgetfds(file_id,filedesc2,filedesclen+1,0);
if (ret==-1) {printf("error from DFANgetfds\n"); exit(1);}
filedesc2[filedesclen+1]='\0';
printf("\nMetadata:\n\n%s\n",filedesc2);
/* close hdf file */
ret = Hclose(file_id);
if (ret==-1) {printf("error from Hclose\n"); exit(1);}


/* open hdf file to read each sds */
sd_id = SDstart(hdf_file, DFACC_RDONLY);
if (sd_id==-1) {printf("error from SDstart\n"); exit(1);}
/* get file information, know how many sds's there are in the file */
ret = SDfileinfo(sd_id,&ndatasets,&nglobal_attr);
if (ret==-1) {printf("error from SDfileinfo\n"); exit(1);}
printf("\n\nPress any key to continue or q to quit:");
ch=getchar(); if (ch=='q' || ch=='Q') exit(1); system("clear");
/* get and display netcdf-style attributes */
printf("netCDF-style global Attributes:\n\n");
attridx = SDfindattr(sd_id,attrname[0]);
if (attridx==-1) {printf("error from SDfindattr\n"); exit(1);}
ret = SDreadattr(sd_id,attridx,&intattr);
if (ret==-1) {printf("error from SDreadattr\n"); exit(1);}
printf("%s=\n",attrname[0]);
for (k=0; k<8; k++) printf("%d ",intattr[k]); printf("\n");
for (k=8; k<14; k++)  printf("%5d ",intattr[k]); printf("\n");
for (k=14; k<20; k++) printf("%5d ",intattr[k]); printf("\n");
for (k=20; k<26; k++) printf("%5d ",intattr[k]); printf("\n");
for (k=26; k<32; k++) printf("%5d ",intattr[k]); printf("\n");
attridx = SDfindattr(sd_id,attrname[1]);
if (attridx==-1) {printf("error from SDfindattr\n"); exit(1);}
ret = SDreadattr(sd_id,attridx,&floatattr[0]);
if (ret==-1) {printf("error from SDreadattr\n"); exit(1);}
attridx = SDfindattr(sd_id,attrname[2]);
if (attridx==-1) {printf("error from SDfindattr\n"); exit(1);}
ret = SDreadattr(sd_id,attridx,&floatattr[6]);
if (ret==-1) {printf("error from SDreadattr\n"); exit(1);}
attridx = SDfindattr(sd_id,attrname[3]);
if (attridx==-1) {printf("error from SDfindattr\n"); exit(1);}
ret = SDreadattr(sd_id,attridx,&floatattr[12]);
if (ret==-1) {printf("error from SDreadattr\n"); exit(1);}
attridx = SDfindattr(sd_id,attrname[4]);
if (attridx==-1) {printf("error from SDfindattr\n"); exit(1);}
ret = SDreadattr(sd_id,attridx,&floatattr[36]);
if (ret==-1) {printf("error from SDreadattr\n"); exit(1);}
printf("%s=\n",attrname[1]);
for (k=0; k<6; k++) printf("%f ",floatattr[k]); printf("\n");
printf("%s=\n",attrname[2]);
for (k=0; k<6; k++) printf("%f ",floatattr[k+6]); printf("\n");
printf("%s=\n",attrname[3]);
for (k=0; k<4; k++) printf("%9.6f ",floatattr[k+12]); printf("\n");
for (k=4; k<8; k++) printf("%9.6f ",floatattr[k+12]); printf("\n");
for (k=8; k<12; k++) printf("%9.6f ",floatattr[k+12]); printf("\n");
for (k=12; k<16; k++) printf("%9.6f ",floatattr[k+12]); printf("\n");
for (k=16; k<20; k++) printf("%9.6f ",floatattr[k+12]); printf("\n");
for (k=20; k<24; k++) printf("%9.6f ",floatattr[k+12]); printf("\n");
printf("%s=\n",attrname[4]);
for (k=0; k<7; k++) printf("%9.6f ",floatattr[k+36]); printf("\n");
```

```
for (k=7; k<14; k++) printf("%9.6f ",floatattr[k+36]); printf("\n");
for (k=14; k<21; k++) printf("%9.6f ",floatattr[k+36]); printf("\n");
for (k=21; k<28; k++) printf("%9.6f ",floatattr[k+36]); printf("\n");
for (k=28; k<35; k++) printf("%9.6f ",floatattr[k+36]); printf("\n");
printf("\n\nPress any key to continue or q to quit:");
ch=getchar(); if (ch=='q' || ch=='Q') exit(1); system("clear");
strcpy(buf,"");
for (num=0; num<ndatasets; num++)
 {/* open each sds */
  sdsid = SDselect(sd_id,num);
  if (sdsid==-1) {printf("error from SDselect\n"); exit(1);}
  /* is coordinate sds or data sds */
  ret = SDiscoordvar(sdsid);
  if (ret==1)
   {sprintf(str,"No.%2d sds is a coordinate sds\n",num+1);
    strcat(buf,str);
   }
  else
   {sprintf(str,"No.%2d sds is a data sds, ",num+1);
    strcat(buf,str);
    sdsref = SDidtoref(sdsid);
    if (sdsref==-1) {printf("error after SDidtoref\n"); exit(1);}
    /* get sds information for data sds,display name and dimensions */
    ret = SDgetinfo(sdsid,sdsname,&rank,dims,&num_datatype,&nlocal_attr);
    if (ret==-1) {printf("error after SDgetinfo\n"); exit(1);}
    strcat(buf,"name="); strcat(buf,sdsname);
    for (k=0; k<20-strlen(sdsname); k++) strcat(buf," ");
    strcat(buf,"dimension=");
    for (k=0; k<rank; k++) {sprintf(str,"%d ",dims[k]); strcat(buf,str);}
    strcat(buf,"\n");
    ret = SDendaccess(sdsid);
    if (ret==-1) {printf("error after SDendaccess\n"); exit(1);}
   }
 }
while (1)
 {
  do
   {
    system("clear");
    printf("%s",buf);
    printf("\n\nEnter the No. of sds desired or q to quit ==> ");
    ch=getchar();
    if (ch=='q' || ch=='Q') want=0;
    else {ungetc(ch,stdin); scanf("%d",&want); ch=getchar();}
    if (want<0 || want>ndatasets)
     {printf("\ninvalid sds No. \n\nPress any key to continue:");
      ch=getchar();
     }
   } while (want<0 || want>ndatasets);
  if (want==0) break;
  /* open the desired sds */
  sdsid = SDselect(sd_id,want-1);
  if (sdsid==-1) {printf("error from SDselect\n"); exit(1);}
  /* is coordinate sds or data sds */
  ret = SDiscoordvar(sdsid);
  if (ret==1)
   {printf("\nthis is not a data sds \n\nPress any key to continue:");
    ch=getchar();
   }
  else
   {sdsref = SDidtoref(sdsid);
    if (sdsref==-1) {printf("error after SDidtoref\n"); exit(1);}
    /* get and display sds information for data sds */
    ret = SDgetinfo(sdsid,sdsname,&rank,dims,&num_datatype,&nlocal_attr);
```

```
   if (ret==-1) {printf("error after SDgetinfo\n"); exit(1);}
   system("clear"); printf("SDS NAME ===> ");
   printf("\"%s\"\nrank=%d\ndims=",sdsname,rank);
   for (i=0; i<rank; i++) printf("%d ",dims[i]);
   printf("\ndatatype=\"%s\"\n",to_strtype(num_datatype));
   for (i=0; i<rank; i++)
    {dimid[i] = SDgetdimid(sdsid,i);
     if (dimid[i]==-1) {printf("error after SDgetdimid\n"); exit(1);}
     /* get and display dimension information for the sds */
     ret = SDdiminfo(dimid[i],dimnamebk,&dimsize,&num_dimtype,&dimnattrs);
     if (ret==-1) {printf("error after SDdiminfo\n"); exit(1);}
     switch (i)
      {case 0: ret = SDgetdimscale(dimid[i],xdimscale); break;
       case 1: ret = SDgetdimscale(dimid[i],ydimscale); break;
       case 2: ret = SDgetdimscale(dimid[i],zdimscale); break;
      }
     if (ret==-1) {printf("error after SDgetdimscale\n"); exit(1);}
       printf("for dim %d: dimname=\"%s\"\n          dimsize=%d\n          dimtype=\"%s\"\n",i,dimnamebk,dim-
size,to_strtype(num_dimtype));
      ret = SDgetdimstrs(dimid[i],dimlabelbk,dimunitbk,dimfmtbk,maxlen);
      if (ret==-1) {printf("error after SDgetdimstrs\n"); exit(1);}
     printf("     dimlabel=\"%s\"\n     dimunit=\"%s\"\n     dimfmt=\"%s\"\n",dimlabelbk,dimunitbk,dimfmtbk);
      start[i]=0; stride[i]=1; edge[i]=dims[i];
     }
   for (i=rank; i<3; i++) {dims[i]=start[i]=stride[i]=edge[i]=0;}
   /* get data description length and data description and display it */
   datadesclen = DFANgetdesclen(hdf_file,DFTAG_NDG,sdsref);
   if (datadesclen==-1) {printf("error after DFANgetdesclen\n"); exit(1);}
   ret = DFANgetdesc(hdf_file,DFTAG_NDG,sdsref,datadescbk,datadesclen);
   if (ret==-1) {printf("error after DFANgetdesc\n"); exit(1);}
   datadescbk[datadesclen]='\0';
   printf("datadesc=\"%s\"\n",datadescbk);
   /* get calibration information and display it */
   ret = SDgetcal(sdsid,&cal,&cal_err,&offset,&offset_err,&num_caltype);
   if (ret==-1) {printf("error after SDgetcal\n"); exit(1);}
printf("cal=%.4lf\ncal_err=%.1lf\noffset=%.1lf\noffset_err=%.1lf\ncaltype=\"%s\"\n",
   cal,cal_err,offset,offset_err,to_strtype(num_caltype));
   /* get data strings and display them */
   ret = SDgetdatastrs(sdsid,datalabelbk,dataunitbk,datafmtbk,coordsysbk,maxlen);
   if (ret==-1) {printf("error after SDgetdatastrs\n"); exit(1);}
printf("datalabel=\"%s\"\ndataunit=\"%s\"\ndatafmt=\"%s\"\ncoordsys=\"%s\"\n",
   datalabelbk,dataunitbk,datafmtbk,coordsysbk);
   /* get fill value and display it */
   if (num_datatype==DFNT_UINT8)
    {ret = SDgetfillvalue(sdsid,&i1fillval);
     if (ret==-1) {printf("error after SDgetfillvalue\n"); exit(1);}
     ret = SDgetrange(sdsid,&i1max,&i1min);
     if (ret==-1) {printf("error after SDgetrange\n"); exit(1);}
     printf("fillval=%u\nmin=%u\nmax=%u\n",i1fillval,i1min,i1max);
    }
   else if (num_datatype==DFNT_INT16)
    {ret = SDgetfillvalue(sdsid,&i2fillval);
     if (ret==-1) {printf("error after SDgetfillvalue\n"); exit(1);}
     ret = SDgetrange(sdsid,&i2max,&i2min);
     if (ret==-1) {printf("error after SDgetrange\n"); exit(1);}
     printf("fillval=%hd\nmin=%hd\nmax=%hd\n",i2fillval,i2min,i2max);
    }
   else if (num_datatype==DFNT_INT32)
    {ret = SDgetfillvalue(sdsid,&i4fillval);
     if (ret==-1) {printf("error after SDgetfillvalue\n"); exit(1);}
     ret = SDgetrange(sdsid,&i4max,&i4min);
     if (ret==-1) {printf("error after SDgetrange\n"); exit(1);}
     printf("fillval=%d\nmin=%d\nmax=%d\n",i4fillval,i4min,i4max);
    }
```

```c
printf("\n\nPress any key to continue or q to break:");
ch=getchar();
if (ch=='q' || ch=='Q');
else
 {system("clear");
 /* read data and display it */
 printf("reading data...\n");
 if (num_datatype==DFNT_UINT8)
  ret = SDreaddata(sdsid,start,stride,edge,i1arr);
  else if (num_datatype==DFNT_INT16)
  ret = SDreaddata(sdsid,start,stride,edge,i2arr);
  else if (num_datatype==DFNT_INT32)
  ret = SDreaddata(sdsid,start,stride,edge,i4arr);
  else {printf("data type invalid\n"); exit(1);}
  if (ret==-1) {printf("error after SDreaddata\n"); exit(1);}
  system("clear");
  m=ext=0;
  if (rank==1)
  {printf("%s\n",sdsname);
   printf("%3d: ",1);
   for (k=0; k<dims[0]; k++)
    {if (num_datatype==DFNT_UINT8) printf("%6u ",i1arr[m++]);
     else if (num_datatype==DFNT_INT16) printf("%6hd ",i2arr[m++]);
     else if (num_datatype==DFNT_INT32) printf("%6d ",i4arr[m++]);
     if ((k+1)%10==0) printf("\n%3d: ",(k+1)/10+1);
    }
   printf("\nPress any key to continue:"); ch=getchar();
  }
  else if (rank==2)
  {for (j=0; j<dims[0]; j++)
    for (k=0; k<dims[1]; k++)
    {if (num_datatype==DFNT_UINT8)     i1_tmp[j][k][0]=i1arr[m++];
     else if (num_datatype==DFNT_INT16) i2_tmp[j][k][0]=i2arr[m++];
     else if (num_datatype==DFNT_INT32) i4_tmp[j][k][0]=i4arr[m++];
    }
   m=0;
   j=1;
   printf("%s\n",sdsname);
   do
    {printf("\nScan %3d:\n",j);
     for (k=0; k<dims[1]; k++)
     {if (num_datatype==DFNT_UINT8) printf("%6u ",i1_tmp[j-1][k][0]);
      else if (num_datatype==DFNT_INT16) printf("%6hd ",i2_tmp[j-1][k][0]);
      else if (num_datatype==DFNT_INT32) printf("%6d ",i4_tmp[j-1][k][0]);
      if ((k+1)%10==0) printf("\n");
     }
    printf("\n"); m++;
    j++;
    if (m%5==0)
     {printf("\n\nPress any key to continue or q to break or enter the Scan number desired:");
      ch=getchar();
      if (ch=='q' || ch=='Q') {ch=getchar(); ext=1; break;}
      else if (ch=='\n');
      else {ungetc(ch,stdin);
          scanf("%d",&j); ch=getchar();
          if (j<1 || j>dims[0])
           {printf("\ninvalid input \n\nPress any key to continue:");
            ch=getchar();
            j=1;
           }
          }
     system("clear");
     printf("%s\n",sdsname);
     }
```

```
      } while (j>=1 && j<=dims[0]);
     if (!ext)
      {printf("\n\nPress any key to continue:");
       ch=getchar();
      }
    }
   else if (rank==3)
    {for (i=0; i<dims[0]; i++)
     for (j=0; j<dims[1]; j++)
      for (k=0; k<dims[2]; k++)
       {if (num_datatype==DFNT_UINT8) i1_tmp[i][j][k]=i1arr[m++];
        else if (num_datatype==DFNT_INT16) i2_tmp[i][j][k]=i2arr[m++];
        else if (num_datatype==DFNT_INT32) i4_tmp[i][j][k]=i4arr[m++];
       }
     i=1;
     do
      {system("clear");
       printf("%s\n",sdsname);
       printf("Scan %3d:\n\n",i);
       for (j=0; j<dims[1]; j++)
        {printf("Scene %2d: ",j+1);
         for (k=0; k<dims[2]; k++)
          {if (num_datatype==DFNT_UINT8) printf("%6u ",i1_tmp[i-1][j][k]);
           else if (num_datatype==DFNT_INT16) printf("%6hd ",i2_tmp[i-1][j][k]);
           else if (num_datatype==DFNT_INT32) printf("%6d ",i4_tmp[i-1][j][k]);
          }
         printf("\n");
        }
       printf("\n\nPress any key to continue or q to break or enter Scan number desired:");
       ch=getchar();
       if (ch=='q' || ch=='Q') {ch=getchar(); break;}
       else if (ch=='\n') i++;
       else {ungetc(ch,stdin);
            scanf("%d",&i); ch=getchar();
            if (i<1 || i>dims[0])
             {printf("\ninvalid input \n\nPress any key to continue:");
              ch=getchar();
              i=1;
             }
            }
      } while (i>=1 && i<=dims[0]);
     }
    }
   }
  /* close sds */
  ret = SDendaccess(sdsid);
  if (ret==-1) {printf("error after SDendaccess\n"); exit(1);}
  }
 /* close hdf file */
 ret = SDend(sd_id);
 if (ret==-1) {printf("error from SDend\n"); exit(1);}
}
```

The program v3hdfread.c can be used to read the TOMS Level–3 HDF file. It is executed using the command v3hdfread.exe level3-hdf-filename, where v3hdfread.exe is the compiled version of v3hdfread.c.

Immediately after execution, the program will display the following information:

- File label
- Text: "File description is stored in the file: filedesc.v3"
- (This description may be large.)
- Metadata

The next keystroke will display a numbered list of the SDS's providing the name and dimension of the SDS corresponding to each number: 1 is ozone, 4 is reflectivity. (Numbers 2 and 3 are coordinate data sets and not displayed by this software.) The user can display either SDS by entering its number or can exit the program by entering q. For the selected SDS, the program will display a description of the axes, the units, and the scale factors between values in the HDF data set and the physical values. The user can then press q to go back to the SDS list or any other key to browse the data. After the user enters the number of the desired SDS, data from one latitude band can be displayed. The default latitude band is one. The user can select another latitude band by entering its number, go back to the SDS list by entering q, or press any other key to continue to the next latitude band.

The program displays the unscaled data in the HDF file. To display the ozone or reflectivity in physical units, users will require software to apply the appropriate offsets and scale factors, shown when the SDS is selected.

```
program name: v3hdfread.c
****************************************************************/
#include <stdio.h>
#include "hdf.h"
#define maxlen100
#define maxattr20

char *to_strtype(intype)
int intype;
{char *str;
 switch (intype)
 {case DFNT_UINT8:  str="UINT8";  break;
  case DFNT_INT8:  str="INT8";  break;
  case DFNT_INT16: str="INT16"; break;
  case DFNT_INT32: str="INT32"; break;
  case DFNT_FLOAT32: str="FLOAT32"; break;
  otherwise: str="unknown"; break;
 }
 return(str);
}

main(argc,argv)
int argc;
char *argv[];
{
 FILE *desc;
 int sd_id, sdsid;
 int ret, num, i, j, k;
 char *hdf_file, filelabel[maxlen];
 char filedesc1[maxlen*400], filedesc2[maxlen*100];
 int file_id, ndatasets, nglobal_attr, filelabellen, filedesclen;
 char sdsname[40];
 int rank, dims[2];
 int i4fillval, i4arr[180][288];
 short int i2fillval, i2arr[180][288];
 unsigned char i1fillval, i1arr[180][288];
 double cal, cal_err, offset, offset_err;
 int xdimscale[180], ydimscale[288];
 int i4max, i4min;
 short int i2max, i2min;
 unsigned char i1max, i1min;
 unsigned short int sdsref;
 char dimnamebk[maxlen],dimlabelbk[maxlen], dimunitbk[maxlen],
     dimfmtbk[maxlen], datalabelbk[maxlen], dataunitbk[maxlen],
     datafmtbk[maxlen], coordsysbk[maxlen], datadescbk[10*maxlen];
 int num_datatype, num_caltype, dimsize, num_dimtype;
 int dimid[2], nlocal_attr, dimnattrs, datadesclen;
 int start[2], stride[2], edge[2];
 int want;
 char ch, buf[maxlen*50], str[maxlen];
```

```
system("clear");
if (argc<2) {printf("usage: v3hdfread.exe level3-hdf-filename\n"); exit(1);}
hdf_file = argv[1];
/* open hdf file to read annotation */
file_id = Hopen(hdf_file, DFACC_RDONLY, 0);
if (file_id==-1) {printf("error from Hopen\n"); exit(1);}
/* get file label length and file label and display it */
filelabellen = DFANgetfidlen(file_id,1);
if (filelabellen==-1) {printf("error from DFANgetfidlen\n"); exit(1);}
ret = DFANgetfid(file_id,filelabel,filelabellen+1,1);
if (ret==-1) {printf("error from DFANgetfid\n"); exit(1);}
filelabel[filelabellen+1]='\0';
printf("filelabel=%s\n",filelabel);
/* get file description length and file description for 1st */
filedesclen = DFANgetfdslen(file_id,1);
if (filedesclen==-1) {printf("error from DFANgetfdslen\n"); exit(1);}
ret = DFANgetfds(file_id,filedesc1,filedesclen+1,1);
if (ret==-1) {printf("error from DFANgetfds\n"); exit(1);}
filedesc1[filedesclen+1]='\0';
/* write 1st file description to an external file */
printf("file description is in: filedesc.v3\n");
desc=fopen("filedesc.v3","w");
fprintf(desc,"%s\n",filedesc1);
fclose(desc);
/* get file description length and file description for 2nd and display it */
filedesclen = DFANgetfdslen(file_id,0);
if (filedesclen==-1) {printf("error from DFANgetfdslen\n"); exit(1);}
ret = DFANgetfds(file_id,filedesc2,filedesclen+1,0);
if (ret==-1) {printf("error from DFANgetfds\n"); exit(1);}
filedesc2[filedesclen+1]='\0';
printf("\nMetadata:\n\n%s\n",filedesc2);
/* close hdf file */
ret = Hclose(file_id);
if (ret==-1) {printf("error from Hclose\n"); exit(1);}
/* open hdf file to read each sds */
sd_id = SDstart(hdf_file, DFACC_RDONLY);
if (sd_id==-1) {printf("error from SDstart\n"); exit(1);}
/* get file information, know how many sds's there are in the file */
ret = SDfileinfo(sd_id,&ndatasets,&nglobal_attr);
if (ret==-1) {printf("error from SDfileinfo\n"); exit(1);}
printf("\n\nPress any key to continue or q to quit:");
ch=getchar(); if (ch=='q' || ch=='Q') exit(1); system("clear");
strcpy(buf,"");
for (num=0; num<ndatasets; num++)
 {/* open each sds */
  sdsid = SDselect(sd_id,num);
  if (sdsid==-1) {printf("error from SDselect\n"); exit(1);}
  /* is coordinate sds or data sds */
  ret = SDiscoordvar(sdsid);
  if (ret==1)
   {sprintf(str,"No.%2d sds is a coordinate sds\n",num+1);
    strcat(buf,str);
   }
  else
   {sprintf(str,"No.%2d sds is a data sds, ",num+1);
    strcat(buf,str);
    sdsref = SDidtoref(sdsid);
    if (sdsref==-1) {printf("error after SDidtoref\n"); exit(1);}
    /* get sds information for data sds,display name and dimensions */
    ret = SDgetinfo(sdsid,sdsname,&rank,dims,&num_datatype,&nlocal_attr);
    if (ret==-1) {printf("error after SDgetinfo\n"); exit(1);}
    strcat(buf,"name="); strcat(buf,sdsname);
    for (k=0; k<20-strlen(sdsname); k++) strcat(buf," ");
```

63

```c
        strcat(buf,"dimension=");
        for (k=0; k<rank; k++) {sprintf(str,"%d ",dims[k]); strcat(buf,str);}
        strcat(buf,"\n");
        ret = SDendaccess(sdsid);
        if (ret==-1) {printf("error after SDendaccess\n"); exit(1);}
      }
  }
 while (1)
  {
   do
    {
    system("clear");
    printf("%s",buf);
    printf("\n\nEnter the No. of sds desired or q to quit ==> ");
    ch=getchar();
    if (ch=='q' || ch=='Q') want=0;
    else {ungetc(ch,stdin); scanf("%d",&want); ch=getchar();}
    if (want<0 || want>ndatasets)
     {printf("\ninvalid sds No. \n\nPress any key to continue:");
      ch=getchar();
     }
    } while (want<0 || want>ndatasets);
   if (want==0) break;
   /* open the desired sds */
   sdsid = SDselect(sd_id,want-1);
   if (sdsid==-1) {printf("error from SDselect\n"); exit(1);}
   /* is coordinate sds or data sds */
   ret = SDiscoordvar(sdsid);
   if (ret==1)
    {printf("\nthis is not a data sds \n\nPress any key to continue:");
     ch=getchar();
    }
   else
    {sdsref = SDidtoref(sdsid);
     if (sdsref==-1) {printf("error after SDidtoref\n"); exit(1);}
     /* get and display sds information for data sds */
     ret = SDgetinfo(sdsid,sdsname,&rank,dims,&num_datatype,&nlocal_attr);
     if (ret==-1) {printf("error after SDgetinfo\n"); exit(1);}
     system("clear"); printf("SDS NAME ===> ");
     printf("\"%s\"\nrank=%d\ndims=",sdsname,rank);
     for (i=0; i<rank; i++) printf("%d ",dims[i]);
     printf("\ndatatype=\"%s\"\n",to_strtype(num_datatype));
     for (i=0; i<rank; i++)
      {dimid[i] = SDgetdimid(sdsid,i);
       if (dimid[i]==-1) {printf("error after SDgetdimid\n"); exit(1);}
       /* get and display dimension information for the sds */
       ret = SDdiminfo(dimid[i],dimnamebk,&dimsize,&num_dimtype,&dimnattrs);
       if (ret==-1) {printf("error after SDdiminfo\n"); exit(1);}
       switch (i)
        {case 0: ret = SDgetdimscale(dimid[i],xdimscale); break;
         case 1: ret = SDgetdimscale(dimid[i],ydimscale); break;
        }
       if (ret==-1) {printf("error after SDgetdimscale\n"); exit(1);}
        printf("for dim %d: dimname=\"%s\"\n          dimsize=%d\n          dimtype=\"%s\"\n",i,dimnamebk,dim-
size,to_strtype(num_dimtype));
        ret = SDgetdimstrs(dimid[i],dimlabelbk,dimunitbk,dimfmtbk,maxlen);
       if (ret==-1) {printf("error after SDgetdimstrs\n"); exit(1);}
      printf("    dimlabel=\"%s\"\n     dimunit=\"%s\"\n     dimfmt=\"%s\"\n",dimlabelbk,dimunitbk,dimfmtbk);
       start[i]=0; stride[i]=1; edge[i]=dims[i];
      }
     for (i=rank; i<2; i++) {dims[i]=start[i]=stride[i]=edge[i]=0;}
     /* get data description length and data description and display it */
     datadesclen = DFANgetdesclen(hdf_file,DFTAG_NDG,sdsref);
     if (datadesclen==-1) {printf("error after DFANgetdesclen\n"); exit(1);}
```

```
ret = DFANgetdesc(hdf_file,DFTAG_NDG,sdsref,datadescbk,datadesclen);
if (ret==-1) {printf("error after DFANgetdesc\n"); exit(1);}
datadescbk[datadesclen]='\0';
printf("datadesc=\"%s\"\n",datadescbk);
/* get calibration information and display it */
ret = SDgetcal(sdsid,&cal,&cal_err,&offset,&offset_err,&num_caltype);
if (ret==-1) {printf("error after SDgetcal\n"); exit(1);}
printf("cal=%.4lf\ncal_err=%.1lf\noffset=%.1lf\noffset_err=%.1lf\ncaltype=\"%s\"\n",
       cal,cal_err,offset,offset_err,to_strtype(num_caltype));
/* get data strings and display them */
ret = SDgetdatastrs(sdsid,datalabelbk,dataunitbk,datafmtbk,coordsysbk,maxlen);
if (ret==-1) {printf("error after SDgetdatastrs\n"); exit(1);}
printf("datalabel=\"%s\"\ndataunit=\"%s\"\ndatafmt=\"%s\"\ncoordsys=\"%s\"\n",
       datalabelbk,dataunitbk,datafmtbk,coordsysbk);
/* get fill value and display it */
if (num_datatype==DFNT_UINT8)
 {ret = SDgetfillvalue(sdsid,&i1fillval);
  if (ret==-1) {printf("error after SDgetfillvalue\n"); exit(1);}
  ret = SDgetrange(sdsid,&i1max,&i1min);
  if (ret==-1) {printf("error after SDgetrange\n"); exit(1);}
  printf("fillval=%u\nmin=%u\nmax=%u\n",i1fillval,i1min,i1max);
 }
else if (num_datatype==DFNT_INT16)
 {ret = SDgetfillvalue(sdsid,&i2fillval);
  if (ret==-1) {printf("error after SDgetfillvalue\n"); exit(1);}
  ret = SDgetrange(sdsid,&i2max,&i2min);
  if (ret==-1) {printf("error after SDgetrange\n"); exit(1);}
  printf("fillval=%hd\nmin=%hd\nmax=%hd\n",i2fillval,i2min,i2max);
 }
else if (num_datatype==DFNT_INT32)
 {ret = SDgetfillvalue(sdsid,&i4fillval);
  if (ret==-1) {printf("error after SDgetfillvalue\n"); exit(1);}
  ret = SDgetrange(sdsid,&i4max,&i4min);
  if (ret==-1) {printf("error after SDgetrange\n"); exit(1);}
  printf("fillval=%d\nmin=%d\nmax=%d\n",i4fillval,i4min,i4max);
 }
printf("\n\nPress any key to continue or q to break:");
ch=getchar();
if (ch=='q' || ch=='Q');
else
 {system("clear");
  /* read data and display it */
  printf("reading data...\n");
  if (num_datatype==DFNT_UINT8)
   ret = SDreaddata(sdsid,start,stride,edge,i1arr);
  else if (num_datatype==DFNT_INT16)
   ret = SDreaddata(sdsid,start,stride,edge,i2arr);
  else if (num_datatype==DFNT_INT32)
   ret = SDreaddata(sdsid,start,stride,edge,i4arr);
  else {printf("data type invalid\n"); exit(1);}
  if (ret==-1) {printf("error after SDreaddata\n"); exit(1);}
  j=1;
  do
    {system("clear");
     printf("%s\n",sdsname);
     printf("\nLatitude band %3d:\n",j);
     for (k=0; k<dims[1]; k++)
      {if (num_datatype==DFNT_UINT8) printf("%6u ",i1arr[j-1][k]);
       else if (num_datatype==DFNT_INT16) printf("%6hd ",i2arr[j-1][k]);
       else if (num_datatype==DFNT_INT32) printf("%6d ",i4arr[j-1][k]);
       if ((k+1)%10==0) printf("\n");
      }
     printf("\n\nPress any key to continue or q to break or enter the Latitude band desired:");
     ch=getchar();
```

```
        if (ch=='q' || ch=='Q') {ch=getchar(); break;}
        else if (ch=='\n') j++;
        else {ungetc(ch,stdin);
            scanf("%d",&j); ch=getchar();
            if (j<1 || j>dims[0])
             {printf("\ninvalid input \n\nPress any key to continue:");
              ch=getchar();
              j=1;
              }
            }
        } while (j>=1 && j<=dims[0]);
    }
  }
 /* close sds */
 ret = SDendaccess(sdsid);
 if (ret==-1) {printf("error after SDendaccess\n"); exit(1);}
 }
 /* close hdf file */
 ret = SDend(sd_id);
 if (ret==-1) {printf("error from SDend\n"); exit(1);}
}
```

APPENDIX C. DATA AVAILABILITY

The derivative data products defined in this User's Guide are archived at and available from the NASA Goddard Space Flight Center Distributed Active Archive Center (NASA/GSFC/DAAC). All data and services offered by the Goddard DAAC are free. For very high volume data orders, users may be asked to provide the magnetic tapes for the requested data.

The DAAC may be accessed on World Wide Web at http://daac.gsfc.nasa.gov/. Options for locating and accessing data are listed on the DAAC home page. Information about TOMS and other ozone data archived at the Goddard DAAC can be found at http://daac.gsfc.nasa.gov/CAMPAIGN_DOCS/ATM_CHEM/ac_main.html. In addition to data, the DAAC Web pages contain information about HDF, the format in which it provides the Level–2 and Level–3 TOMS products, available from ftp://daac.gsfc.nasa.gov/pub/hdf/. Get the README file.

The DAAC maintains a help desk, which provides assistance with its on-line ordering services. It can be reached as follows:

Electronic Mail:daacuso@daac.gsfc.nasa.gov
Telephone: +1-301-286-3209
FAX: +1-301-286-0268

The postal address of the DAAC is

Goddard Distributed Active Archive Center
Global Change Data Center

Code 902.2

NASA/Goddard Space Flight Center
Greenbelt, MD 20771